Spherical Nanoindentation:

Insights And Improvements, Including Stress-Strain Curves and Effective Zero Point Determination

A Thesis

Submitted to the Faculty

of

Drexel University

by

Alexander J. Moseson

in partial fulfillment of the

requirements for the degree

of

Master of Science in Materials Science And Engineering

September 2007

DEDICATIONS

This work is dedicated to my family, both they who raised me from birth, and she who will soon be family by love and marriage. I thank them for all their support, and praise God for His unfathomable grace and love, in the years of work which culminate in this thesis.

ACKNOWLEDGEMENTS

I would first like to thank Dr. M. W. Barsoum for his invaluable teaching in the classroom, lab, and life. I would also like to thank my colleague Mr. Sandip Basu, a mentor and partner in this work, and Mr. Aiguo Zhou, for his help with bulk compression tests and other training. I could not name them all here, but my thanks go as well to the faculty, staff, and students in the Materials Science And Engineering Department, without whose teaching and support none of this would have been possible. Last but not least, I am also gladly indebted to the Mechanical Engineering And Mechanics Department, especially Dr. Mun Y. Choi, and the College of Engineering, especially Dr. Selçuk Güçeri, for their support, guidance, and encouragement. This work was supported by the Army Research Office (DAAD19-03-1-0213).

TABLE OF CONTENTS

LIST OF TABLES vi

LIST OF FIGURES vii

ABSTRACT ix

CHAPTER 1. BACKGROUND 1

1.1 Background on Instrumented Indentation 1

1.3 Spherical Indentation Model 10

1.4 Experimental Details 17

CHAPTER 2. STRESS-STRAIN CURVES FROM SPHERICAL NANOINDENTATION 20

2.1 Background On Obtaining Stress-Strain Curves From Spherical Indentation 20

2.2 Results And Discussion 22

CHAPTER 3. EFFECTIVE ZERO POINT DETERMINATION 39

3.2 Effective Zero Point Determination Methodology 44

3.3 Results 46

3.4 Discussion 57

3.5 Potential Applications 59

3.6 Critical Analysis Of Method 61

3.7 Summary And Conclusions: Effective Zero Point 63

CHAPTER 4. SPHERICAL NANOINDENTATION TO CHARACTERIZE INDIVIDUAL GRAINS 64

4.1 Three Different Grains on Iron$_B$ 64

4.2 The Effect Of Compression on Iron$_C$ 71

4.3 Summary of Work on Iron$_B$ and Iron$_C$ 78

CHAPTER 5. SUMMARY AND CONCLUSIONS 78

5.1 Summary And Conclusions 78

5.2 Future Work 81

LIST OF REFERENCES 83

APPENDIX 1: Provisional Patent #60/953,361 89

APPENDIX 2: Detailed Example Of Zero Point Determination Method 117

LIST OF TABLES

1. Mechanical Values From Literature And Our Work 24

2. Comparison of $Iron_C$ Vickers Hardness Values,
Before And After Compression 75

3. Comparison of $Iron_C$ Vickers Indents, Before And After compression 75

4. Detailed Example - Raw Data 117

5. Detailed Example - Data After X_j Shift 120

6. Detailed Example - Data With Calculations 121

7. Detailed Example - Regression Results - One Case 122

8. Detailed Example - Composite Regression Results 124

LIST OF FIGURES

1. Schematic of Nanoindenter 4
2. Berkovich Tip Indentation 5
3. Spherical Indentation Tip 5
4. CSM Oscillations 7
5. MTS CSM Operation 8
6. Spherical Indentation Model Schematic 10
7. S vs. a And Berkovich vs. Spherical 23
8. Aluminum - Stress vs. Strain, Before And After Original δ-Correction 26
9. Fused Silica - Stress vs. Strain, Before And After Original δ-Correction 29
10. ZnO – Load vs. Displacement And Stress vs. Strain 31
11. Sapphire – Stress vs. Strain 33
12. Iron$_A$ - Stress vs. Strain, Before And After Original δ-Correction 35
13. Silica - Load Vs. Displacement Before Correction 41
14. Fused Silica - Zero Point Results 47
15. Iron$_B$ – Zero Point Results 49
16. Sapphire – Zero Point Results 50
17. Effect of P on Stress-Strain 51
18. Eeff vs. δ 53
19. Our Method vs. Oliver & Pharr - Fused Silica, S vs. a 55
20. Our Method vs. Oliver & Pharr - Fused Silica, Stress vs. Strain 56

21. Micrograph of Iron$_B$ Sample 65

22. Annealed Iron$_B$ Map, Load vs. Displacement 67

23. Annealed Iron$_B$ Map, Stiffness vs. Contact Radius 68

24. Annealed Iron$_B$ Map, Indentation Stress vs. Indentation Strain 69

25. Compression Sample Results, Load vs. Displacement 72

26. Compression Sample Results, S vs. a 73

27. Compression Sample Results, Indentation Stress vs. Strain 74

28. P vs. h_t for raw data 119

29. Detailed Example - S vs. a The dashed line is the linear regression. 122

30. Detailed Example - Composite S vs. a 124

31. Detailed Example - Regression Results Comparison 125

ABSTRACT

Spherical Nanoindentation: Insights And Improvements, Including Stress-Strain Curves and Zero Point Determination

Alexander J. Moseson
Dr. M. W. Barsoum

Instrumented nanoindentation is a valuable method for mechanical characterization. Typically, sharp tips are used to indent surfaces and well-established techniques used to determine the hardness and moduli values of a wide range of materials. Spherical indentation tips, though less common, offer the distinct advantage of providing useful insight into the elasto-plastic transition region. In this thesis the results of continuous stiffness measurements with spherical indenters - with radii of 1 μm and/or 13.5 μm - and Hertzian theory are used to convert indentation load/depth curves to their corresponding stress-strain curves. We applied the technique to a wide range of materials, including fused silica, aluminum, iron and single crystals of sapphire and ZnO. In all cases, the stress-strain curves clearly showed the elastic, plastic, and elasto-plastic regions. The modulus and hardness obtained by our method show, for the most part, a strong correlation with bulk and Vickers values obtained on the same surface, respectively. When both the 1 μm and 13.5 μm indenters were used on the same material, for the most part, the indentation stress-strain curves traced one trajectory. Furthermore, accurate determination of the "zero point", first contact between an indenter tip and sample surface, has to date remained elusive. Herein a relatively simple, objective procedure by which that zero point can be determined accurately and reproducibly using a nanoindenter equipped with CSM option and a spherical tip is described. The method relies on applying a data shift, which insures that stiffness versus contact radius curves are linear and go through the origin. The method was applied to fused silica, sapphire single crystals and polycrystalline iron with various indenter sizes, to a zero point resolution of 2 nm. Errors of even a few nm can drastically alter plots and calculations which use the data, including stress vs. strain curves. The method is the first to use a parameter inherently *not* affected by zero point to correct the displacement and all subsequent uses thereof, which *is* highly sensitive to zero point. The applications of this method range from increased accuracy for all tests including stress vs. strain, to sample leveling, to individual grain characterization, and beyond. Finally, I herein present our most recent work, including further insights into the characterization of individual grains.

CHAPTER 1. BACKGROUND

Please Note: The content of this section has been adapted from two papers for which Alex Moseson was a primary or co-author.[1,2]

1.1 Background on Instrumented Indentation

The field of Materials Science and Engineering has three primary purposes: i) understand current materials, ii) develop new materials, and iii) develop and support applications of materials. For all three intertwined paths, characterization, whereby the properties and behavior of materials are observed, is critical. With limitless applications, as every physical object is by definition made of some material(s), nearly all material properties are of interest, be they mechanical, electrical, chemical, or otherwise. Temperature can be observed with a thermometer, and length with a ruler, but more complex and/or subtle properties require ever more sophisticated characterization techniques. Our theoretical understanding of materials advances in step with our ability to experiment and observe, as the scientific method demands, in the real world.

In this thesis, I present work done over the course of two years, which adds accuracy and functionality to a mechanical characterization method known as “instrumented indentation” or “nanoindentation.” The concept of the technique is simple: a tip with known geometry is pushed into the surface of a material, and the applied force and tip displacement are precisely measured. The result is essentially a hybrid of the information-rich stress-strain curves typically obtained from bulk compression tests and indentation hardness testing, with all its valuable advantages. It is assumed that the reader already has a working understanding of these two techniques.

Bulk compression applies a force along some linear axis of a bulk material, and measures the force, displacement, and perhaps other parameters such as strain. The most common representation of the data is a stress-strain curve.

Instrumented Indentation arose as a research field in the mid-1980's. Compared to other well-established techniques, this one is in its infancy. It is based however, on the much simpler "hardness" testing. In its simplest form, this was a test of a material's ability to resist scratching by another material. It was expressed on the semi-quantitative Mohs scale, developed by German Friedrich Mohs in 1812.[3] Next came indentation hardness, wherein typically, a single indent is made with a tip of known size, hardness, and geometry, and the dimensions of the residual indent examined. Harder materials will resist the material more, and thus have a smaller residual indent. and the size of the These indentation hardness tests (as opposed to the antiquated scratch tests) apply a known force with a tip of known geometry, and hardness is proportional to the size of the permanent indent created, squared. A schematic of a typical modern nanoindenter is shown in Figure 1. The actual electronic and physical configuration will vary by device, but the concept remains the same. An indenter tip, on the end of a shaft, is forced onto a sample by a load actuator. Sensors, such as LVDTs (Linear Variable Differential Transducers) precisely measure depth and force, on the order of nanometers and mN, respectively. The key advantages of nanoindentation above competing methods are extremely high precision, the ability to investigate the material microstructure such as individual grains and orientations, essentially non-destructive testing, and the ability to characterize thin films.

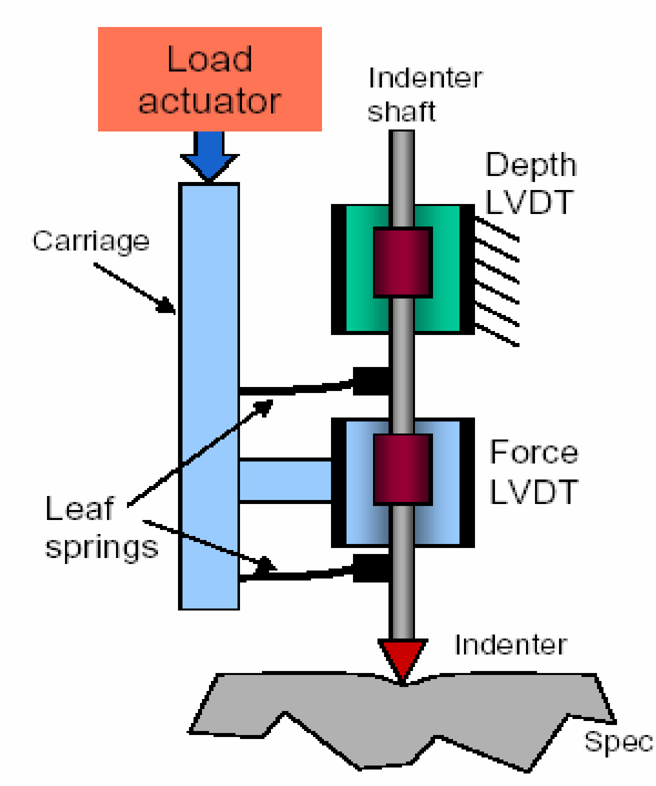

Figure 1: Schematic of Nanoindenter[4]

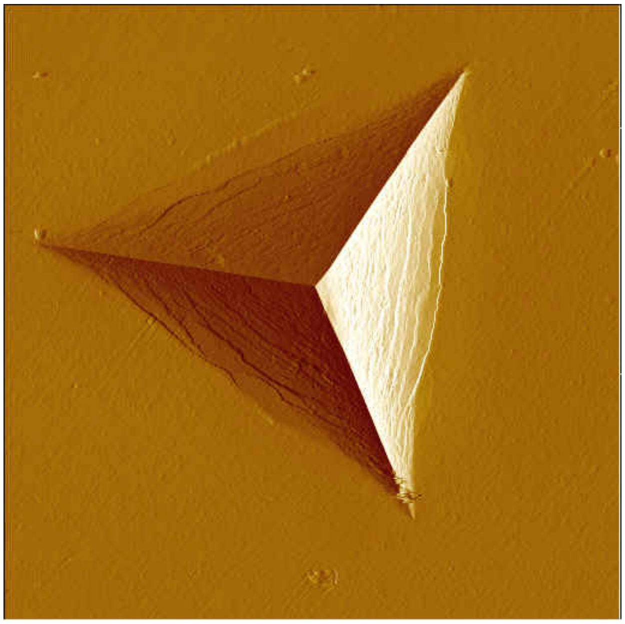

Figure 2: Berkovich Tip Indentation[4]

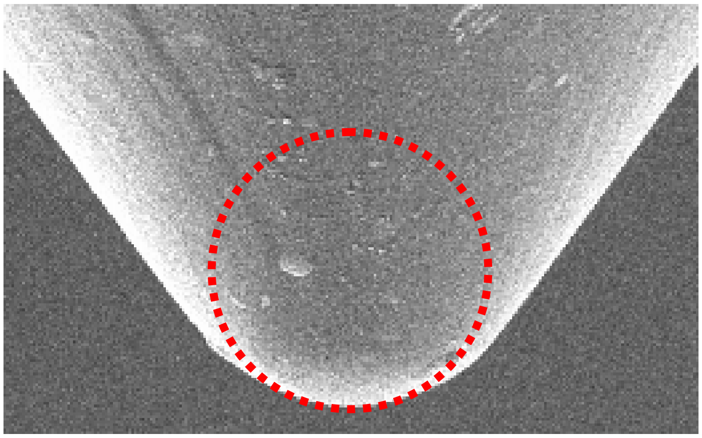

Figure 3: Spherical Indentation Tip[4,5]

Figure 2 shows the residual cavity from a Berkovich indentation, and Figure 3 shows a spherical, also sometimes referred to as conical, tip. The dotted line represents the area where the tip is assumed spherical. These are two common tip geometries. For reasons explained below, we have chosen to focus on spherical nanoindentation. In short, the technique has several advantages over sharp tip geometries, including the ability to characterize the elastic-to-plastic transition and parameters such as hardening rates.

For this work, we also utilize a Continuous Stiffness Measurement (CSM) Attachment on the nanoindenter. As depicted in Figure 4, CSM applies a superimposed oscillating load to the indenter tip, with force amplitudes that are roughly an order of magnitude smaller than the nominal load.[6] This technique is thus capable of accurately measuring the contact stiffness (otherwise the slope of the load-displacement curve) at every load and eliminates the need to carry out multiple loading-unloading measurements, as described in the Field and Swain method,[7,8] to calculate the variations in hardness and moduli values with load and displacement into the surface.

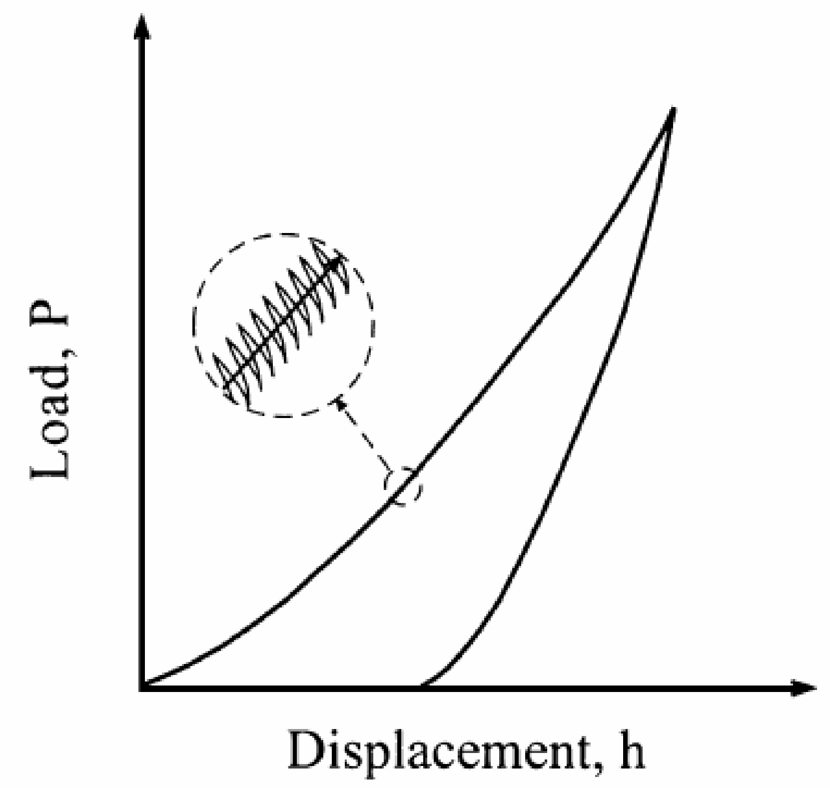

Figure 4: CSM Oscillations[4,9]

Figure 5 shows a representative schematic of the measurement actually taken in the MTS system used for this work. The details are proprietary, but the literature for the device states that "amplitude, ratio, and phase shift" are used to continuously determine the stiffness.

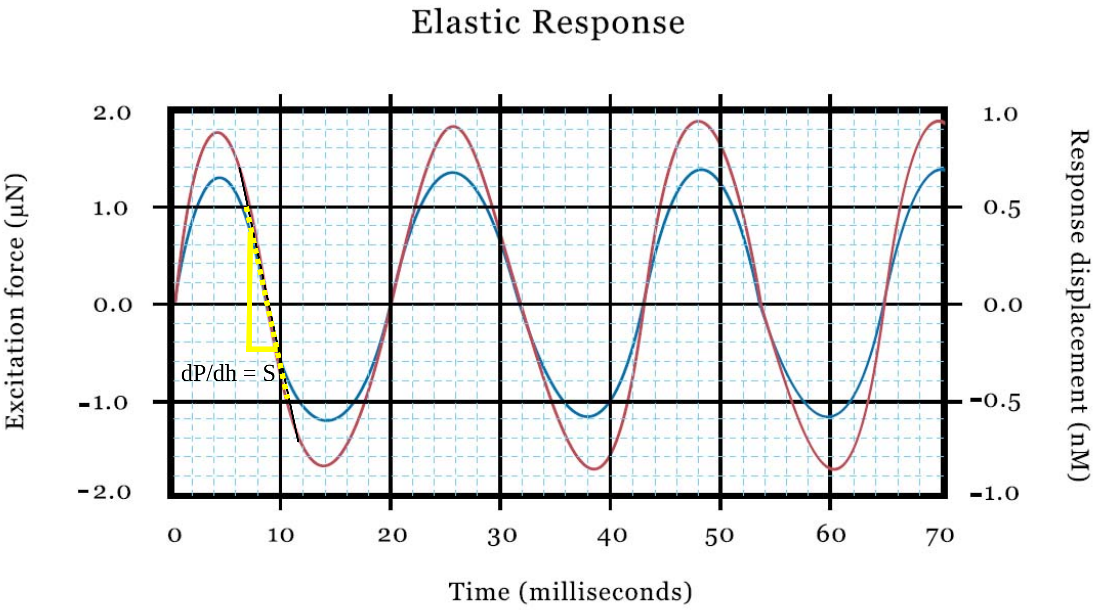

Figure 5: MTS CSM Operation(Modified From 10)

1.2 Previous Work on KNE Solids With Spherical Nanoindentation

A volume of previous work was done by primarily by Ph.D Candidate Anand Murugaiah, also from our research group, culminating in his 2004 thesis.[11] This work utilized nanoindentation and other techniques to characterize what have since become known as Kinking Nonlinear Elastic (KNE) Solids. These are defined as "solids with high c/a ratios (though that ratio is not a strictly necessary condition) that do not twin"[11], and have some remarkable properties; namely the ability to absorb and release energy with "incipient kink bands", yielding hysteresis loops in load-displacement curves obtained by nanoindentation. These also necessarily appear in stress-strain curves created from those load-displacement curves. Not having a CSM attachment to use in his work, Murugaiah relied on a variation of published methods to perform the conversion to stress-strain curves which did *not* use the CSM.[7,11-17] The key difference between this method and that presented below, is that a relationship for contact area, based on load and displacement, *not* including stiffness, is used, rather than a contact radius, which does include the stiffness value. The relationships are:[11]

$$Area = \frac{3\pi}{8}\left(\frac{\sigma^2}{E^*}\right) \qquad \text{where} \quad \sigma = \frac{P}{\pi R_t h_e}$$

(R_t is the indenter radius, and h_e the elastic displacement into the surface.)

The results, including those for nanoindentation, are reasonable and sound, and allowed great insight into the mechanical behavior of KNE solids and their deformation modes.

1.3 Spherical Indentation Model[1]

The model described here is essential to our work, and is partially based upon previous developments of others in the field, especially Herbert et al.[18]

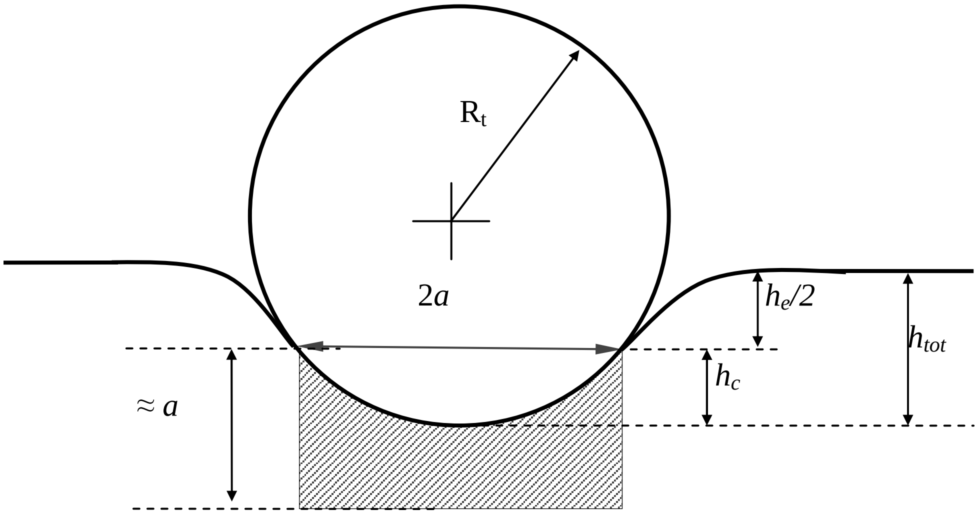

Figure 6: Spherical Indentation Model Schematic[1]

As described in Section 1.1, the primary data channels output by nanoindenters are load on the sample (P) and the vertical displacement of the tip. Typically, the displacement is given with reference to the surface of the sample as the zero datum plane, with depth into the surface given as positive. This value, hereafter just "displacement", we term h_t. See Figure 6 above for a schematic of the dimensional terms used. In addition to those basic channels, nanoindenters equipped with CSM, either as part of the main unit or as an attachment provide the harmonic contact stiffness, S, for the entirety of the test. These three data channels, combined with important static parameters, combine to form the theory on which our method is based.

Most analytical theory related to spherical nanoindentation is based on the Hertz equation in the elastic region. This theory, developed as early as 1881, is amazingly becoming more and more relevant, rather than the opposite, as technology enables us to make greater use of it. It is given below, as Eq. 1.[1,8,15,19]

$$P = \frac{3}{4} E_{eff} R_t^{1/2} h_e^{3/2} \tag{1}$$

where R_t is the radius of the indenter, h_e is the elastic distance into the surface (Figure 6) and E_{eff} is the system composite modulus given by:

$$\frac{1}{E_{eff}} = \frac{1-\upsilon^2}{E} + \frac{1-\upsilon_i^2}{E_i} \tag{2}$$

In Eq. 2, E_i and υ_i, respectively, refer to the modulus and Poisson's ratio of the diamond indenter (typically 1140 GPa and 0.07). E and υ are the terms for the sample. Note that for soft materials, i.e. most metals, the correction makes little difference, but nonetheless must be accounted for.

The next relationship, proven by Sneddon[20] for a rigid spherical indenter, shows that the *elastic* displacements of a plane surface above and below the contact circle are equal, and given by,

$$h_e = h_t = \frac{a^2}{R_t} \tag{3}$$

where a is the contact radius during indentation (Figure 6). That is, when the indentation is only in the elastic regime, the entire indentation depth is elastic, and determined by the term on the right. Combining Eqs. 1 and 3 yields,

$$\frac{P}{\pi a^2} = \frac{4}{3\pi} E_{eff} \left(\frac{a}{R_t} \right) \tag{4}$$ [1]

Though not obvious, this is where stress and strain enter. The left hand side of this equation represents the Meyer hardness, also known as the indentation stress or mean contact pressure.[15] The expression in parentheses on the right-hand side represents the indentation strain.[15] For the remainder of this thesis, these will be referred to as indentation stress and indentation strain, respectively. Note these are not the same as the stresses and strains measured in uniaxial

---

[1] In Chapter 3, E_{eff} in Eq. 4 is renamed E* to avoid confusion of this modulus with that shown in Eq. 14.

compression tests, nor even the same as those for other nanoindenter tip geometries.[21]

Thus far, we have only presented two well understood and accepted relationships, and combined them to form a lesser known one. Our innovation comes however, in the determination of the contact radius a. To do so, we need only the data channels of P, S, and h_t. We show in the following subsections how this is done first in the elastic regime, and then in the elasto-plastic regime.

1.3.1 Elastic Regime:

The most typical plot for nanoindentation is that of load (P) versus displacement (h). Both the Oliver & Pharr[22] and Field & Swain[8] methods use the slopes of the initial portions of the unloading curves dP/dh, (loading is more complex), to calculate h_e. Differentiating Eq. 1 with respect to h yields:

$$\frac{dP}{dh} = 2E_{eff} R_t^{1/2} h_e^{1/2} \tag{5}$$

When this result is substituted back into Eq. 1, the result is:

$$P = \frac{2}{3}\frac{dP}{dh} h_e \tag{6}$$

And therefore,

$$h_e = \frac{3}{2} P \frac{dh}{dP} \tag{7}$$

Since dP/dh is nothing but the stiffness, S_s, of the system comprised of the specimen and the load frame, we can substitute S_s for the reciprocal of dh/dP in Eq. 7. We thus have:

$$h_e = \frac{3}{2}\frac{P}{S} \tag{8}$$

where the stiffness of the material itself can be calculated from (similar to the modulus in Eq. 2)

$$\frac{1}{S} = \frac{1}{S_s} - \frac{1}{S_f} \tag{9}$$

where S_s is the stiffness of the system, reported by the CSM, and S_f is the load-frame stiffness given by the instrument manufacturer. In our case this was 5.5 MN/m. We obtained this value from the manufacturer of the instrument, but calibration procedures are available to determine it experimentally.[21]

Eq. 8 gives h_e in terms of P and S, and with that knowledge, we calculate *a* from Eq. 3, so a is now known in terms of P and S.

1.3.2 Elasto-Plastic Regime

Again taking our lead from Oliver & Pharr[22] and Field & Swain[8] we define the "contact depth", h_c, as the distance from the circle of contact to the maximum penetration depth (Figure 6) as follows:

$$h_c \approx h_t - \frac{h_e}{2} \tag{10}$$

Combining Eqs. 8 and 10 yields:

$$h_c = h_t - \frac{3}{4}\frac{P}{S} \tag{11}$$

For reasons discussed in Section 3, we originally modified this equation to read:

$$h_c = h_t - \frac{3}{4}\frac{P}{S} + \delta \tag{12}$$

where δ is an adjustable parameters of the order of a few nm needed to obtain the correct elastic moduli. The origin, or need for δ was not clear at that time.[1] We have since discovered that δ arose from using an incorrect zero point, motivating us to develop the method to find the correct zero point described in Section 3.

Once h_c is known, a can be calculated as follows:

$$a = \sqrt{2R_t h_c - h_c^{\ 2}} \ \approx \sqrt{2R_t h_c} \tag{13}$$

Note that the right-hand expression is only valid if h_c << a, and the indenter tip is perfectly spherical. In the purely elastic regime, $h_c = h_t/2 = h_e/2$ and Eqs. 3 and 13 become identical. Also note that for the most part in the plastic regime, $h_t \gg h_e/2$ and thus $h_c \approx h_t$ (Eq. 10).

We also know that for an *isotropic* elastic solid indented with a spherical indenter,[22]

$$a = \frac{S}{2E_{eff}} \tag{14}$$

To date the most commonly used method for measuring nanoindentation hardness values is the Oliver and Pharr method, in which h_c is calculated from Eq. 11, and the contact area, A, is determined from a calibrated area function of the form:[22]

$$A(h_c) = C_0 h_c^2 + C_1 h_c + C_2 h_c^{1/2} + C_3 h_c^{1/4} + C_4 h_c^{1/8} + \ldots. \tag{15}$$

In our method, we calculate a from Eq. 13 for the entirety of the curve, essentially extending the well-understood elastic region into the elasto-plastic region by the relationships shown above. We then judge the results by two criteria: First, the initial portion of the indentation stress-strain curves should be linear, with the higher of two slopes: either the slope obtained from Eq. 14, or the one measured by the standard method, viz. a Berkovich indenter and the Oliver and Pharr method. Second, the stress level at higher strains should be comparable to the stress measured on the *same* material using a Vickers microhardness indenter, within a reasonable margin. As previously mentioned, some conversion must be made between the various hardness measurement methods and tip geometries, but, being of similar principle, should be reasonably similar.

1.4 Experimental Details[1]

The nanoindenter (XP System, MTS, Oak Ridge, TN) used in this work was equipped with a CSM attachment. All tests were carried out with a load rate over load factor of 0.1 and an allowable drift rate of between 0.05 and 0.1 nm/s. The harmonic displacement for the CSM was 2 nm, with a frequency of 45 Hz. The tests were carried out to various loads for different materials depending on their hardness. Once the surface is detected, the indenter is loaded at a constant value of $(\mathrm{d}P/\mathrm{d}t)/P = 0.1$ (the loading rate divided by the load), which logarithmically scales the data density so that it is more or less even across the entire loading regime. Constant $(\mathrm{d}P/\mathrm{d}t)/P$ tests also have the advantage of producing a constant indentation strain rate, $(\mathrm{d}h/\mathrm{d}t)/h$, provided the hardness is not a function of the depth.[1,23]

Two diamond spherical tips - with radii of 13.5 μm and 1 μm - were used. As noted above we used a number of materials: fused silica (GM Associates Inc., Oakland, CA); sapphire single crystal (C-orientation) (Kyocera Industrial Ceramics, Vancouver, WA); C-orientation ZnO single crystal (Wafer World, Inc., West Palm Beach, FL) and several metals. The first is Al (Puratronic 99.999%, Alfa Aesar, MA). The remainder are iron samples as follows (subscript indicating the sample, though all are iron) Iron_A (99.99 % Alfa Aesar, MA), Iron_B (99.65%, SurePure Chemetals, Florham Park, NJ, annealed at 1450°C for 8 hours, average grain size of 1.7 millimeter), and Iron$_c$ (99.65%, SurePure Chemetals, Florham Park, NJ, annealed at 1450°C for 12 hours, average grain size of 300 μm, though some grains were up to several mm in size) Iron$_B$ and Iron$_C$ were from the same raw stock, but were annealed separately, and Iron$_C$ was machined as a compression sample (13mm diameter x 38mm long, parallel flats 3 – 5 mm wide machined along axial direction), while Iron$_B$ had dimensions 13mm diameter x 5mm long).[1]

In all cases, the Vickers microhardness values of the same surfaces used for the nanoindentations were measured using a microhardness indenter (M-400 Hardness Tester, LECO Corp., St. Joseph, MI), with loads ranging from a 2 to 10 N. We also used the Oliver and Pharr[22] method and a Berkovich indenter tip to measure the hardness, H_{Br}, and moduli, E_{Br}, of all samples. As noted above, the latter will henceforth be referred to as the standard method.[1]

To compare the indentation stress-strain curves with those measured in uniaxial compression, and later, to study the effect of compression on nanoindentation results, the Iron$_A$ cylinder (9.7mm diameter x 35mm long) and Iron$_C$ cylinder (13mm diameter x 38mm long, parallel flats 3 – 5 mm wide machined along axial direction) were loaded at a nominal stress rate of approximately 13.5 MPa/s. The strain was measured using an extensometer attached to the sample.

CHAPTER 2. STRESS-STRAIN CURVES FROM SPHERICAL NANOINDENTATION

Please Note: The content of this section has been adapted from a paper for which Alex Moseson was a co-author.[1]

2.1 Background On Obtaining Stress-Strain Curves From Spherical Indentation

The key advantage of instrumented indentation, or more commonly, “nanoindentation”, is its ability to characterize the mechanical properties of bulk samples, single grains, and thick films with high accuracy. Primarily, Berkovich (Figure 2), or similar indenters such as “cube corner” have been successfully used over the past two decades primarily to determine moduli and hardness values for a variety of materials.[22] Berkovich indenters are sharp however, causing plastic deformation almost instantly, so data in the elastic-to-plastic transition is lost.[15] Our answer to this dilemma is the use of a spherical tip, and the appropriate theory to accompany it. As described above, this involves knowledge of the load and displacement from the nominal loading, as well as stiffness from continuous stiffness measurement (CSM).

Attempts have been made for quite some time to convert load/displacement curves to indentation stress/strain curves.[15] Spherical indenters are sometimes used for the conversion, but these techniques are not widely used. [7,14,18,24,25] Even the apparently superior method by Field and Swain[8,19], published about ten years ago, has not been widely used, even by Swain himself, with some exceptions.[14,18,24-28] Instead, in some recent publications,[24,26-28] Swain presents plots of hardness vs. indentation penetration, but none as indentation stress/strain curves. Another promising method was published by Herbert et al[18], yet this as well has fallen out of interest, for reasons which are unclear. In short, though some have attempted to use spherical nanoindenters to convert load-displacement to stress-strain, and the apparent ease with which this could be done, there has been little effort to systematically study and refine the process.

In the remainder of this chapter, we present the results of applying the method described in Section 1.3 to a wide variety of materials. In all cases, we compared the results to the moduli reported in the literature and those measured using the Oliver and Pharr[22] method and a Berkovich indenter. The hardness values obtained here were, in turn, compared to the results obtained using Vickers and Berkovich indenters. The results show that our method is quite powerful and versatile.[1]

2.2 Results And Discussion

2.2.1 Stiffness vs. Contact Radii

Figure 7a shows the S vs. a plot for various materials tested. Using Eq. 14, we can easily correlate these clean and reproducible slopes to the effective modulus, $E_{eff.}$ Figure 7b shows the correlation between moduli determined by Berkovich and spherical indenters, and the excellent agreement between the two.

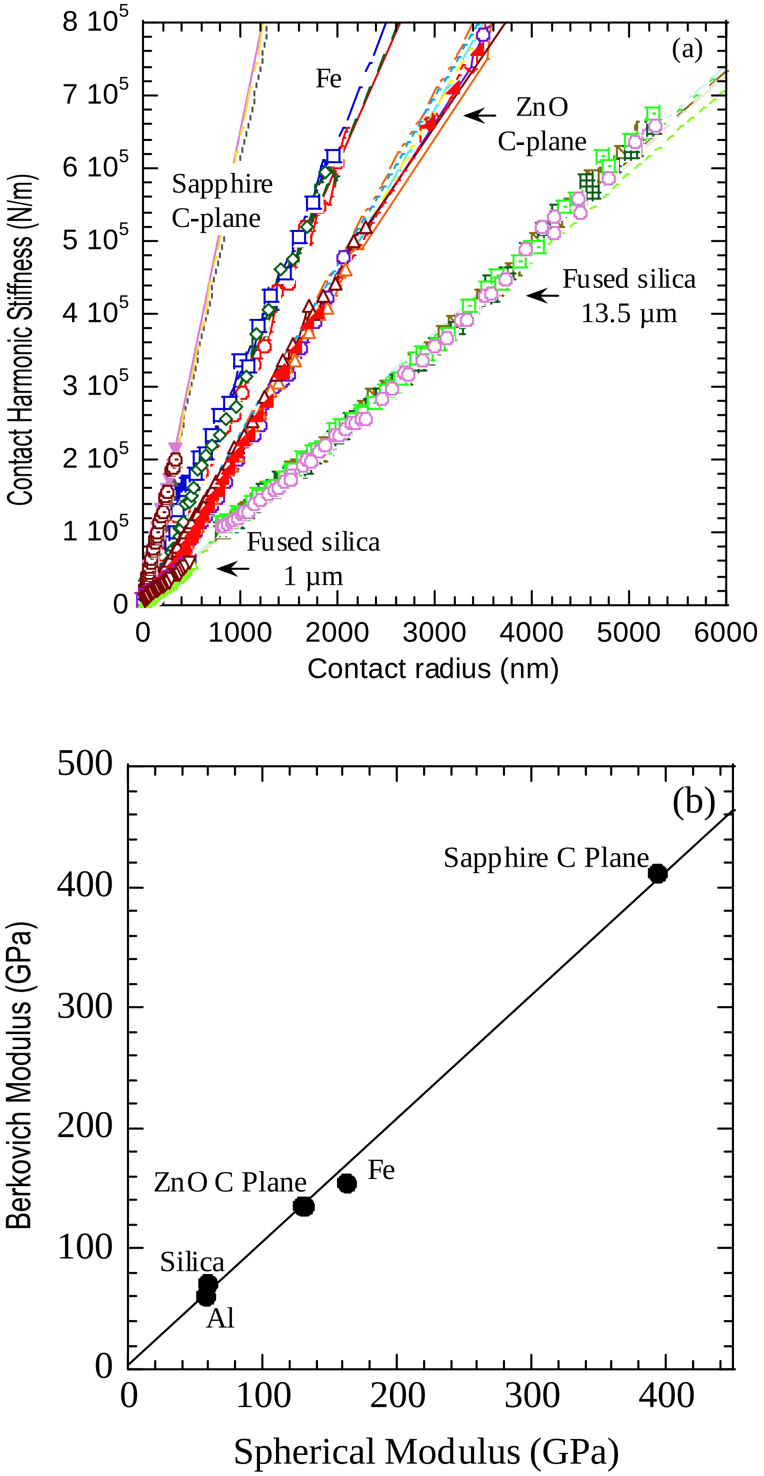

Figure 7: S vs. a And Berkovich vs. Spherical

a) Contact harmonic stiffness versus contact radius, a. b) Comparison of modulus values obtained from Berkovich and Spherical Indentation models.

The Young's moduli for spherical indentation were calculated from Eqs. 2 and 14, after minor adjustments in δ (in Eq. 12, our original zero point determination method). These are listed in column 4 of Table 1 as E_{Sp}, along with the literature data, E in column 3 and the values determined using Berkovich indentation in column 5. For all cases, $E_{Sp} < E$. Some difference between methods is to be expected, and that they are consistent at least in direction is encouraging. Also, with the exception of Fe_A, $E_{Sp} < E_{Br}$.

Table 1: Mechanical Values From Literature And Our Work[1]

Summary of Poisson's ratios, v, and Young's moduli, E, or 1/s33 taken from the literature, the moduli values measured in this work using the spherical indenters, ESp, a Berkovich indenter, EBr, and the hardness values using the latter, HBr. Also listed in last column are the Vickers microhardness values measured herein using a load of 10 N.

Material	υ	E or $1/s_{33}$ (GPa)	E_{Sp} (Figure 7) (GPa)	E_{Br} (GPa)	H_{Br} (GPa)	Vickers μ-Hard. (GPa)
Silica 13.5 μm	0.18	72	59±1	71.7±0.7	9.3±0.2	5.6±0.6[b]
SiO_2 1 μm			59±2			
Al 13.5 μm	0.3	70	58±4	60±4	0.48±0.02	0.29±0.02
Fe_A 13.5 μm	0.3	210 203[a]	163±9	155±1	1.2±0.1	1.3±0.1
C-ZnO 13.5 μm	0.2	$1/s_{33} = 149$	130±4	135±3	4.8±0.2	3.3±0.1
C-ZnO 1 μm			131±4			
C-Al_2O_3 1 μm	0.2	$1/s_{33}= 458$	394±4	412±8	25±1	22.5[c]

a) This work. B) Value depends on load; lower loads yield higher values.
C) According to manufacturer

2.2.2 Moduli Corrections

For this work, we set the adjustable parameter δ in Eq. 12 so that the elastic portion of the stress-strain curve goes through the origin. Secondarily, we attempted to make the slope of the elastic portion of the stress-strain curve match the greater of E_{Br} or E_{Sp} for each sample. In Section 3, we outline an accurate and robust zero point determination method, used to supersede the need for δ in Equation 12. By way of example though, Figure 7 is included here to demonstrate how the previous method was employed.

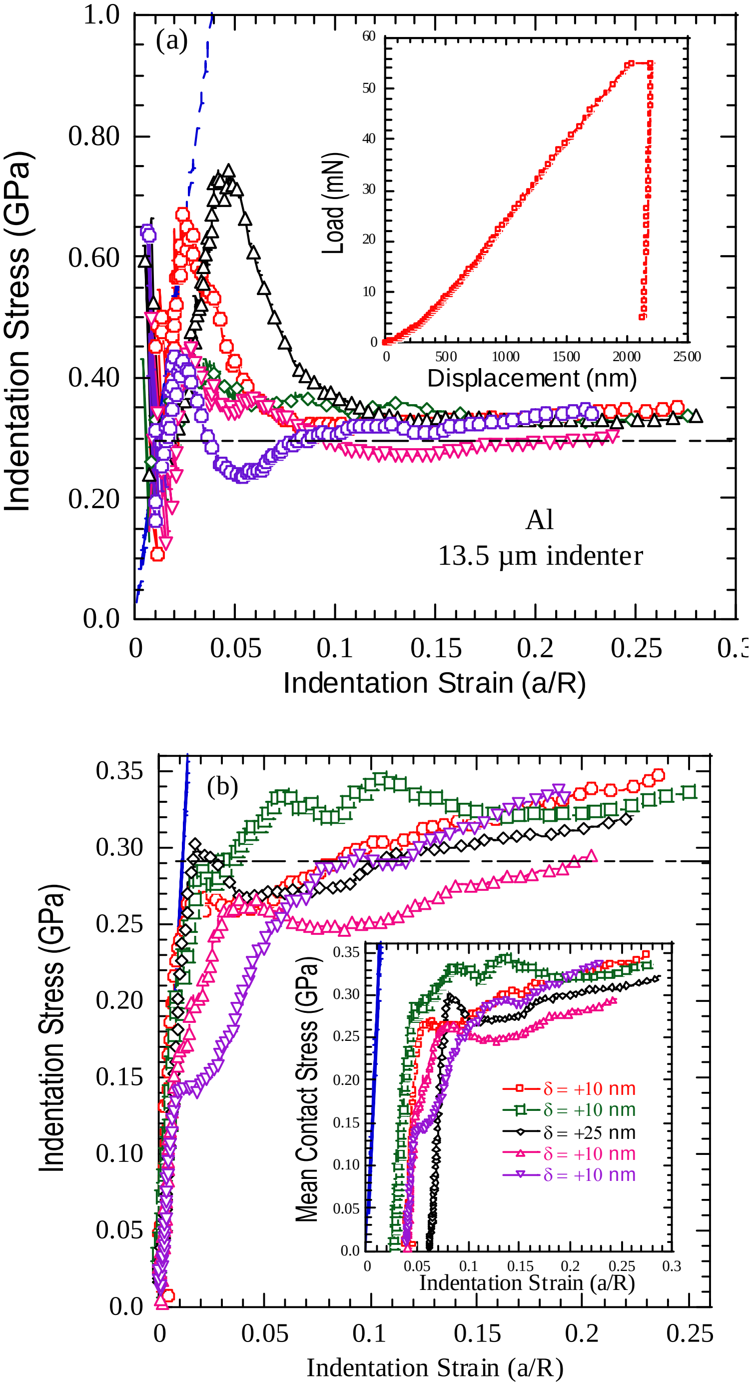

Figure 8: Aluminum - Stress vs. Strain, Before And After Original δ-Correction

Indentation stress/strain curves in pure Al in various locations, a) as-received data. Inset shows a typical load/depth-of-penetration curve, b) same as a, but after δ correction (see text) and mechanical shifting of curves. Inset shows the results before mechanical shifting. The numbers listed in the inset represent the values of δ needed to obtain the correct modulus. Note shifting the curve also rotates the initial nonsensical points counterclockwise and aligns them with the other results. Dashed horizontal lines represent the Vickers microhardness values measured on the same Al sample.

In the remainder of this chapter, we treat each material separately, starting with the most popular standard material, fused silica.

2.2.3 Fused Silica

Figure 9a shows typical load-displacement curves for the 1 μm and 13.5 μm indenters on fused silica. Figure 9b shows the indentation stress-strain curves for 5 different locations, for both the 1 μm and 13.5 μm indenters. Least squares regression of the linear portions in Figure 7a and Figure 9b, yields slopes that correspond to an E_{Sp} 59±2 GPa (Table 1), rather than the expected E_{Br} of 72 GPa. Note though, that in Figure 9b, the 1 μm and 13.5 μm data sets agree very well, especially after the distinct change in slope of the lines. This is significant, because it contradicts the indentation size effect observed elsewhere in the literature and observed below for ZnO. This distinct change (at about 6.5 ± 1 GPa in this case), we deem the yield point, as a working understanding of the term. Note its correspondence to the Vickers microhardness, curiously in the same range. We do not believe the origin of the “microyielding” to correspond to the activation of a slip system, but rather it is most probably due to densification under the indenter tip, or other phenomena.

Please note that our method is valid for the 1 μm indenter tip only up to h_t depths of the order of ≈ 300 nm, and for the 13.5 μm indenter up to ≈ 4500 nm. Beyond those points, the tip can no longer be considered spherical. Recall that the tip as constructed is not actually a sphere, but rather a rounded cone with a tip that behaves as a sphere. It is for this reason that there are no results beyond a strain of 0.7 in Figure 9b.

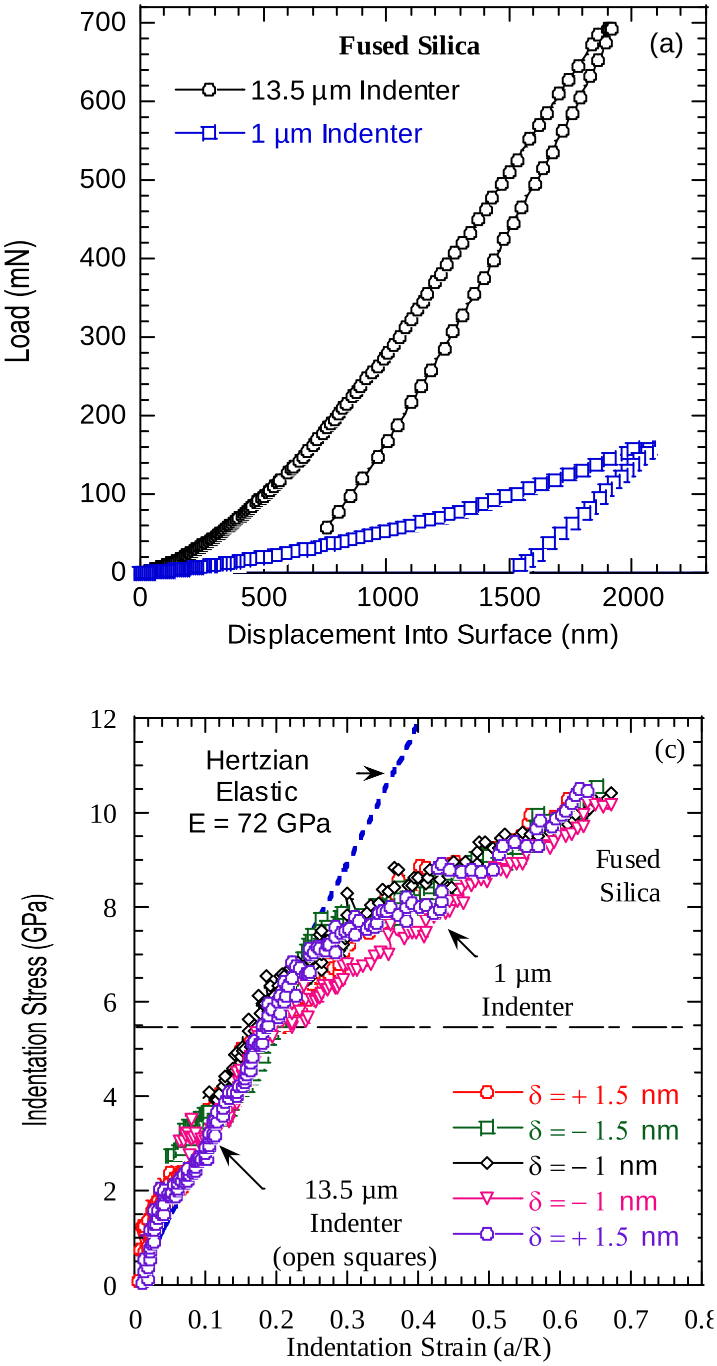

Figure 9: Fused Silica - Stress vs. Strain, Before And After Original δ-Correction

Indentation results for fused silica, a) load/depth-of-penetration results for the 1 µm and 13.5µm indenters used, b) corresponding stress-strain curves after δ –correction. In this figure we eliminated the data points to the left of the blue dashed line, which represents the elastic response of the solid. The agreement between the two sets of results in excellent. Dashed horizontal lines represent the Vickers microhardness values measured on the same silica.

2.2.4 ZnO

For indentation on ZnO C-planes, we observe large pop-ins on the load-displacement curves that occur between 80 mN and 120 mN (Figure 10a). The stress-strain plots (Figure 10b) give a clearer understanding of what is happening, wherein the material appears elastic up to 6.5±1 GPa, and then abruptly falls to about 3 GPa, and slowly rising with what appears to be strain hardening.

Recent work by Basu and Barsoum[29] explored ZnO further, with nanoindentation and microscopy, in both the C-plane and A-plane orientations. The phenomena is well explained by the concept of incipient kink bands, as ZnO is now understood to be a KNE, like that reported on by Murugaiah (See section 1.2). Though this is beyond the scope of this thesis, suffice it to say that the results are indeed valid observations of real physical phenomena.

Kucheyev et al.[28] report a value of 111±5 GPa for the modulus of ZnO, while ours, calculated from Figure 7a, is 130±4 GPa. Kucheyev et al used a 4.2 μm radius indenter and the Field & Swain method. This provides good corroboration for our work.

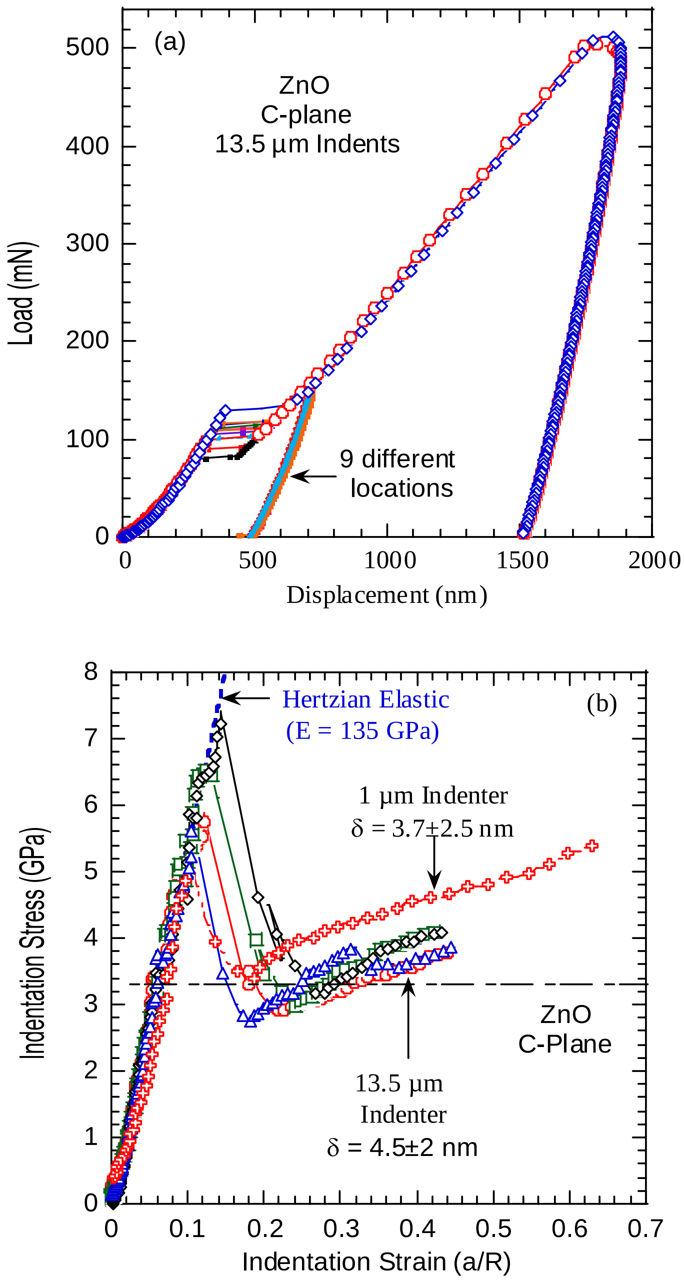

Figure 10: ZnO – Load vs. Displacement And Stress vs. Strain

Indentation results for single crystal ZnO C-planes, a) load/depth-of penetration results 13.5µm indenter, Note large pop-ins around 100 mN. b) corresponding stress-strain curves after δ -correction and mechanical shifting. Here again data points to the left of the blue dashed line were removed. Dashed horizontal lines represent the Vickers microhardness values measured on the same ZnO C-planes.

2.2.5 Sapphire

The shape of the stress-strain curves for sapphire look like that of ZnO i.e. linear elastic behavior to a maximum, then a sudden drop and continued linear growth with a lower slope. Here, the material appears elastic up to a stress of 45±4 GPa, until at a load of ≈ 15 mN, a 'pop-in' occurs. at which point it drops to about 28 GPa, and then increases steadily. Typical load-displacement curves obtained when the C-planes of sapphire are loaded with the 1 μm indenter are characterized by a 'pop-in' event at a load of ≈ 15 mN. Again, recent work by Basu, Barsoum, et. al have identified sapphire as a KNE, and successfully explained its behavior with that model. [30] In short, the 'pop-in' is based on the activation of dislocation slip systems.

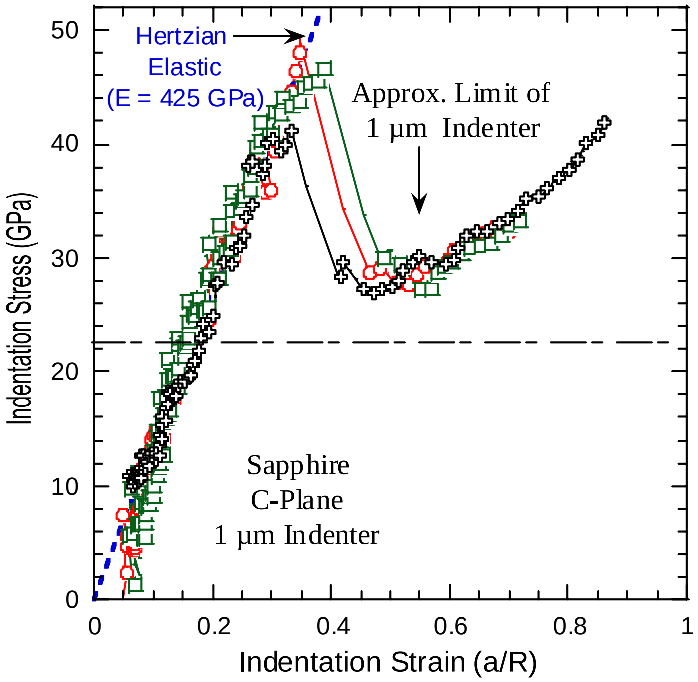

Figure 11: Sapphire – Stress vs. Strain

Indentation stress-strain curves after δ -correction and mechanical shifting for single crystal sapphire C-planes loaded with a 1μm radius spherical indenter. Note large pop-ins in the 40-50 GPa range. Dashed horizontal lines represent the Vickers microhardness values reported by the manufacturer for the same surface.

2.2.6 Iron$_A$

The hardness value shown in Figure 12 (1.1±0.1 GPa) is reasonably close to that found by Vickers microhardness (1.3±0.1 GPa). The nanoindentation data, though scattered, is clustered well, and likely represents indentation on grains of different orientations, though on this un-annealed sample, the indentation almost assuredly impacted several grains at once. We also compared the results with a uniaxial compression test, by scaling the stress and strain values for that test by 3 and 10, respectively. Note that this was merely done for the sake of illustration, but interestingly, for some other samples where work hardening was prevalent, the hardening rates were comparable, which was not intentionally sought. While the scaling of the uniaxial compression data may seem arbitrary, we already have the well-understood relationships of Meyer hardness (the hardness shown on our nanoindentation curves), and the bulk yield stress. In general,

$$\frac{P}{\pi a^2} \approx 3\sigma_y$$

where σ_y is the yield point.[15] Similarly,[15]

$$\frac{a}{R} \approx 5\varepsilon$$

Here we used 10 instead of 5 in order to make the data fit.

More recent work, on Iron_B and Iron_C is described in Chapters 3 and 4. The results to date remain perplexing, but progress is certainly being made.

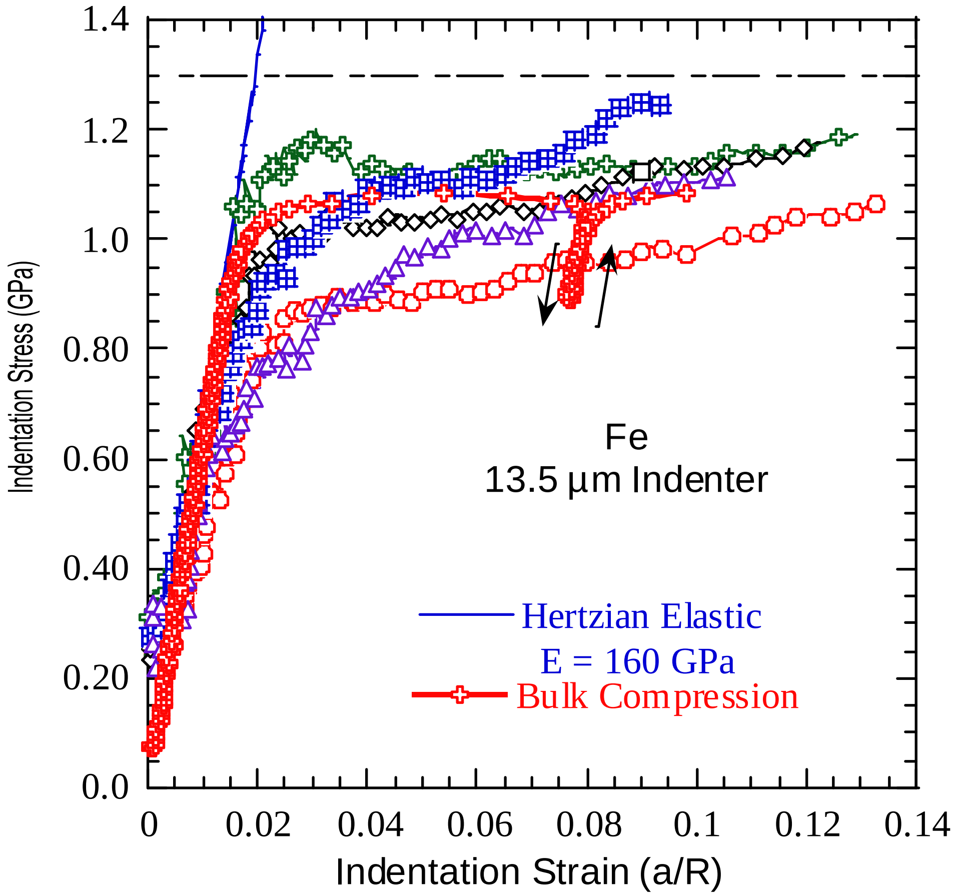

Figure 12: Iron$_A$ - Stress vs. Strain, Before And After Original δ-Correction

Indentation stress-strain curves for Fe$_A$ loaded with a 13.5 µm radius spherical indenter, with mechanical shifting and δ –correction. Also plotted are bulk compression results (open squares) on the same Fe after multiplying the stress by 3 and the strain by 10. The agreement between the two sets of results is excellent. Dashed horizontal lines represent the Vickers microhardness values measured herein on the same sample.

2.2.7 Aluminum

The aluminum data was presented in Figure 8, above. After using our original δ correction, the Al results appeared clean, with a clear modulus, yield point and Meyer's hardness. The latter was very close to the Vickers hardness measured. We were originally concerned about the magnitude of δ for this sample, being up to 25 nm, where others were limited to less than 3 nm, but as explained in Chapter 3, this is no longer a concern.

Though our results on Al agree internally, there is some discrepancy between our work and that of others. Our hardness values are roughly 1/3 of the values reported by Field and Swain[8] for pure Al. One possible source of this difference is that but Field and Swain used their original method, without CSM. Also, the indentation stress-strain curves obtained by Herbert et al.[18] from spherical nano-indentation experiments on 6066-T1 Al - essentially using the same technique described here – had a decidedly different shape. The hardness values did not asymptote or reach a steady state, but continually increased with strain. Two possible sources for this discrepancy are that Herbert et al. used an Al-alloy rather than pure Al and/or the fact that they used much larger spherical indenters.

2.3 Summary And Conclusions: Stress-Strain

As demonstrated in this chapter, our method is a relatively simple way to convert indentation load-penetration results into the much more informative and useful indentation stress-strain curves. The usefulness of the method lies of course in that phrase "much more informative", which we believe to be true already, but with further refinement (including that described in Chapters 2 and 3), we expect it to become even more so. To its credit, the method is versatile and applicable to materials at least from soft polycrystalline metals such as Al to hard and stiff sapphire. The main caveats were i) the adjustable parameter δ (though methods such as that proposed by Oliver and Pharr use many such parameters to fit data, to a much greater extent) and, ii) phenomena which we observed, and were not certain were real physics and not artifacts of the method. The former has been solved for the most part, as described in Chapter 3, though the method used for this work is not terribly different in the value eventually chosen. The latter concern seems to be ebbing away as we research the observations further, offering insight into KNE solids, and having found further external corroboration.

In this chapter we have combined CSM measurements, Hertzian theory, and the Oliver & Pharr and Herbert et. al methods to convert spherical nanoindentation load/displacement curves to indentation stress/strain curves. Corroboration is offered by Vickers microhardness measurements on the same solids (in our understanding, never done before), Berkovich nanoindentation, and values from the literature. Still however, the key advantage of using spherical indenters is the elastic-to-plastic transition and the associated yield point, which we are actively researching to better understand. We will continue studying this and other phenomena to better understand not only the method, but the materials which we are studying.

CHAPTER 3. EFFECTIVE ZERO POINT DETERMINATION

Please Note: The content of this section has been adapted from a paper for which Alex Moseson, the author of this thesis, was the primary author. [2]

3.1 Background On The Zero Point Dilemma

Instrumented indentation is a valuable method for characterizing the mechanical behavior of materials, especially that of single crystals and thin films. Instrumented indentation was born in the mid-1980's, and pioneered by Doerner, Newey, Loubet, Oliver, and others.[31] Their experimental setup controlled the load or displacement of a tip of known geometry as it indents into a material. During the indentation, they continuously measured the load and displacement into the surface. This was deemed "instrumented" indentation, with obvious differences between it and its predecessor indentation hardness testing, wherein only the residual indent was analyzed for its size. Though the concept is simple, the successful application of the technique is challenging. This is due both to the models used to interpret the data, and the hardware used to obtain it. Advances in complementary empirical and analytical paths continue to help with the former. For example, Finite Element Analysis is today used to simulate nanoindentation, allowing development of theory in an environment without the complications of the real world.[32] Despite this, Hertzian theory, published as early as 1881, remains the model most often used as a basis for spherical nanoindentation. Advances in hardware are also being made, as computers, control systems, and the such advance.[31] Oliver & Pharr, Field & Swain, and others built upon Hertzian theory and have made significant progress in developing the technique, but recognize the significant hurdles yet to overcome.[7,8,21] One such obstacle is the accurate and reliable determination of the zero point, where the indenter tip makes first contact with the sample surface.[21,33-38] At this point, both the applied indentation load, P, and the total displacement, h_t, or indentation depth, should be zero, though the sample stiffness, S, may appear positive. Figure 13 shows the conundrum, wherein a P vs. h_t curve has no clear zero point. The correct δ, by our method, is indicated as a vertical dashed line.

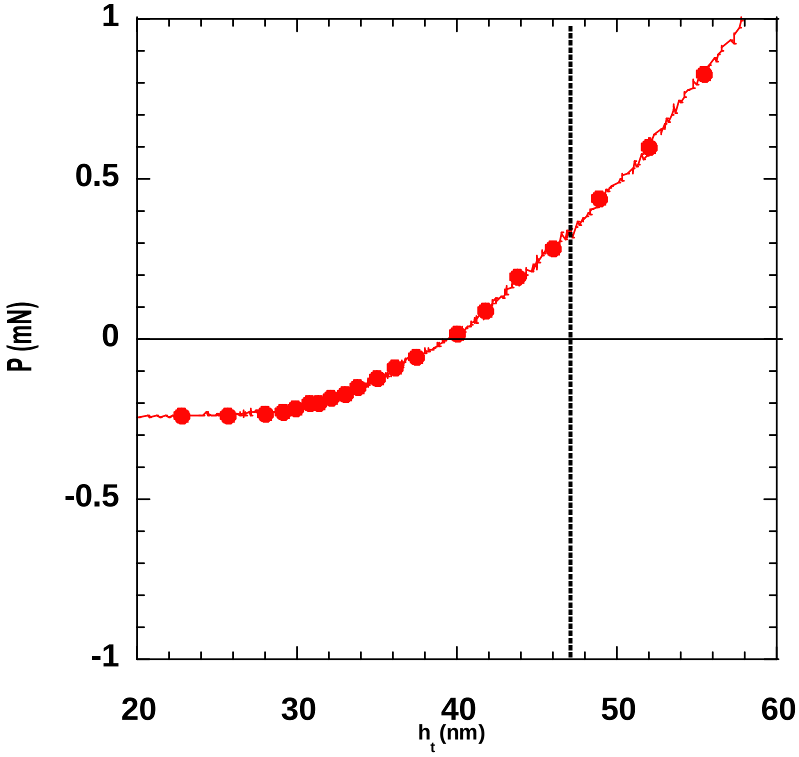

Figure 13: Silica - Load Vs. Displacement Before Correction
P vs. h_t at region near the supposed S = 200 N/m zero point used by manufacturer to define the zero point. Dashed line denotes location of the true effective zero point.

To date, methods of various sophistication have been proposed to qualitatively or quantitatively determine the zero point.[39-46] For example, one is to simply plot P versus h_t and choose a point where P first exceeds a certain threshold, while another uses a video camera.[43,45] For instruments with continuous stiffness measurement (CSM) capabilities, Oliver & Pharr[21] suggest using the point at which *S* reaches a local minimum, before increasing steadily. Alternatively, they suggest using abrupt changes in CSM harmonic displacement or phase angle if they are clearer, but all three options require some subjectivity, however small. They claim the method has an accuracy of 2 nm, but we have found that it identifies the zero point too early, sometimes by as much as 14 nm. This may seem insignificant, but as we show below, the difference can be quite important. Chudoba, Ullner and their colleagues suggest using regression on the P vs. h_t plots.[39,40,46] The former advocates an iterative numerical method to fit the data to a variation of the Hertzian model, replacing the conventional parameters of tip radius and effective modulus with an optimized proportionality constant and forcing the data to go through zero.[39,40] The latter advocates optimizing the terms of a second order polynomial to fit the data.[46]

Finally, a variation on the Oliver & Pharr method is to locate the zero point where S first meets or exceeds 200 N/m. This is based on an assumption that while the tip is hanging free, other factors such as vibration produce values below 200 N/m, and that this small value first appears when the tip makes contact with the surface. This method indeed works in some cases but in the authors' experience, it can falsely locate the surface up to hundreds of nanometers away from the actual zero point. In our deductive data analysis, we found that this is most likely the method employed by the MTS instrument we used, and all δ values (see below) in this chapter are given with respect to the original zero assumed by the instrument. In summary, and while some of these methods may be somewhat successful, they are limited in that both load and displacement values are noisy at low loads and are greatly impacted by the zero point.

Originally, Eq. 11 included a small correction, δ that helped insure that the early regions of the stress-strain curves behaved in a linear elastic fashion. The origin, or need for, δ was not clear at that time.[1] We have since discovered that δ arose from using an incorrect zero point, leading to the method described herein. We thus present a robust, simple, accurate, and objective method for reliably determining the effective zero point for instrumented spherical indentation equipped with the CSM option. In essence, our method shifts the P and h_t columns of a given data set in such a way as to insure that the S versus the contact radius, a, curves are straight lines that go through the origin. The power of the technique lies in the fact that, if needed, the results can be linearly back-extrapolated from a region where the signal-to-noise level is high, viz. at shallow depths, back through the origin thus circumventing the myriad problem encountered at low loads.[3] In that sense our zero point is an "effective" zero point, i.e. the zero point one would have obtained had the surface been atomically flat and perfectly normal to the loading direction. This effective zero point, may, or may not, correspond to the very first point of contact between the indenter and the surface.

3.2 Effective Zero Point Determination Methodology

To create the *S*. vs. *a* plots, the former is known from the CSM, and we use Eqs. 11 and 13 to find *a*. Note that Eq. 14 is *not* used to find *a*. According to Eq. 14 though, for a properly zeroed sample, a plot of *S* vs. *a* should be a straight line, that goes through the origin, with a slope of $2E_{eff}$. The essence of our method lies in finding the datum point which if the effective zero point would make the *S* vs *a* curve go through the origin as predicated by Eq. 14. For the remainder of this chapter, the modulus in Eq. 4 has been renamed to E* to differentiate it from the E_{eff} in Eq. 14. E* relates to the slope of the elastic portion of the stress-strain curve, and would equal E_{eff} as found from the slope of the S-a curve (Eq. 14) if and only if all assumptions made[47] in its derivation (i.e. atomically flat surface, surface perpendicular to tip, isotropic material, perfect sphere, etc.) are valid. Again, in our method, Eqs. 11 and 13 are used to find *a, not* Eq. 14.

The key value we solve for is δ, the difference in h_t between the *correct* effective zero point, X_z, and the first point X_o where $S \geq 200$ N/m – viz. the one given by the instrument. (Note that X_o is defined as such here for convenience, as our instrument was programmed to choose the zero point based on $S \geq 200$ N/m; this may vary by instrument. The δ value itself is not so important as identifying the correct effective zero point.) To start, we choose points X_j near (viz. ± 10 nm) where P definitely becomes positive. To find the correct effective zero point we simply shift the P and h_t columns by subtracting (even if the values are negative) P_j and $h_{t,j}$, respectively, from the entire column. Data points with negative values of h_t are discarded and S vs a is plotted. The shift that results in a S vs. a line that best goes through the origin is the sought after effective zero point.

Linear regression is used to quantitatively determine the degree to which each S vs. a curve is linear *and goes through the origin* (i.e. a straight line forced through the origin). Note that none of the data sets interact. We used two criteria for quantifying the curve fits, though one would suffice. The first is the standard error, defined as the average vertical difference between each datum point and the best-fit line forced through the origin. The second is the well-known correlation coefficient, R^2, again, with respect to the same best-fit line forced through the origin. The value of δ_j that minimizes the error or maximizes R^2 is the correct δ. As shown below, the result is an objective, quantitative determination of the zero point. The method and various applications thereof are patent pending, with the provisional patent 60/953,361 attached as Appendix I. A detailed example of the procedure is given in Appendix 2. Note that for the tests in this chapter, the maximum load was 690 mN for fused silica, and 50 mN for iron$_B$ and sapphire.

3.3 Results

3.3.1 Silica

Figure 14 shows results for fused silica with the 13.5 μm indenter. This is the same data as shown in Figure 13. Note its location in contradistinction to the more intuitive point where P begins increasing, around a δ of 10 nm. Figure 1a shows *S* vs. *a* plotted for three δ's, over a span of 10 nm. Inset 2 shows the entire data set, wherein it is apparent that after ≈ 2500 nm, the value of δ is no longer of consequence. The inset of Figure 14b plots the linear regression R-values and the above-defined standard error from the data *forced through zero*, at various δ's. In this case, δ_z is clearly ≈ 47.2 nm. Figure 14b shows a plot of indentation stress vs. strain, as defined by Eq. 4.

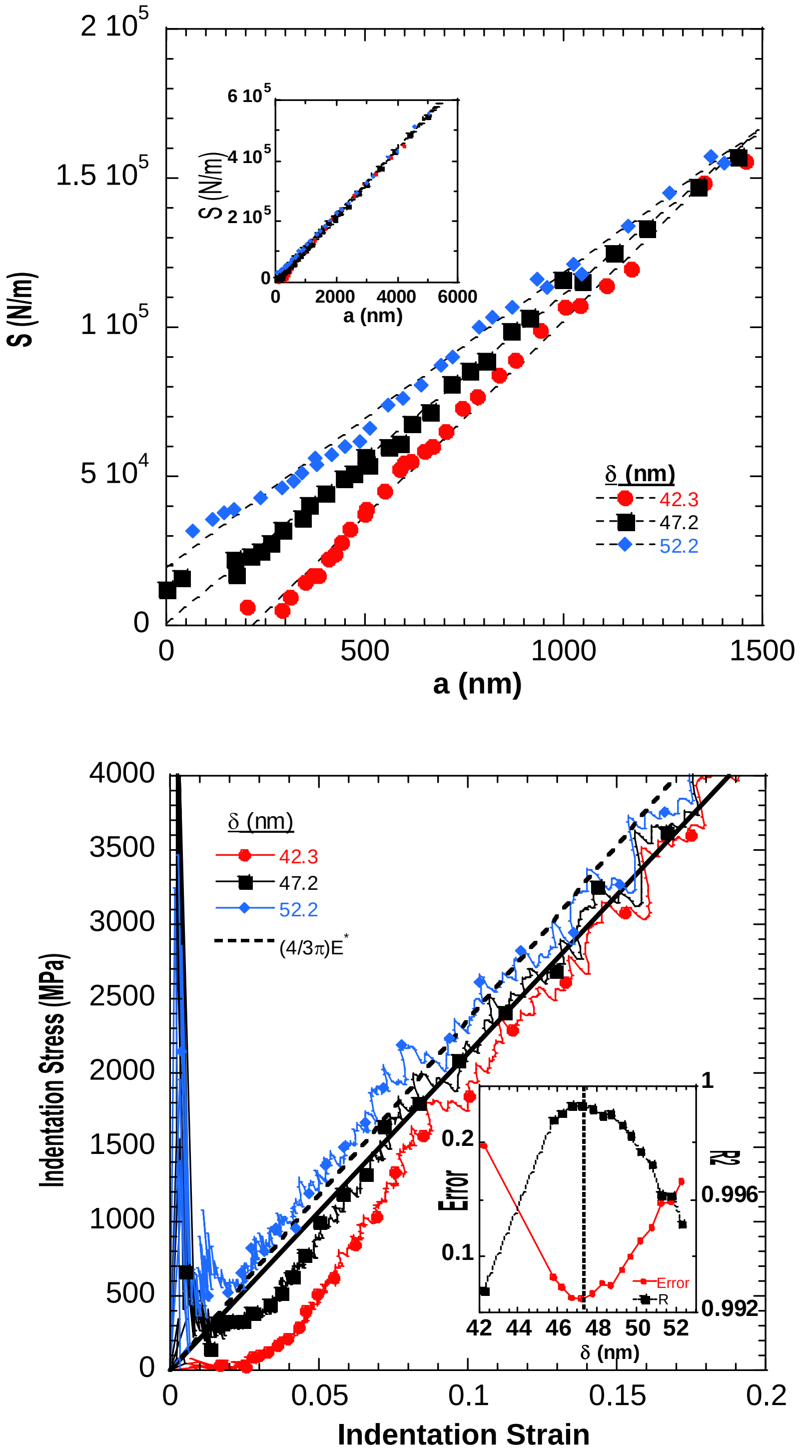

Figure 14: Fused Silica - Zero Point Results

Fused silica, 13.5 µm indenter. a) *S* vs. *a* for various δ's, for region near the origin. Linear regression shown. *Inset:* Full data set. b) Indentation stress vs. strain curves; center curve has the correct δ. Solid line is linear regression of the center curve, dashed line is the expected slope as calculated from $4E^*/3\pi$. *Inset* plots error and R^2 vs. δ.

3.3.2 Iron$_B$, Sapphire, And The "Spike"

Figure 15 and Figure 16 show similar results for iron and sapphire, respectively.

Here again the instrument value for the zero point is slightly off.

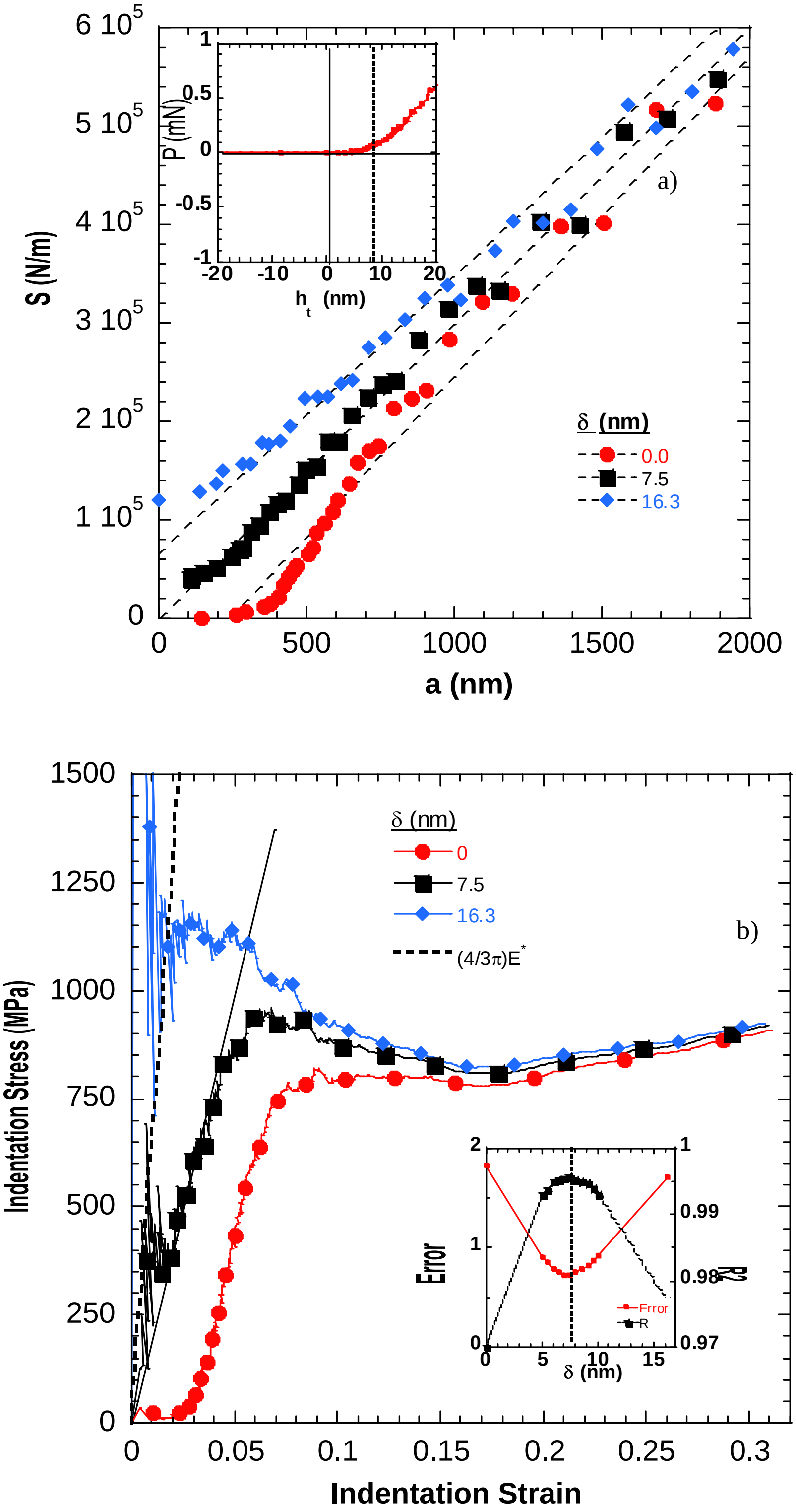

Figure 15: Iron$_B$ – Zero Point Results

Iron$_B$, 13.5 μm indenter. a) *S* vs. *a* for various δ's, for region near the origin. Linear regression shown. *Inset:* Raw P vs. h_t at region near the supposed S = 200 N/m zero point. Dashed line denotes true location of the effective zero point as determined herein. b) Indentation stress vs. strain curves; center curve has the correct δ. Solid line is linear regression of the center curve; dashed line is the expected slope as calculated from $4E^*/3\pi$. *Inset*: Error and R^2 vs. δ.

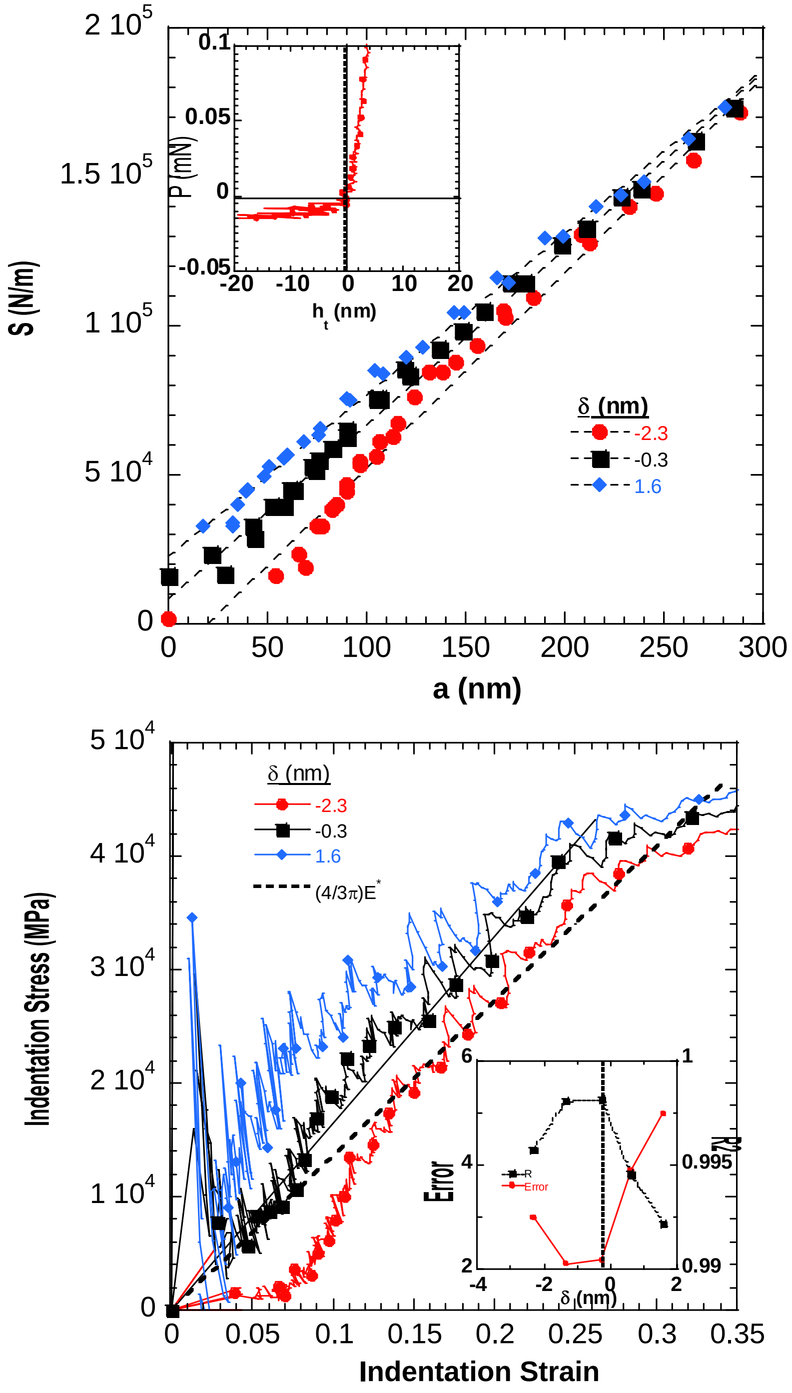

Figure 16: Sapphire – Zero Point Results

Sapphire, 1 μm indenter. a) *S* vs. *a* for various δ's, for region near the origin. Linear regression shown. *Inset:* Raw load vs. displacement at region near the supposed S = 200 N/m zero point. Dashed line denotes true location of the effective zero point as determined herein. b) Indentation stress vs. strain curves; center curve has the correct δ. Solid line is linear regression for first loading region of the center curve, dashed line is the expected slope as calculated from $4E^*/3\pi$. *Inset* plots error and R^2 vs. δ.

Note the early spike in the results that appears in Figure 14b, Figure 15b, and Figure 16b, especially at strains less than 0.01. This spike - to our knowledge not previously highlighted or understood - arises primarily because at low h_t, the stress is quite sensitive to the values of P, through a^2. Its effect on the early region of the stress-strain curve is best seen in Figure 17, which is a re-plot of the center curve of Figure 15, Fe_B where $\delta = 7.5$.

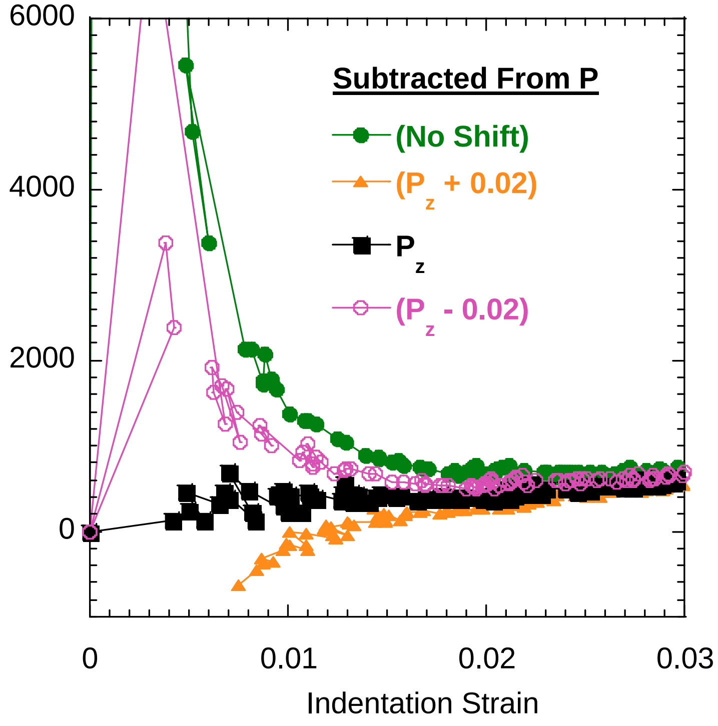

Figure 17: Effect of P on Stress-Strain

Effect of changing the values of the P data column on the stress-strain curves for Fe, $\delta = 7.5$ nm. Filled circles uses as received data, P_0; filled squares, $P_0 - P(\delta = 7.5)$; Open circles, value for filled squares + 0.02 mN; filled triangles, value for filled squares - 0.02 mN.

If the as-received P = 0.04 mN, is used, the spike is huge (solid circles). When P is zeroed according to Pz (the P for the chosen δ), the curve is well behaved and the spike disappears (solid squares). Surprisingly, adding just 0.02 mN, results in a huge spike (open circles); subtracting 0.02 mN results in negative stresses (solid triangles). This result was unanticipated; 0.02 mN is only 0.08% of the maximum load for this test, and 0.003% of the full scale of the hardware. For this reason, discarding the first few early outliers (i.e. the "spike" at strain ≤ 0.1) in the stress-strain plots is permissible and since the stress-strain curves merge at strains > 0.15 would have no effect on the final results or conclusions. Herein they were left intact for the purpose of discussion, and the complete data sets were used in our calculations. Note, that removing these points would not affect the determination of δ, nor any of the S vs. a curves presented here. Removing the early points also greatly mitigates the effects of complex surface phenomena,3 further bolstering the robustness of our method. These comments notwithstanding, gratifyingly, when the correct zero point was chosen the spike all but disappears, indirectly confirming the correctness of our approach. Given the sensitivity of the curves to P, this result is quite remarkable.

3.3.3 Slope Comparison

When E_{eff}, viz. slopes of the *S* vs. *a* curves divided by 2, for all three samples, are plotted as a function of δ (Figure 18) it is clear that E_{eff} is a function δ. This is an important result because the choice of the wrong zero-point can lead to an incorrect determination of E_{eff}. For example, for both Fe and sapphire, an error of only ≈ 2 nm in the choice of the effective zero point results in an error of 4% or more in E_{eff}.

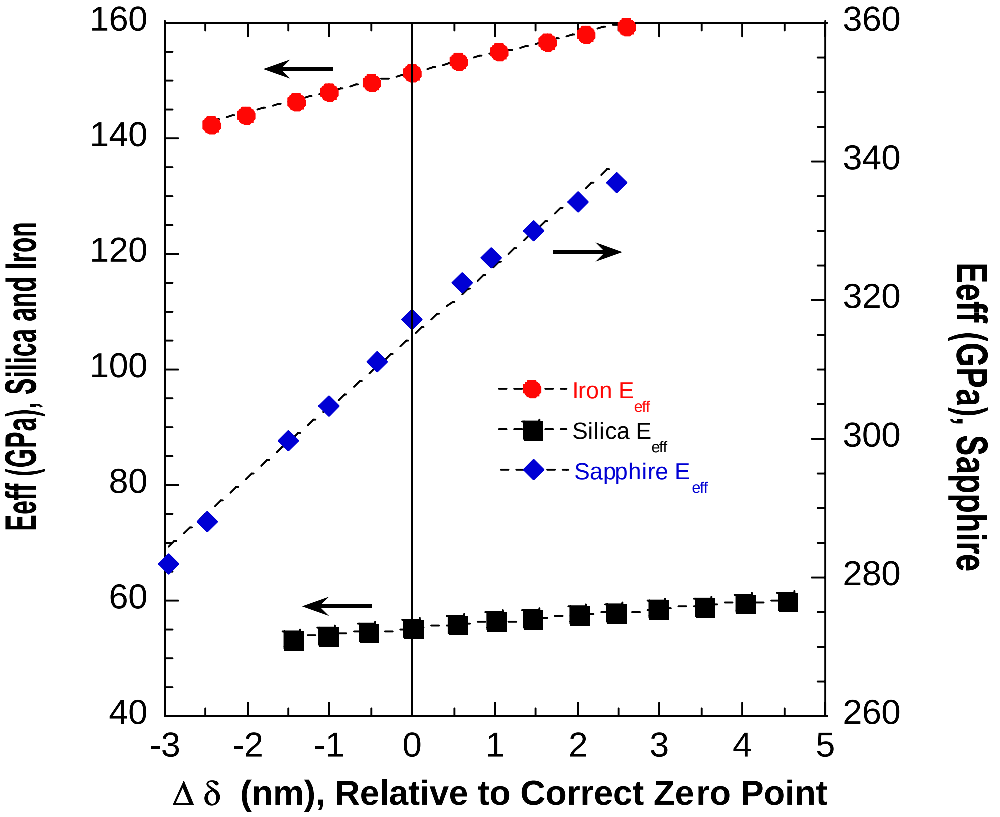

Figure 18: Eeff vs. δ

Dependence of E_{eff} on δ for all three solids tested. Dashed lines are the linear regression for each data set. The change in δ is given with reference to the correct effective zero point for each sample, respectively (i.e. for the correct delta, Δδ = 0). Arrows indicate corresponding y-axis for data.

3.3.4 Comparison With Other Methods

It is instructive to compare the results of our method with those from the methods described above. Consider the methods as follows:

1. The "simple" S=200 method most likely used by MTS (current comparison)
2. The Oliver & Pharr S=200 method (preceding a steady increase in S)[21]
3. Camera method (only claims accuracy of ~5 micron) (Lim / Richter methods)[43,45]
4. Chudoba optimized regression on P vs. ht[39,40]
5. Ullner optimized regression on P vs. ht[46]
6. P exceeding a certain threshold

This chapter is already written with delta in reference to Method 1, with zero identified as that given by the MTS instrument, likely to be the first instance during loading of S ≥ 200 n/m. We have since compared our method to Method 2, that of Oliver & Pharr. It is similar to Method 1, but has a key difference greatly increasing its accuracy. They also suggest using phase angle or harmonic displacement instead of S, depending on which appears to be the most clear, but we have limited our comparison to S, their preferred method. We found that Method 2 identified the zero point lower than that which our method does, by up to 14 nm. Please note that Method 2 is somewhat subjective, but we made every effort to faithfully implement it according to their 2004 review paper.[21] Figure 19 and Figure 20 below show examples of the difference found, and its impact on the results. Note that the sample compared is the same fused silica from above. (Figure 14)

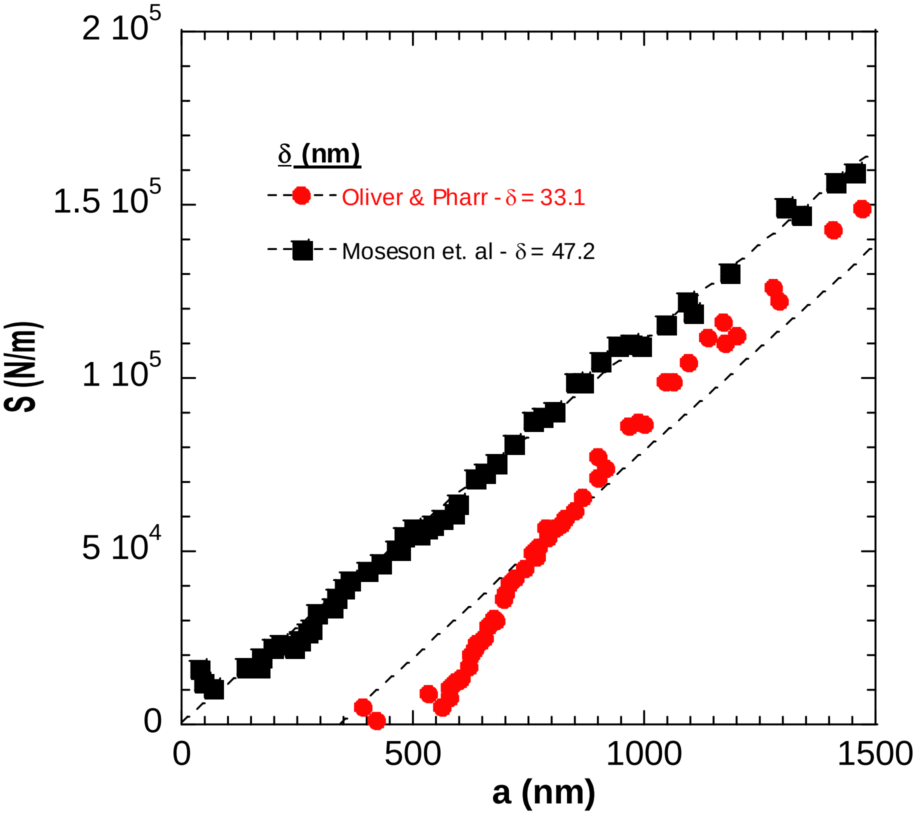

Figure 19: Our Method vs. Oliver & Pharr - Fused Silica, S vs. a

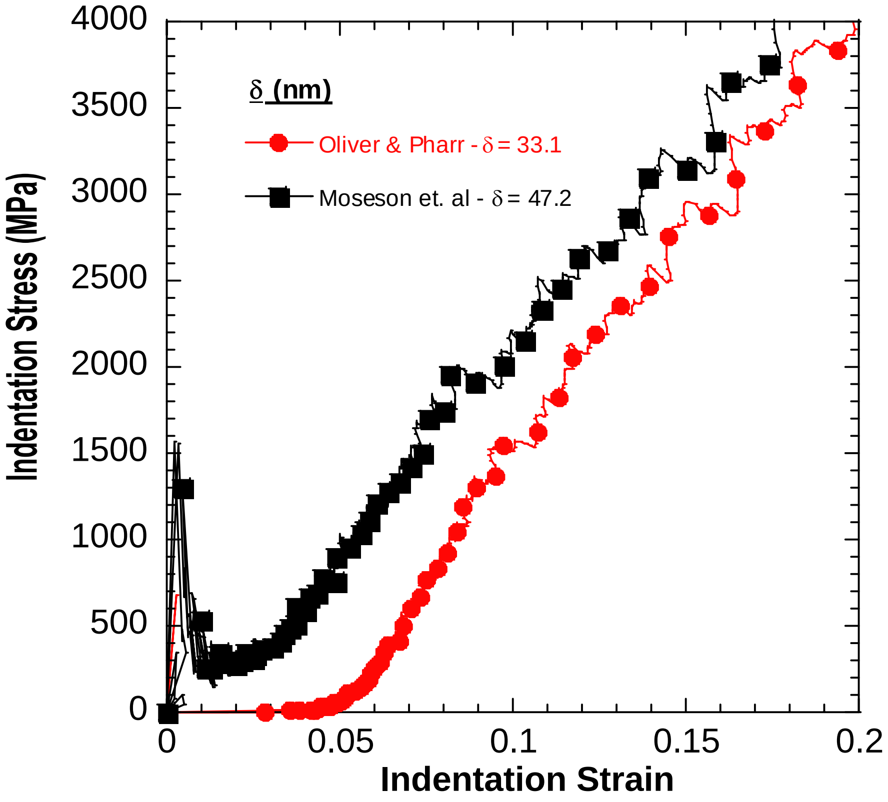

Figure 20: Our Method vs. Oliver & Pharr - Fused Silica, Stress vs. Strain

Comparison with Method 3 would require a significant investment in hardware, and the supposed accuracy is only 5000 nm, three orders of magnitude greater than our method, and Method 2, thus we have chosen not to pursue that method further.

Methods 4 and 5 require the use of complex regression procedures, requiring numerical optimization and associated custom computer programs. The specific details of the method, which would enable us to do a comparison, are either absent or exceedingly difficult, and may require custom computer programs to be procured or written to perform the analysis. In short, we believe the comparison to be valuable, but beyond the scope of this Rapid Communication. We would also like to see a future, more detailed paper which addresses this comparison, be it by ourselves or others.

Method 6 is already well understood to be a poor indicator of the zero point, and thus of little interest. Furthermore, as Oliver & Pharr explain in their 2004 review paper, the transition at the surface is gradual and not distinct; so the method is inherently subjective, and thus not comparable to the methods being discussed here.

3.4 Discussion

According to Eq. 4, the slope of the indentation stress vs. strain curve should equal $4E^*/3\pi$. The inclined dashed lines shown in Figure 14b, Figure 15b and Figure 16b represent the $4E^*/3\pi$ line; the solid inclined lines, on the other hand, represent the least squares fit of the data points shown in the linear regime forced through zero. The following comments are salient: i) In the case of silica and sapphire, $E^* \approx E_{eff}$. This is especially true considering that Eq. 6 was derived assuming a perfect sphere indenting a perfectly perpendicular, atomically smooth, elastically isotropic surface. The latter is probably only true here for fused silica. The agreement would have also been more obvious had we chosen to plot the results for larger increments of δ as done in Figure 16b. The correlation is also excellent for ZnO,[1,29] Al[1], GaN[48] and more recently, $LiNbO_3$.[49] ii) For Fe the dashed line is approximately 3 times steeper than the solid line, i.e $E^* \approx 3\ E_{eff}$. As previously discussed,[1] this difference is not an error in our method, but rather a true physical phenomena – most probably related to the elastic anisotropy of Fe - consistent with previous results and deserving of future research. iii) In principle, the linearity of the stress-strain curves, and the need that they pass through the origin, can also be used to find the actual location of the effective zero point instead of, or in addition to, the method outlined herein.

The results above demonstrate the method on three different materials, including metal and ceramic, and with two spherical indenter sizes. The importance and sensitivity of correctly identifying the effective zero point is highlighted in the stress vs. strain curves. For example, in Figure 15b, a difference of only 2 nm results in large variations in the indentation stress/strain curves, which previously were left unexplained.

The effective zero point resolution for our setup is estimated to be ≈ 2 nm, but this could vary depending on hardware and loading schemes. We hope that this work will inspire further research to make instrumented indentation an ever more valuable characterization tool. We suggest, for future investigation, the expansion of this method to other tip geometries, phenomena such as that seen for Fe, full comparison with other methods, and applications of the method.

3.5 Potential Applications

3.5.1 *Increase Accuracy Of Current Methods*

First and foremost, as demonstrated above, the use of our Zero Point Determination method increases the accuracy of all spherical instrumented indentation techniques. Raw data and the subsequent calculations which use it, can be extremely sensitive to zero point.

3.5.2 *Sample Tilt Determination, Possibly With Correction*

As a specific example of a method which could have its accuracy enhanced, sample tilt is yet another confounding issue for nanoindentation. All models assume an atomically flat surface perpendicular to the indenter tip, so any tilt, even less than one degree, can noticeably impact the results.[32] Sample tilt across a reasonably sized sample appears as an elevation difference on the order of microns, so accuracy to 2 nm would not be necessary, but if software and hardware are developed to sense, and perhaps correct, sample tilt, increasing the accuracy of that process would be welcome.

3.5.3 *Surface Topography With Spherical Nanoindentation*

Oliver and Pharr describe a method by which they used a nanoindenter with a Berkovich tip to map the topography of a deep Berkovich indentation.[21] They essentially scanned the surface and used a "quantitative imaging system" (apparently proprietary or not of great interest for the paper in which they use it) to create a 3D image of the deep indent. The method appears similar to that of atomic force microscopy, (AFM) wherein a tip is scanned across the surface of the sample, and the x, y, and z coordinates logged and compiled. For such experiments, the resolution and accuracy of the scan depend extraordinarily on the location of the surface (zero point). Thus, our method might be used in conjunction with an imaging algorithm to obtain not only accurate topographical, but mechanical data as well.

3.6 Critical Analysis Of Method

It may appear that there is a critical flaw in our logic, which if true would certainly be a serious problem. The criticism, excerpted here from a reviewer decision letter, is:

> *"The most critical flaw and inconsistency is in what follows: Both of Eq. (6) and Eq. (1) (this is the key expression in the authors' technique proposed for adjusting the zero-point contact)* $S = 2 E_{ff} a$ *are easily as well as straightforward derived from the original Hertzian elastic equation of* $P \alpha h^{3/2}$*. This means that Eq. (1) and Eq. (6) are definitely equivalent, meaning that the results for any elastic materials with any surface conditions (roughness, friction, etc.) via Eq. (1) must coincide with those obtained from Eq. (6)…"*

This objection would be true *if and only if* we had calculated S from a. In our work - and it is here that our major contribution comes in – S is <u>completely independent</u> of all the equations shown; it is a raw data channel which comes from the CSM attachment on the instrument. And while we use S to calculate a, we - and this is very important – also only use constants and the totally *independent* variables of h_t and P. The full equation used to calculate a is:

$$a = \sqrt{2R_t\left(h_t - \frac{3}{4}\frac{P}{S}\right) - \left(h_t - \frac{3}{4}\frac{P}{S}\right)^2}$$

What we then do is plot a - which is calculated from the Eq. shown above - and the totally *independently* measured S, and we show that they indeed result in a straight line as expected. There is absolutely no *apriori* reason that the moduli in Eqs. 1 and 6 be the same. In most cases they are.[1,29,49] In the case of iron, they are not. As we note in this thesis, this is *not* a defect in our method, but rather a true physical phenomenon most probably related to the elastic anisotropy of Fe. The results on Fe actually help to prove our point. Had we used a circular argument then *per force* the two slopes would have been identical. The fact that in most cases the moduli are almost identical (see sapphire, silica, and the references noted above) confirms the validity of our approach; the fact that in some cases they are not the same – when we use the *identical algorithm* for data analysis – is the proverbial exception that proves the rule and certainly rules out that we used a circular argument.

We understand of the difference between the two slopes to be a result of deviations from the assumptions made by Hertz and others in developing the model, as well as a very acceptable level of experimental uncertainty. The many samples for which the slopes agree reasonably well are indirect evidence of the validity of the Hertz model, despite its assumptions.

3.7 Summary And Conclusions: Effective Zero Point

We are confident that our method allows the indentation zero point to be objectively and accurately determined, by using data that is *not* sensitive to the zero point to correct something that is. The zero point resolution for our setup is estimated to be ≈ 2 nm but this could vary depending on hardware and loading schemes. We hope that this work will inspire further research to make instrumented indentation an ever more valuable characterization tool. We suggest, for future investigation, the expansion of this method to other tip geometries (such as Berkovich), phenomena such as that seen for Fe, full comparison with other methods, and applications of the method.

CHAPTER 4. SPHERICAL NANOINDENTATION TO CHARACTERIZE INDIVIDUAL GRAINS

Most recently, I conducted experiments on annealed samples with large grains, to explore the characterization of the individual grains of polycrystalline samples. Please note that this work is still in progress, and has offered results which are both tantalizing and befuddling. Once the research is completed to a satisfactory understanding of our observations, we intend to publish the work.

4.1 Three Different Grains on Iron$_B$

First, consider Iron$_B$, which is pure iron which has been annealed at 1450°C for 8 hours. The average grain size, at least in the region tested, is 1.7mm. Figure 16 shows a map of the locations of nanoindents made (numbers), as well as the Vickers indents (appearing as dark squares). Note that the outer perimeter of the Vickers indents were used to mark the grain boundary, and not for gathering data. The surface was highly polished, with guidance from Struers' E-Metalog recommendations. Grain boundaries were made visible by lightly etching the sample with a common etchant, 10% Nital (10% Nitric Acid, 90% Methanol). The red lines indicate the grain boundaries, for clarity.

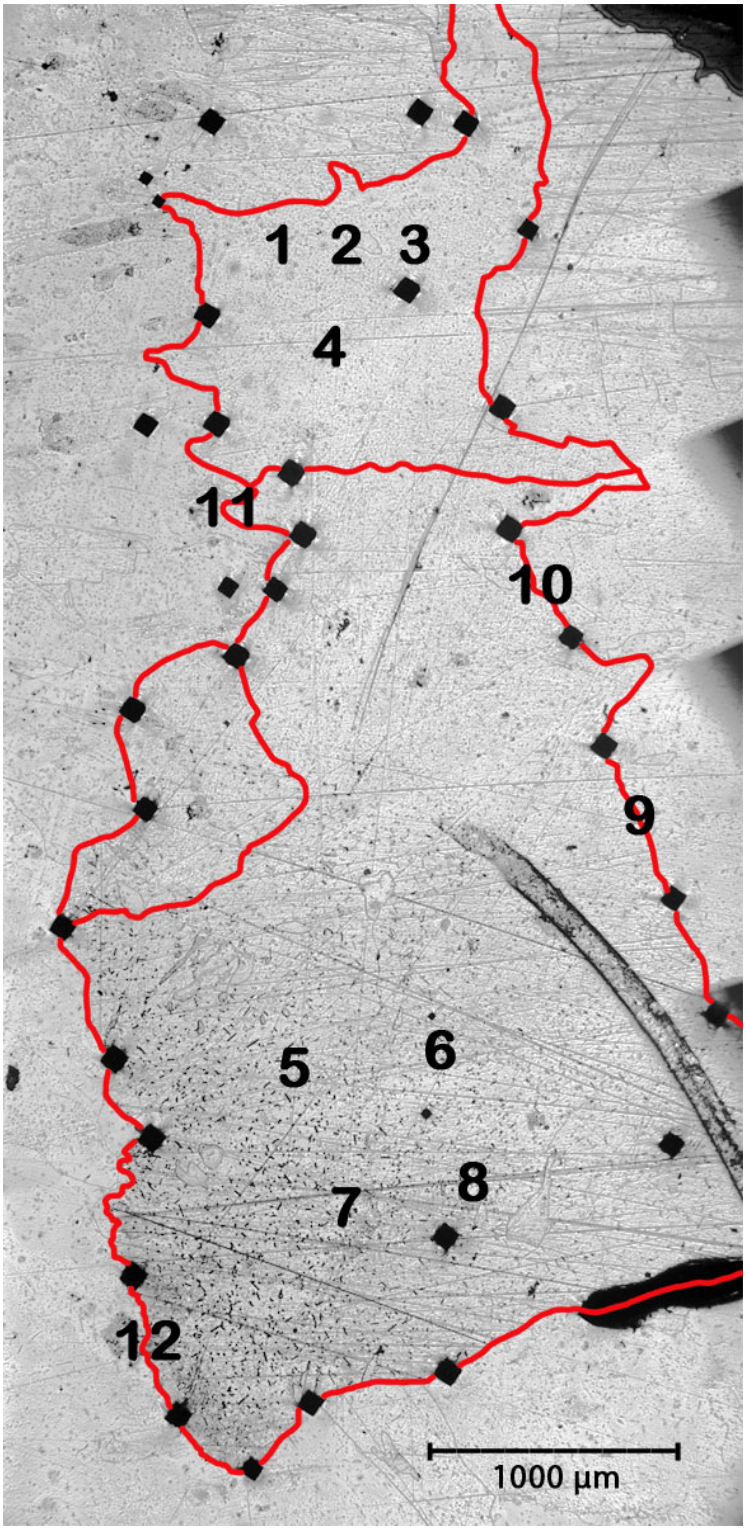

Figure 21: Micrograph of IronB Sample
Numbers correspond to approximate nanoindentation locations. The indents are too small to see at this magnification. Dark squares are Vickers indents, most used only to mark the grain boundary. The red line outlines the grains.

Note that locations 9 through 12 were intentionally placed on the grain boundary, to investigate the effects of indenting on a boundary. Locations 13 through 16 are on a single grain located some distance away from the grain pictured in the micrograph, and that grain cannot be readily identified. Figure 22 through Figure 24 show the load-displacement, S-a, and stress-strain curves, respectively. The stress-strain curve was produced by the method described in Chapters 1 and 3.

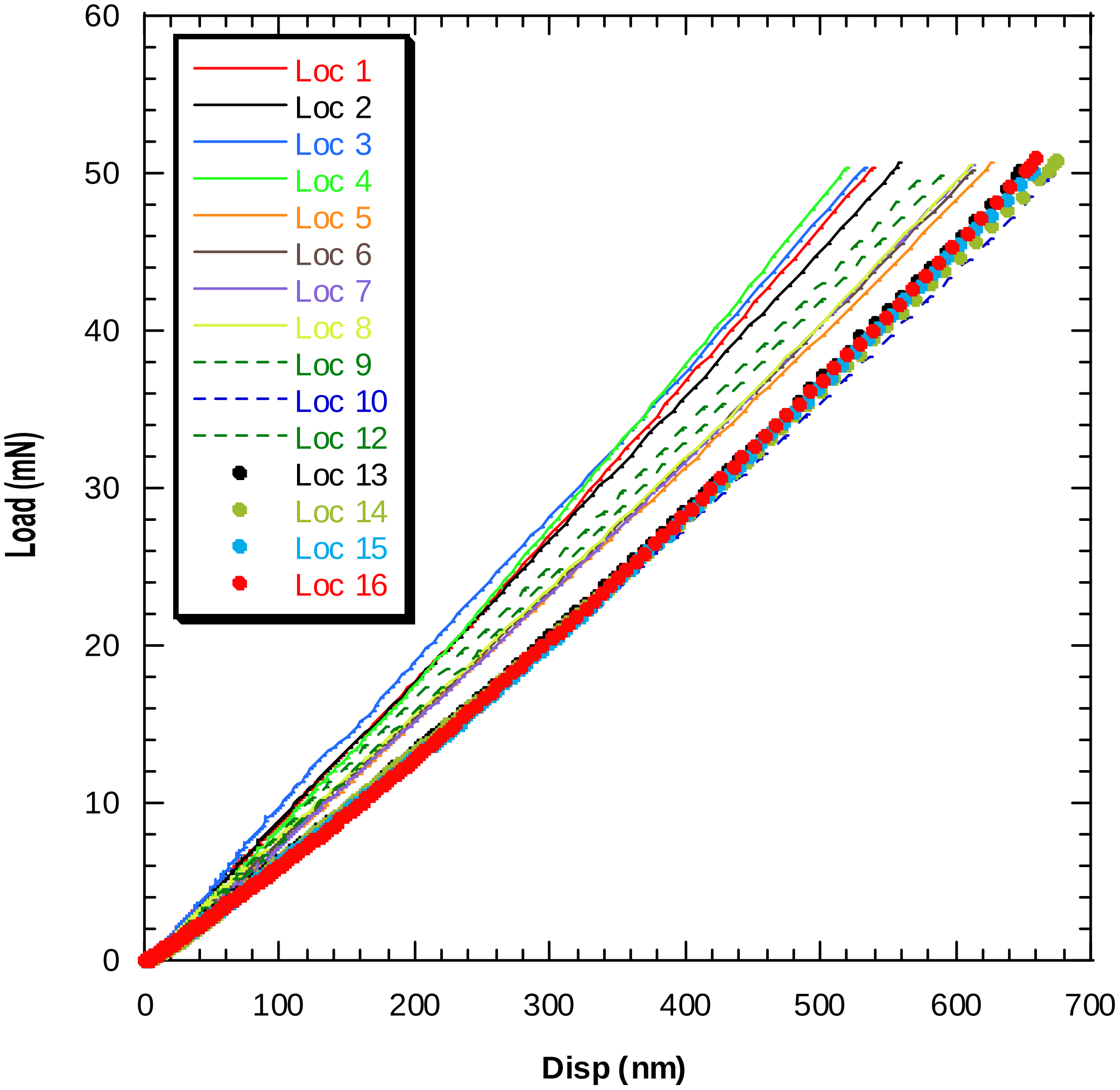

Figure 22: Annealed Iron$_B$ Map, Load vs. Displacement

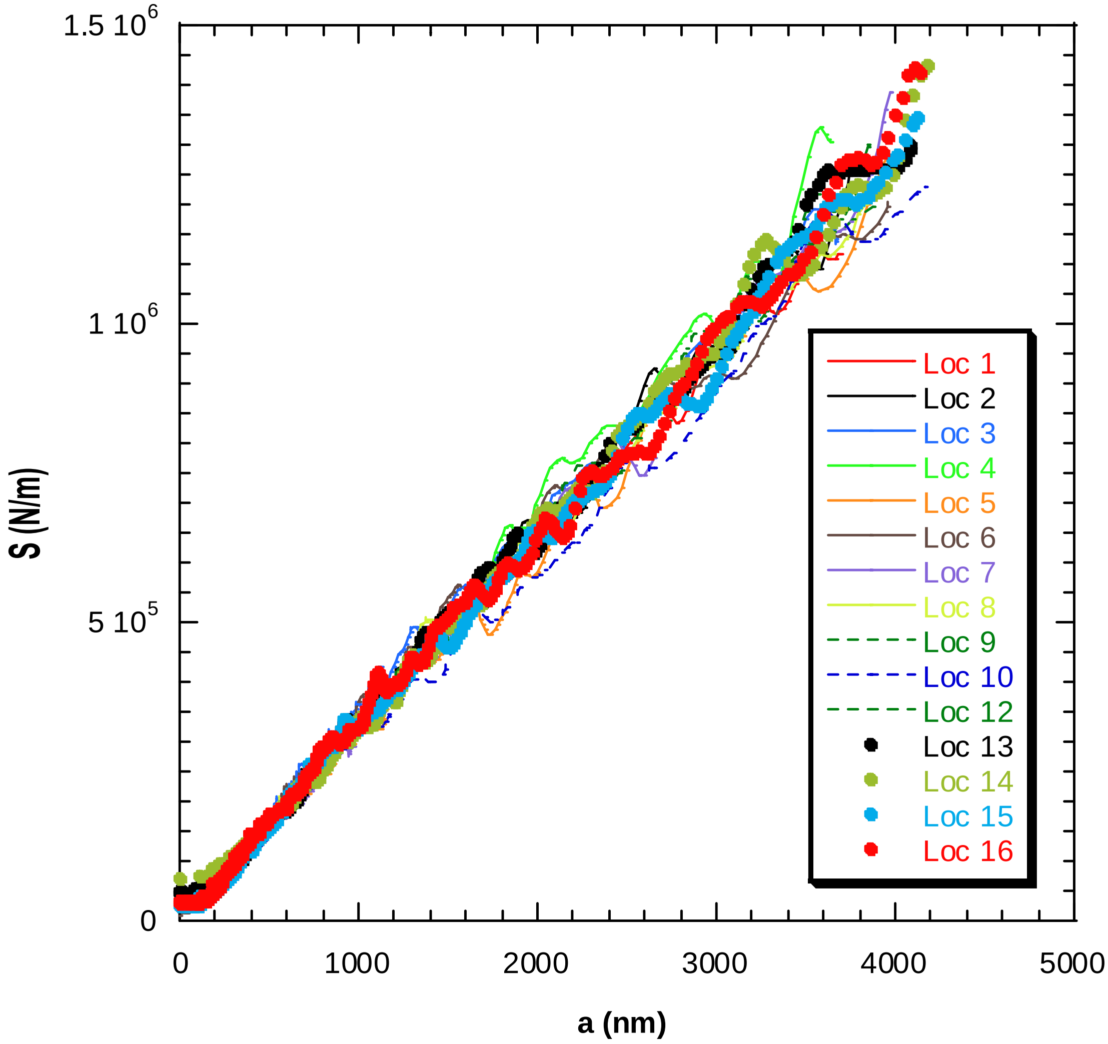

Figure 23: Annealed Iron$_B$ Map, Stiffness vs. Contact Radius

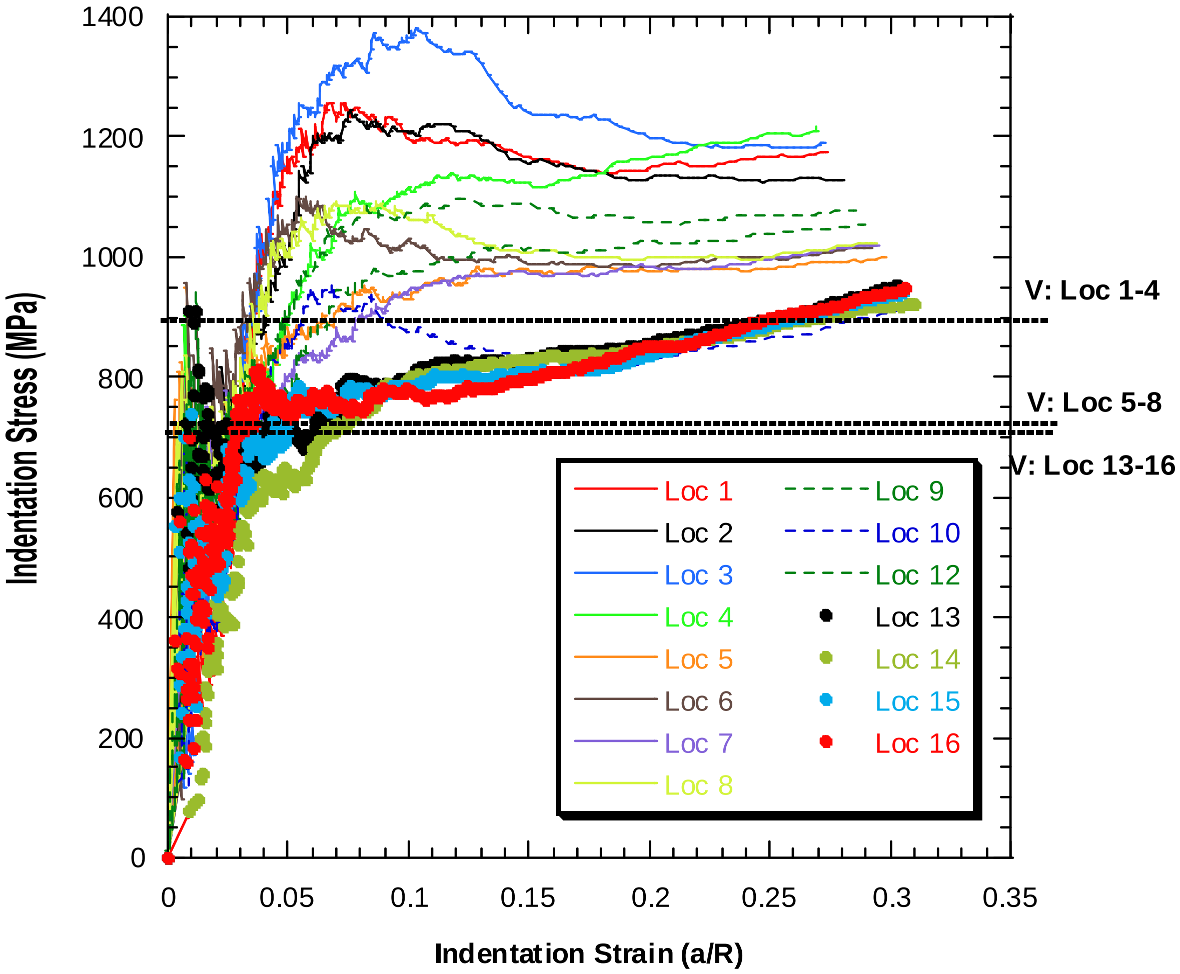

Figure 24: Annealed Iron$_B$ Map, Indentation Stress vs. Indentation Strain

The three data sets (one from each of the three grains), cluster well for load-displacement, yet are superimposed for the S-a curve. This indicates that the grains are indeed distinct, but have the same elastic modulus. Even more fantastic is the clustering of data in the stress-strain curve, Figure 24. The moduli appear to be essentially the same, but each grain has a different yield point. The best explanation for this is that the grains have different orientations, and as was demonstrated for ZnO[29] and sapphire[30], this exposes different slip systems, each requiring different stresses to yield. The fact that the grains differ with such magnitude and distinction is remarkable and indirectly confirms our methodology in converting nanoindentation load-displacement to stress-strain curves. Note the clusters for locations 1 though 4, 5 through 8, and 13 through 16. Also, as expected the data for locations 9 through 12, located on or very close to a grain boundary, does not exhibit the same clustering. The dashed lines in the figure indicate the Vickers hardness for the three grains, though the location for tests 13 – 16 is a best guess. The magnitude of the Vickers microhardness is lower than the Meyers hardness for locations 1-4 and 5-8 by arguably *exactly* the same amount. That is, if one were to shift those two Vickers lines up by approximately 150 MPa, both would coincide perfectly with the Meyers hardness. The key here is not the absolute value, which we can expect to differ by some amount because the two methods differ, but the fact that the two grains differ in yield point by the same amount as they do for Vickers. Needless to say, this is gratifying, and deserving of further investigation. One such research path would be conducting Orientation Imaging Microscopy (OIM) to determine the orientations of the grains, first to determine if they are different, and second to see if the associated expected Critical Resolved Shear Stress (CRSS) corresponds to the yield points observed.

4.2 The Effect Of Compression on Iron$_C$

Here we come to the confusing potion of our latest research. For Iron$_C$, we prepared a compression sample with nominal dimensions 13mm diameter x 38 mm long. We then machined flat parallel surfaces along the entire length of the sample, each 3mm wide. This sample was annealed for 12 h at 1450°C (not 8 h as with Iron$_B$, since growing the grains is more difficult for this larger sample.) I then machined one of the flat surfaces to expand its width to 5.5mm, ensuring that we would have enough surface area to conduct testing, and to further ensure that the surface was parallel to the other flat. I polished the larger flat surface for nanoindentation, with nearly the same procedure as that used for Iron$_B$, except that the sample had to be held by hand instead of mounted to the polisher. I followed this with the identical etching procedure as for Iron$_B$.

Following this preparation, I performed the following steps on the sample, in the order indicated, on the same three large grains: i) Vickers Microhardness ii) Nanoindentation iii) uniaxial compression to 6.3% strain (obviously for the entire sample) iv) Nanoindentation and v) Vickers microhardness. We expected to see an increase in both the Vickers and Meyers hardness values. The results show evidence of the sensitivity of the method to many, many factors which in other characterization techniques might be overlooked. Figure 25 through Figure 27 show the results of nanoindentation for the same sample, before and after compression. The legend notes "tape" or "wax" for each location. This indicates the layer used to adhere the custom built sample holder (top to bottom: sample, wax, steel mounting cylinder, wax, Bakelite mounting cylinder, wax, glass slide, wax, glass slide) to the sample stage. (The sample would not fit in the regular sample holder.)

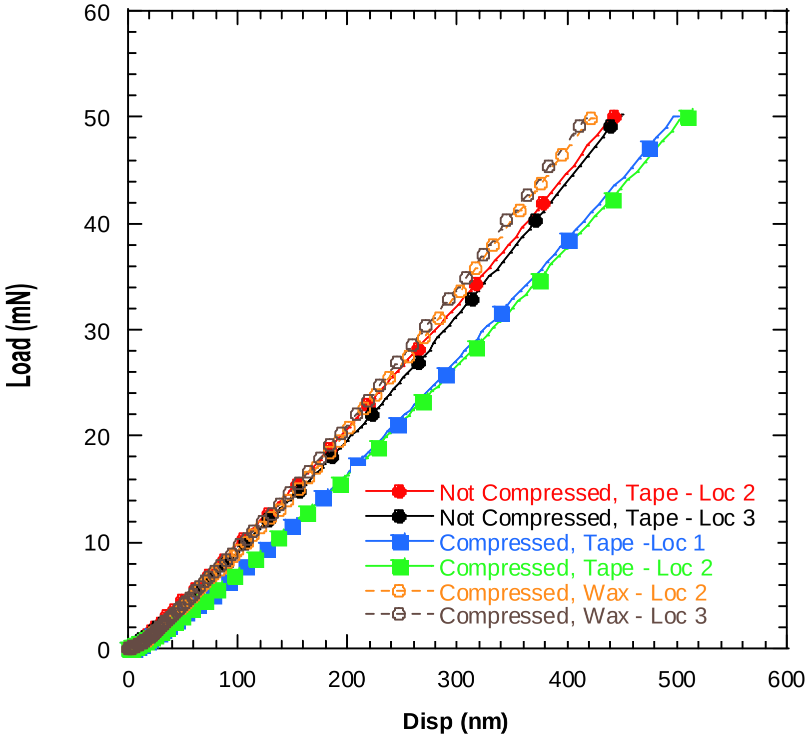

Figure 25: Compression Sample Results, Load vs. Displacement

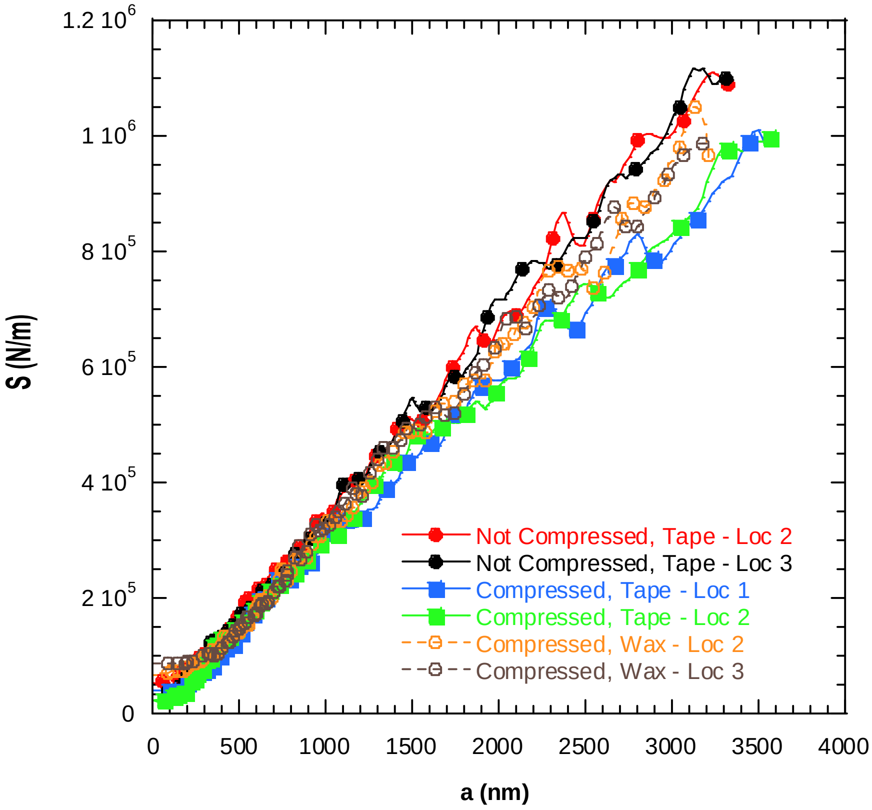

Figure 26: Compression Sample Results, S vs. a

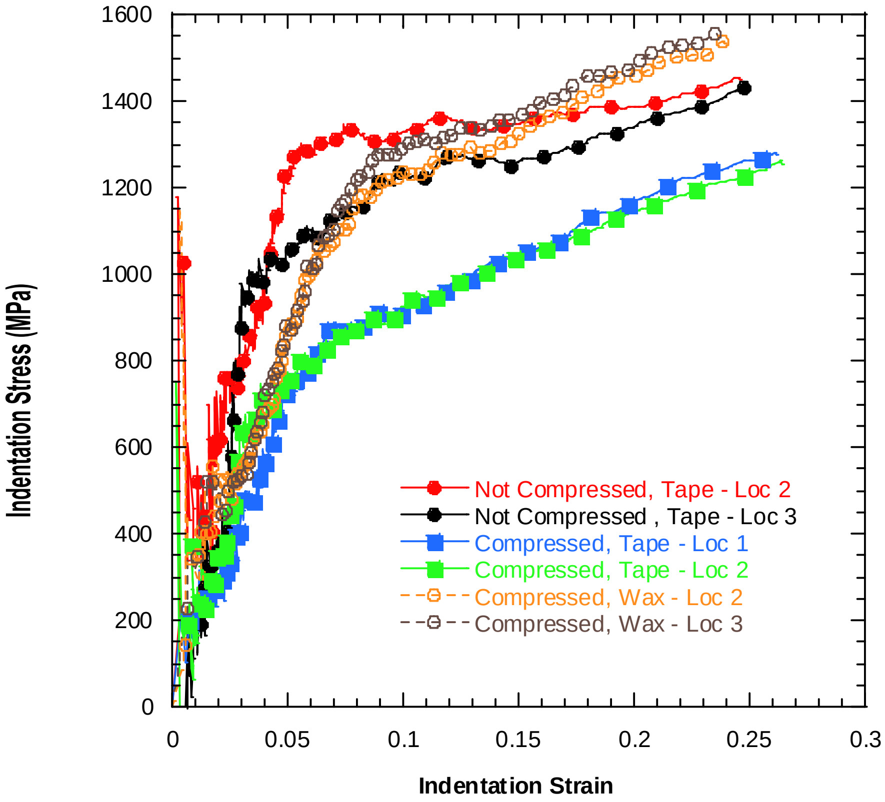

Figure 27: Compression Sample Results, Indentation Stress vs. Strain

The above results show that apparently, the sample becomes less hard upon compression. This is certainly counterintuitive. It is comforting however that the modulus remained more or less constant, though this was not the case for the other two locations tested (not shown here). When the sample holder was adhered to the sample carrier with wax instead of the much more compressible tape though, the results change dramatically. This is an example of just one of the many factors affecting the sensitive results. As another standard of measure to investigate the results, I performed Vickers indentation after compression (Table

2) and also re-measured the Vickers indents which had been created before compression (Table 3).

Table 2: Comparison of IronC Vickers Hardness Values, Before And After Compression

	S (Pre-Compression)		**T (Post Compression)**		
Grain	Vickers (MPa)	St.Dev	Vickers (MPa)	St.Dev	**Change In Vickers**
1	1141.4	55.4	1294.9	1.9	13.4%
2	989.8	20.0	1091.6	9.3	10.3%
3	1220.7	47.3	1343.9	33.0	10.1%

Table 3: Comparison of IronC Vickers Indents, Before And After compression

	Pre-Compresion		**Post-Compression**		**Change In…**		
Grain	**D1 Average**	**D2 Avg.**	**D1 Avg**	**D2 Avg**	**D1**	**D2**	**Avg D**
1	111.8	114.1	91.8	103.1	-17.9%	-9.6%	-13.7%
2	118.6	123.9	75.7	81.9	-36.1%	-33.9%	-35.0%
3	108.9	109.5	101.2	108.5	-7.1%	-0.9%	-4.0%

Table 2 shows that for all three grains, the Vickers hardness increased by about 10% after compression. We should thus expect to see the Meyers hardness increase after compression by the same 10%, which we do not. As strain is nothing but the change in sample length divided by the original length (at least for the engineering strain), I thought it valuable to compare the sizes of the original Vickers indents before and after compression. Dimension D1 was aligned with the axis of the cylinder, and we see that indeed, these decrease substantially for all grains, and decrease more so than D2, which is perpendicular to the axis. The magnitudes vary between grains though, and have no apparent correlation to the change in Vickers hardness, which are more or less equal.

After much deliberation, we have identified the following as possible sources of error. First, the figures above demonstrate that using tape anywhere in the sample mounting column, albeit over 50 mm away from the indentation surface, has some effect on the results. Second, the sample surface may not have been as nearly perpendicular to the indenter tip after compression as before. As all of the theory assumes a flat, perpendicular surface, this aberration would alter the results. Even a fraction of a degree can have significant effects.[32] Our loss of perpendicularity occurred for two reasons: i) Because of the necessary lack of shear stress on the surface of the sample, where the indentations were performed, the polished flat "crinkled" along what appear to be the grain boundaries, creating a surface which is no longer uniformly flat. The phenomena can perhaps best be described as the effect seen when compressing a stiff piece of common aluminum foil. Even after re-polishing, some effects remained. ii) the sample buckled slightly under compression, before the test was terminated to prevent further buckling. This contributed to the loss of perpendicularity. Furthermore, grain 3 was located at a portion of the sample where the buckling caused additional compression, and "ripples" in the grain easily visible under the microscope. For this reason, we will not be considering the results of grain 3 any further. The third area of concern is that of surface roughness, which would alter results for obvious reasons. Fourth, Oliver & Pharr note "near-surface forces" such as water meniscus formation, and other effects such as thermal and physical vibration as contributing to uncertainty, especially at extremely shallow depths. Fifth, the sample holder designed for the nanoindentation of this experiment included a piece of double-stick tape, albeit several centimeters away from the sample, which could compress under the load of the indenter. Though the compression would be seemingly insignificant at normal scales, that significance could be magnified enough to interfere with the results, at the nanoscale. Lastly, the surface polishing is in question, because the sample was held by hand rather than mounted properly in a sample holder.

The sheer volume of possible problems described above point towards a new experimental design, mitigating or eliminating as many of those unknowns as reasonably possible. This is likely to be our next course, possibly in collaboration with others doing similar work at Drexel University.

4.3 Summary of Work on $Iron_B$ and $Iron_C$

In summary, the preliminary results on $Iron_B$ are very interesting, point towards the success of our method and the tests on that sample, and could offer solid proof of something rarely shown before, if ever. The work on $Iron_C$ is interesting, but will require a new design of experiment to carry out the work properly.

CHAPTER 5. SUMMARY AND CONCLUSIONS

5.1 Summary And Conclusions

In this thesis, I have provided valuable insights into spherical nanoindentation, through original research by myself and my colleagues.

First, we demonstrated the validity of a method to accurately transform indentation load-displacement plots to stress-strain plots. Stress-strain plots, having information throughout the regions of elasticity, transition, and plasticity, are quite valuable, and are a major improvement over the load-displacement plots from which they are derived. We validated our method on a wide variety of materials, and confirmed results with literature, Berkovich indentation, and

Vickers indentation. Note that included in those samples were ceramics, and our work is thus one of the earliest times in history where meaningful stress-strain curves were produced for ceramic materials. (In traditional tests, the brittle sample fractures suddenly and before much data can be gathered.) We also performed the work with two indenter sizes, and saw excellent agreement between the results. Later work on ZnO and $LiNbO_3$, using the technique, offered insight into the behavior of KNE solids and further evidence of the technique's validity. In short, we are able to reliably convert spherical indentation load-displacement curves to stress-strain curves for a variety of materials and tip sizes, offering insights into mechanical behavior never observed as such before. One question originally left unanswered though, was that of a δ correction factor, which brings us to the next discovery reported in this thesis.

Second, I described and showed evidence for a robust, quantitative method to determine the effective zero point, a problem which has plagued the field since its inception. The method is simple, based on well-accepted theory, and even in comparison to our closest competitor (Oliver & Pharr), offers a critical increase in accuracy. The sensitivity of nanoindentation data to the zero point is astounding, and our ability to operate despite that is perhaps even more so. Again, we demonstrated the method on a variety of materials and indenter sizes. Even under intense scrutiny, the method holds firm. As it explains so much which was not previously understood, and removes a major barrier to research, this advancement could enable great progress in the field,

Third, I showed our most recent results on iron. The work on iron$_B$ offers a tantalizing glimpse of the results which may be possible, thanks to the techniques described earlier. Validation and extension of the results, showing clear differentiation between the mechanical properties of individual grains, would be truly remarkable. The work on iron$_C$ was a valuable exercise in experimental design. It forced our research group to carefully consider all of the factors which affect the results, and how to mitigate or isolate them. Further work on compression samples will hopefully yield powerful results as well.

In summary, we have demonstrated a reliable method to convert spherical nanoindentation load-displacement curves to stress-strain curves, a robust and quantitative method to determine the effective zero point, and remarkable results on individual grains. We are privileged to have contributed to the field, and as described below, will endeavor to continue doing so.

5.2 Future Work

The following is recommended future work, to continue that described thus far. Our research group, including the author of this thesis, intends to continue the work, but we would also encourage any others who might be interested in pursuing them to do so.

i. Extend the stress-strain and effective zero point methods to other sizes of spherical tip

ii. Extend the stress-strain and effective zero point methods to other tip geometries, including and especially Berkovich

iii. Gain a better understanding of the yield point, including the correlation between it and the Vickers (or other) hardness

iv. Quantitatively compare our effective zero point determination method with competing methods

v. Test our methods on thin and/or thick films

vi. Investigate the effect of sample tilt on our methods

vii. Continue work on large distinct grains to search for differences in mechanical behavior. This would include performing OIM on the Iron$_B$ sample, and extending the experimental design used for that material to others.

viii. Investigate the effect of compression on nanoindentation results, especially modulus and hardness.

ix. Investigate the effect of surface roughness, preparation procedures (including polishing), and other near-surface effects on our methods

x. Collaborate with the research group of Dr. Surya Kalidindi (Drexel University, Philadelphia, PA), which has expertise in simulation and microstructure, and is currently working to answer similar questions as those raised here.

LIST OF REFERENCES

1. S. Basu, A. Moseson, and M. W. Barsoum: On the determination of spherical nanoindentation stress-strain curves. Journal of Materials Research **21,** 2628-2637 (2006).

2. A. J. Moseson, S. Basu, and M. W. Barsoum: Determination of The Zero Point Of Contact For Spherical Nanoindentation. Journal of Materials Research **Submitted For Publication** (2007).

3. Encyclopedia Britannica, Friedrich Mohs (German Mineralogist), Available From,<http://www.britannica.com/eb/topic-387712/Friedrich-Mohs>

4. S. Basu, (Drexel University, Graduate Seminar Presentation Slides, 2006).

5. MTS: MTS Technical Data Sheet, “Spherical Indenters”. (Distributed 2005).

6. X. Li and B. Bhusan: A review of nanoindentation continuous stiffness measurement technique and its applications. Materials Characterization **48,** 11-36 (2002).

7. J. S. Field and M. V. Swain: THE INDENTATION CHARACTERISATION OF THE MECHANICAL PROPERTIES OF VARIOUS CARBON MATERIALS: GLASSY CARBON, COKE AND PYROLYTIC GRAPHITE. Carbon **34,** 1357 (1996).

8. J. S. Field and M. V. Swain: Determining The Mechanical-Properties Of Small Volumes Of Material From Submicrometer Spherical Indentations. Journal Of Materials Research **10,** 101-112 (1995).

9. W. C. Oliver and G. M. Pharr: Nanoindentation creep of quartz, with implications for rate- and state-variable friction laws relevant to earthquake mechanics. Journal of Materials Research **19,** 357-365 (2004).

10. MTS, Nano CSM, Product Information Sheet, Available From,<http://www.mtsnano.com/pdf/Nano_CSM.pdf>

11. A. Murugaiah, Thesis, Drexel University, 2004.

12. A. C. Fischer-Cripps: A review of analysis methods for sub-micron indentation testing. Vacuum **58,** 569-585 (2000).

13. F. Guiberteau, N. P. Padture, and B. R. Lawn: Effect of Grain Size on Hertzian Contact Damage in Alumina. J. Amer. Cer. Soc. **77,** 1825-1831 (1994).

14. N. Iwashita, M. V. Swain, J. S. Field, N. Ohta, and S. Bitoh: Elasto-plastic deformation of glass-like carbons heat-treated at different temperatures. Carbon **39,** 1525-1532 (2001).

15. D. Tabor. *Hardness of Metals* (Clarendon, Oxford, U.K., 1951),

16. K. L. Johnson. *Indentation Contact Mechanics* (Cambridge University Press, Cambridge, MA, 1985),

17. B. R. Lawn, N. P. Padture, H. Cait, and F. Guiberteau: Making Ceramics "Ductile". Science **263,** 1114-1116 (1994).

18. E. G. Herbert, G. M. Pharr, W. C. Oliver, B. N. Lucas, and J. L. Hay: On the Measurement of stress-strain curves by spherical indentation. Thin Solid Films **398-399,** 331-335 (2001).

19. J. S. Field and M. V. Swain: A Simple Predictive Model For Spherical Indentation. Journal Of Materials Research **8,** 297-306 (1993).

20. I. N. Sneddon: The relaxation between load and penetration in the axisymmetric boussinesq problem for a punch of arbitrary profile. Int. J. Engineering Science, **3,** 47 (1965).

21. W. C. Oliver and G. M. Pharr: Measurement of hardness and elastic modulus by instrumented indentation: Advances in understanding and refinements to methodology. Journal of Materials Research **19,** 3-20 (2004).

22. W. C. Oliver and G. M. Pharr: Measurement of hardness and elastic modulus by instrumented indentation: Advances in understanding and refinements to methodology. J. Mater. Res. **19,** 3-20 (2004).

23. B. N. Lucas and W. C. Oliver: Indentation power-law creep of high-purity indium. Metallurgical And Materials Transactions A-Physical Metallurgy And Materials Science **30,** 601-610 (1999).

24. J. E. Bradby, J. S. Williams, and M. V. Swain: Pop-in events induced by spherical indentation in compound semiconductors. J. Mater. Res. **19,** 380-386 (2004).

25. N. Iwashita, J. S. Field, and M. V. Swain: Indentation Hysteresis of Glassy Carbon Materials. Phil. Mag. A **82,** 1873-1881 (2002).

26. J. E. Bradby, S. O. Kucheyev, J. S. Williams, C. Jagadish, M. V. Swain, P. Munroe, and M. R. Phillips: Contact-induced defect propagation in ZnO. App. Phys. Lett **80,** 4537-4539 (2002).

27. S. O. Kucheyev, J. E. Bradby, J. S. Williams, C. Jagadish, and M. V. Swain: Nanoindentation of epitaxial GaN films. Appl. Phys. Lett. **77,** 3373-3375 (2000).

28. S. O. Kucheyev, J. E. Bradby, J. S. Williams, C. Jagadish, and M. V. Swain: Mechanical deformation of single-crystal ZnO. App. Phys. Lett **80,** 956-958 (2002).

29. S. Basu and M. W. Barsoum: Deformation Micromechanisms of ZnO Single Crystals as Determined From Spherical Nanoindentation Stress-Strain Curves. J. Mater. Res. **22** (2007).

30. S. Basu, M. W. Barsoum, and S. R. Kalidindi: Sapphire: A Kinking Nonlinear Elastic Solid. J. Appl. Phys. **99,** 063501 (2006).

31. M. R. VanLandingham: Review of Instrumented Indentation. Journal of Research of the National Institute of Standards and Technology **108,** 249-265 (2003).

32. Z. H. Xu and X. Li: Effect Of Sample Tilt On Nanoindentation Behaviour Of Materials. Philosophical Magazine **87,** 2299-2312 (2007).

33. J. L. Bucaille, E. Felder, and G. Hochstetter: Identification of the viscoplastic behavior of a polycarbonate based on experiments and numerical modeling of the nano-indentation test. Journal of Materials Science **37** (2002).

34. P. Grau, G. Berg, W. Fraenzel, and H. Meinhard: Recording hardness testing problems of measurement at small indentation depths PHYS STATUS SOLIDI A **146,** 537-548 (1994).

35. N. Huber and E. Tyulyukovskiy: A new loading history for identification of viscoplastic properties by spherical indentation. Journal of Materials Research **19,** 101-113 (2004).

36. Z. Li, K. Herrmann, and F. Pohlenz: A comparative approach for calibration of the depth measuring system in a nanoindentation instrument. Measurement **39,** 547-552 (2006).

37. B. Rother, A. Steiner, D. A. Dietrich, H. A. Jehn, J. Haupt, and W. Gissler: Depth-sensing indentation measurements with Vickers and Berkovich indenters. Journal of Materials Research **13** (1998).

38. E. Tyulyukovskiy and N. Huber: Neural networks for tip correction of spherical indentation curves from bulk metals and thin metal films. Journal of the Mechanics and Physics of Solids **55,** 391-418 (2007).

39. T. Chudoba, M. Griepentrog, A. Dück, D. Schneider, and F. Richter: Young's modulus measurements on ultra-thin coatings. Journal of Materials Research **19,** 301-314 (2004).

40. T. Chudoba, N. Schwarzer, and F. Richter: Determination of elastic properties of thin films by indentation measurements with a spherical indenter. Surface and Coatings Technology **127,** 9-17 (2000).

41. A. C. Fischer-Cripps: Critical review of analysis and interpretation of nanoindentation test data. Surface and Coatings Technology **200,** 4153-4165 (2006).

42. Y.-H. Liang, Y. Arai, K. Ozasa, M. Ohashi, and E. Tsuchida: Simultaneous measurement of nanoprobe indentation force and photoluminescence of InGaAs/GaAs quantum dots and its simulation. Physica E: Low-dimensional Systems and Nanostructures **36,** 1-11 (2007).

43. Y. Y. Lim and M. Munawar Chaudhri: Indentation of elastic solids with a rigid Vickers pyramidal indenter. Mechanics of Materials **38,** 1213-1228 (2006).

44. V. Linss, N. Schwarzer, T. Chudoba, M. Karniychuk, and F. Richter: Mechanical properties of a graded B-C-N sputtered coating with varying Young's modulus: deposition, theoretical modelling and nanoindentation. Surface and Coatings Technology **195,** 287-297 (2005).

45. F. Richter, M. Herrmann, F. Molnar, T. Chudoba, N. Schwarzer, M. Keunecke, K. Bewilogua, X. W. Zhang, H. G. Boyen, and P. Ziemann: Substrate influence in Young's modulus determination of thin films by indentation methods: Cubic boron nitride as an example. Surface and Coatings Technology **201,** 3577-3587 (2006).

46. C. Ullner: Requirement of a robust method for the precise determination of the contact point in the depth sensing hardness test. Measurement **27,** 43-51 (2000).

47. K. L. Johnson. *Contact Mechanics* (Cambridge, Cambridge University Press, 1985),

48. S. Basu, M. W. Barsoum, A. D. Williams, and T. D. Moustakas: Spherical nanoindentation and deformation mechanisms in free-standing GaN films. J. App. Phys. **In Print** (2007).

49. S. Basu, A. Zhou, and M. W. Barsoum: Micromechanics of Deformation Under a Spherical Indenter and Indirect Observation of Reversible Dislocation Motion in a LiNbO3 Single Crystal. Physics Review Letters **Submitted For Publication** (2007).

APPENDIX 1: Provisional Patent #60/953,361

“A Novel Method for Zero Point Detection”

A NOVEL METHOD FOR ZERO POINT DETECTION

BACKGROUND OF THE INVENTION

1. Statement of Government Interest

This invention was reduced to practice with Government support under Grant No. DAAD19-03-1-0213 awarded by Army Research Office; the Government is therefore entitled to certain rights to this invention.

2. Field of the Invention

The present invention relates to a method for objectively and accurately determining the zero point of a nano-indented material. The novel method of the present application may be particularly useful in enhancing the accuracy of nano-indentation analysis, providing a better understanding of contact mechanics, and positioning a nanoindenter relative to a surface of an object. Additionally, the method may be used to analyze the surface topography and mechanical characteristics of a material.

3. Description of the Related Technology

Instrumented indentation is a valuable and effective method for characterizing the mechanical behavior of materials, especially that of single crystals and thin films. Scientists, such as Hertz, Oliver, Pharr, Field and Swain, have developed a variety of techniques for instrumented indentation but recognize that there are significant hurdles that have yet to be overcome.[1-3] One such obstacle is the accurate and reliable determination of the zero point, the location where the indenter tip makes first contact with the surface of a solid.[3-9] At this point, although the sample stiffness may appear positive, both the applied indentation load, P, and the total displacement or indentation depth, h_t,, are zero.

To date, methods of various sophistication have been proposed to qualitatively or quantitatively determine the location of the zero point.[10-17] One conventional method involves plotting the applied indentation load P versus the indentation depth h_t; the zero point is identified as the point where P first exceeds a selected threshold value. Another known method uses a video camera positioned perpendicular to the indentation axis to visually determine when the tip of a sensor has contacted the surface of a material, by analyzing the absence of light passing through a non-existent gap between the tip and surface. This method, however, has limited accuracy of approximately 5 μm (microns).[14,16] According to Oliver and Pharr,[3] it is also possible to determine the location of the zero point using an instrument capable of continuous stiffness measurement; the zero point is the point at which the stiffness, S, first exceeds 200 N/m. This method operates on the assumption that while the tip is hanging free, other factors such as vibration produce stiffness values below 200 N/m and that the small value of 200 N/m first appears when the tip makes contact with the surface. Although the method of Oliver and Pharr can be used to determine the zero point in certain instances, for various reasons it is prone to erroneous identification of the location of interest up to about 450 nm away from the actual zero point. In yet another method, Chudoba, Ullner and their colleagues suggest using regression analysis on a graph of P versus h_t.[10,11,17] The method of Chudoba involves using an iterative numerical function to fit the data of P versus h_t to a variation of the Hertzian model, replacing the conventional parameters of tip geometry, in the case of a spherical shaped tip, the radius, and effective modulus with an optimized proportionality constant, forcing the data to go through an origin of the graph.[11] Ullner's method uses a similar technique for analyzing the data of P versus h_t, but further suggests optimizing to a second order polynomial.[17] These methods are limited in that both load and displacement values are greatly impacted by the zero point, especially at very shallow depths. Although these methods may produce some successful results, because both P and h_t, are significantly affected by the zero point, they do not provide an objective determination of the zero point. Furthermore, especially at very shallow depths, other factors such as vibration and thermal drift can impact the determination of the zero point, and, in many cases, separating these factors using these conventional methods may not be possible.

Current methods for identifying the zero point of a nano-indented material are typically subjective, inaccurate and/or susceptible to factors that impact and interfere with the accuracy of the determination of the zero point. A method capable of objectively, robustly and accurately determining the location of the zero point has, to date, remained elusive. Therefore, there exists a need to develop a method that would enable an accurate and objective means for reliably and reproducibly determining from an existing data set the zero point for a material.

SUMMARY OF THE INVENTION

The present invention is directed to a method for objectively and accurately determining the zero point of a nano-indented material. The method comprises the steps of: obtaining continuous stiffness measurement oscillation data for a nano-indented material; plotting a stiffness of the material as a function of a contact parameter of the material for at least one identified data point; and applying a linear regression analysis to determine the degree to which the data point approximates a line that passes through the origin.

BRIEF DESCRIPTION OF THE DRAWINGS

Figure 1(a) is a graph of stiffness S versus contact parameter a for various δ values for a fused silica sample. Inset 1 is a graph of applied load P versus indentation depth h_t at a region near the point where S= 200 N/m. Inset 2 is a graph of S versus a for the full data set.

Figure 1(b) is a graph of indentation stress versus indentation strain for various δ values for the fused silica sample. The solid line is linear regression for a first loading region of the center curve; the dashed line is the expected slope as calculated from $4E_{eff}/3\pi$. The inset is a graph of the linear regression R-values and the standard error of the S versus a lines of Figure 1(a) forced through the origin of the graph, at various δ.

Figure 2(a) is a graph of indentation stress versus indentation strain for various δ values for an annealed iron sample. The inset is a graph of applied load P versus indentation depth h_t at a region near the point where S= 200 N/m.

Figure 2(b) is a graph of indentation stress versus indentation strain for various δ values for the annealed iron sample. The solid line is linear regression for first loading region of the center curve, the dashed line is the expected slope as calculated from $4E_{eff}/3\pi$. The inset is a graph of the linear regression R-values and the standard error of the S versus a lines of Figure 2(a) forced through the origin of the graph, at various δ.

Figure 3(a) is a graph of indentation stress versus indentation strain for various δ values for a sapphire sample. The inset is a graph of applied load *P* versus indentation depth h_t at a region near the point where S= 200 N/m.

Figure 3(b) is a graph of indentation stress versus indentation strain for various δ values for the sapphire sample. The solid line is linear regression for first loading region of the center curve, the dashed line is the expected slope as calculated from $4E_{eff}/3\pi$. The iset is a graph of the linear regression *R*-values and the standard error of the *S* versus *a* lines of Figure 3(a) forced through the origin of the graph, at various δ.

Figure 4 is a graph of the slope of *S* versus *a*, such as those curves shown in figures 1(a), 2(a), and 3(b), versus δ for samples of fused silica, iron and sapphire. The arrows indicate the proper corresponding y-axis for each data set.

DETAILED DESCRIPTION OF THE PREFERRED EMBODIMENTS

The present invention is directed to a novel method for determining the zero point of a nano-indented material, i.e. the point of first contact between an indenter tip and the surface of a material. According to the present invention, it is possible to determine the location of the zero point of any material, including solid materials such as metals or ceramics and semi-solid materials, using a simple and objective procedure that produces accurate results, which can be reproduced using a sensor capable of continuous stiffness measurement (CSM).

The method of the present invention utilizes a sensor that is equipped with a means for continuous stiffness measurement. Preferably, the sensor is a nanoindenter or an instrumented indenter with a CSM option, attachment or capability. The sensor comprises a tip, which can have any geometrical shape, a means for controlling and/or determining the displacement of the tip relative to any chosen datum and a means for controlling and/or measuring the force applied by the tip onto a solid or semi-solid material.

The sensor may be used for a variety of applications, including but not limited to producing load-displacement curves, marking samples for further inspection, calculating values from the data obtained and mapping data to indentation stress-strain curves.[18,19,20] In the present invention, the sensor may be used to produce indentation stress-strain curves from load displacement curves by detecting CSM oscillations. CSM is a technique which applies an oscillating force superimposed on the indenting motion of a sensor tip, with both load and displacement on scales considerably smaller than the primary indentation. Resolution of the sensor and the sensitivity of the method of the present invention which uses said sensor, are dependant upon many instrument factors including but not limited to vibration, thermal drift, testing factors such as loading rate and characteristics of the material being tested such as surface roughness. In a preferred embodiment, the sensor has a displacement resolution of about 1 nm or less and a force resolution of about 0.5 millinewtons (mN).

The method of the present invention generally comprises the steps of using a sensor to detect a load and displacement for the primary indentation and for oscillations from continuous stiffness measurements which are superimposed on the primary indentation; systematically shifting the data, creating a data set for each shift; plotting a graph of a stiffness of said material versus a contact parameter of the material for each data point in the data sets; using at least one linear regression means to determine the degree to which each data set approximates a straight lines that passes through the origin of the graph; and selecting a zero point from said data sets. Optionally, the last step may be carried out based on a data shift for which the linear regression most closely approximates a line that passes through the origin of said graph.

Using the data collected by the sensor, the method of the present invention involves generating a graph of material stiffness S as a function of a contact parameter a to determine the zero point of a nanoindented material. The graph of S as a function of a should produce a line that passes through the origin of the graph with a slope of twice the effective modulus for a properly zeroed sample. The graph of S versus a will be linear and pass through the origin of the graph, if and only if, the correct zero point is chosen. Even small errors regarding the location of the zero point will yield significant S versus a errors for small displacements.

The method of the present invention determines the location of the datum point at which first contact is made, δ, which is the difference in h_t between the true zero point X_z and the first point X_o. To find δ, points X_j are chosen near the measured zero point, where the load becomes positive. Preferably, points X_j are within about ± 100 nm of the zero point, more preferably within about ± 50 nm of the zero point, and most preferably within about ± 10 nm of the zero point in order to reduce the number of calculations necessary to determine the true zero point. Each of these points are treated as if they were X_z. At X_z, both P and h_t should be zero; to fulfill this requirement, δ_j must be defined by the value of $h_{t,j}$ and P_j and $h_{t,j}$ must be subtracted from all data points. Since S is actually measured from the CSM oscillations, and thus not affected by the zero point, its value remains unchanged for each point. Points with negative h_t are then discarded. The result is several data sets, each assuming that X_j, with its corresponding δ_j, is X_z, the zero point. A graph of S as a function of a is then plotted for these data sets, and linear regression is used to quantitatively determine the degree to which each set approximates a straight line forced through the origin, which is the ideal form. The slope of these lines is not forced, nor do any of the data sets interact. At least one measure may be used to analyze and quantify the curve fit. In a preferred embodiment, the fit of the curve is analyzed by determining the standard error, which is defined as the average vertical difference between each data point and the line of best fit, which for the purpose of determining the zero point is the line which passes through the origin of the graph of S versus a, and by determining correlation coefficient, R. The value of δ_j that minimizes the error or maximizes R is assumed to be δ.

According to this method, the zero point may be determined within a resolution of about 2 nm or less and more preferably within a resolution of about 1 nm or less. This is however, dependant upon the resolution of the instrument, as previously indicated. There is no theoretical limit to the resolution of this invention. Errors in determining the zero point of even a few nm can drastically alter further calculations and other uses of the data, such as producing stress-strain curves and S vs. a curves.

Using a similar method by mapping a graph of indentation stress as a function of indentation strain, identifying a set of relevant δ points, fitting a curve of indentation stress versus indentation strain for each δ point so that the curve is forced through the origin of the graph, and determining the accuracy of the fit, it is possible to determine the zero point. The linearity of the stress-strain curves, and the requirement that they pass through the origin of the graph of S as a function of a, can also be used to find the actual location of the zero point instead of, or in addition to, the method outlined herein.

The method of the present invention is unique in that it is a simple, objective, robust, accurate and reproducible method for determining the zero point of a nano-indented material from an existing data set using CSM. In contrast to the prior art, the method of the present invention is advantageous because it relies on actual stiffness measurements collected from the CSM data, which is not inherently sensitive to the zero point or significantly sensitive to vibrations or drift. Therefore, excipient factors that can skew zero point determination do not substantially interfere with the CSM data. Essentially, the method of the present invention uses non zero point sensitive CSM data to correct something without significant interference from other factors. .

The method of the present invention may be used to enhance the accuracy and execution of a variety of applications. Currently nearly all indentation models erroneously assume that the indentation is perfectly perpendicular to a flat surface of the solid. The orientation of an indentation relative to a surface of a solid, however, is dependent upon the angle of the solid surface. Therefore, an assumption that the indentation is perpendicular to the sample surface generally results in some degree of inaccuracy regarding the location of the zero point. Using our zero point and the absolute displacement of the indenter tip, we can, by using a minimum of three points, determine the pitch and roll (x and y angle) of a solid. This information may be used to correspondingly position the sample stage via some mechanical, hydraulic or other physical means, so that the solid is perpendicularly oriented with respect to the indenter tip.

Additionally, the present method may also be used with a nanoindenter as well as a surface profilometer, similar to Atomic Force Microscopy (AFM). The surface of the solid may be scanned with the nanoindenter and indented at multiple points along the surface of the solid. This application would enable one to obtain information regarding surface topography and mechanical properties of the solids.

The method of the present application may also be applicable for enhancing the accuracy of nanoindentation analysis and providing a better understanding of contact mechanics.

EXAMPLES

Example 1

A graph of S as a function of a may be used to determine the zero point of the nano-indented material using a sensor having a spherical shaped indenter tip. The following equations, which pertain to a spherical shaped indenter tip and are based upon the Hertzian model, disclose a means for calculating contact parameter a. Modified equations that represent other tip geometries are not enumerated but would be obvious to one of ordinary skill in the art.

The stress-strain curve for a nanoindented isotropic elastic material may be calculated from the contact parameter a, the stiffness of the isotropic elastic material S and the composite modulus E_{eff} of Equation 1,[3]

$$a = \frac{S}{2E_{eff}} \qquad \text{(Equation 1)}$$

where S is defined by Equation 2.

$$\frac{1}{S} = \frac{1}{S*} - \frac{1}{S_f} \qquad \text{(Equation 2)}$$

$S*$ is the stiffness value of the system, reported by the CSM, and S_f is the load-frame stiffness, given by the instrument manufacturer. The composite modulus, E_{eff}, is defined by Equation 3,

$$\frac{1}{E_{eff}} = \frac{1-\upsilon^2}{E} + \frac{1-\upsilon'^2}{E'} \qquad \text{(Equation 3)}$$

where E' and υ', respectively, refer to the Young's modulus and Poisson's ratio of an indenter, preferably a diamond indenter; E and υ are Young's modulus and Poisson's ratio of the nano-indented isotropic elastic material. According to Oliver and Pharr[3] and Field and Swain[1], the contact parameter a may also be determined by Equation 4,

$$a = \sqrt{2Rh_c - h_c^2} \qquad \text{(Equation 4)}$$

where R is the indenter parameter and the contact depth, h_c, is the distance from the circle of contact (i.e. the highest point on the tip where the sample actually touches the surface of the tip) to the maximum penetration depth (i.e. at the apex of the tip) is given by Equation 5,[1,3,18]

$$h_c = h_t - \frac{3}{4}\frac{P}{S} \qquad \text{(Equation 5)}$$

where P is the indentation load applied to the solid and h_t is the depth of the indentation in the surface of the solid, measured between an assumed datum parallel to the sample surface and the apex of the indenter tip. Finally, the indentation stress and strain, as defined by Equation 6, is derived from the Hertz equation[1,3,21,22] and the work of Sneddon[23]

$$\frac{P}{\pi a^2} = \frac{4}{3\pi} E_{eff}\left(\frac{a}{R}\right) \qquad \text{(Equation 6)}$$

The left side of Equation 6 is defined as the indentation stress, mean contact hardness or Meyer hardness.[18,22] The expression in parenthesis is the indentation strain.[18,22]

From these equations, a graph of S versus a may be used to determine the zero point of the nanoindented material. S may be obtained from the CSM data collected by the sensor, and Equations 4 and 5 may be used to calculate contact parameter a.

Example 2

The method of the present invention was found to be effective for determining the zero point of fused silica, sapphire single crystals and polycrystalline iron using indenters of various sizes having a resolution of 1 nm.

A Nano-indenter XP system (MTS, Oak Ridge, TN) with a CSM attachment was used to perform the method of the present invention. The nano-indenter sensor comprises a diamond spherical tip. In this experiment, two tips, with radii of 13.5 μm and 1 μm, were used. The Young's modulus and Poisson's ratio of the diamond indenters were 1140 GPa and 0.07, respectively.

The three sample materials that were in the experiment include: fused silica (GM Associates Inc., Oakland, CA); C-orientation sapphire single crystal (Kyocera Industrial Ceramics, Vancouver, WA); and iron (99.65%, SurePure Chemetals, Florham Park, NJ). The Vickers microhardness value was measured on the same surface used for the nanoindentation with an M-400 Hardness Tester, (LECO Corp., St. Joseph, MI).

All the tests were carried out with a load rate over load factor of $(dP/dt)/P = 0.1$ and an allowable drift rate of 0.05 nm/s. The load frame stiffness, S_f was provided by the manufacturer, and has a value of ~5.5 MN/m. Maximum load was 690 mN for the fused silica sample and 50 mN for the iron and sapphire samples. The harmonic displacement for the CSM was 2 nm with a frequency of 45 Hz.

Figure 1(a) shows an analysis of S versus a using the method of the present invention for three datum points δ, over a span of 10 nm, for a fused silica sample using a 13.5 μm indenter. Linear regression of the three datum points δ is represented by dashed lines. Figure 1(a) shows that datum point δ=47.2 nm has a fitted line that passes through the origin of the graph and is therefore the true zero point for the fused silica sample. Inset 2 of Figure 1(a) shows the entire data set, wherein it is apparent that after ≈ 2500 nm, the value of δ is no longer of consequence.

Figure 1(b) shows a graph of indentation stress versus strain, as defined by Equation 6, of the fused silica sample, where the center curve is the true zero point and the solid line represents the linear regression for a first loading region of the center curve. The early data spike is reduced in both magnitude and prevalence as δ increases because: 1) some of the data points occur in the air before the indenter reaches the zero point, identified by having a negative h_t after the δ correction, and are thus discarded and 2) the magnitude of a, and thus that of the indentation stress, becomes more accurate as δ approaches the zero point. The dashed line represents the expected slope, calculated from $4E_{eff}/3\pi$, and the Inset of Figure 1(b) is a graph of the linear regression R-values and the standard error of the data that is forced through the origin of the graph, at various δ values.

As shown by Inset 1 of Figure 1(a), the conventional method of graphing P versus h_t at a region near the point where S= 200 N/m, which according to the prior art supposedly corresponds to the zero point, does not clearly indicate the zero point, which is represented by the dashed line. Notably, the datum point δ= 47.2 nm is counterintuitive when compared to Inset 1 of Figure 1(a), which suggests that P begins to increase around a δ of 10 nm.

Figures 2 and 3 similarly show a zero point analysis for samples of iron and sapphire. Figure 2(a) is a graph of S versus a using the method of the present invention for three datum points δ, over a span of 10 nm, for a sample of iron sample using a 13.5 μm indenter. The zero point occurs at δ=7.5 nm, which is also represented by the dashed line in the Inset of Figure 2(a). Figure 2(b) shows a graph of indentation stress versus strain for various datum points δ of the iron sample, where the center curve is the true zero point. The solid line represents a linear regression for first loading region of the center curve, and the dashed line is the expected slope as calculated from $4E_{eff}/3\pi$. The Vickers hardness value, shown by the dashed horizontal line in Figure 2(b), is within a reasonable range of the value expected from our stress versus strain curve, where the curve becomes horizontal. The Inset of Figure 2(b) shows a graph of the linear regression R-values and the standard error from the data forced through zero, at various δ.

Similarly, Figure 3(a) shows a graph of S versus a using the method of the present invention for three datum points δ, over a span of 10 nm, for a sample of iron sample using a 1 μm indenter. The zero point occurs at δ=40.4 nm, which is also represented by the dashed line in the Inset of Figure 3(a). In Figure 3(b), the center curve of the stress versus strain graph represents the true zero point. The solid line represents a linear regression for first loading region of the center curve, and the dashed line is the expected slope as calculated from $4E_{eff}/3\pi$. The Inset of Figure 3(b) shows a graph of the linear regression R-values and the standard error from the data forced through zero, at various δ. The importance and sensitivity of correctly identifying the zero point is highlighted in the stress versus strain curves. For example, in Figure 3(b), a difference of only approximately 2 to 3 nm results in significant variations in the indentation stress/strain curves, which previously were left unexplained.

Figure 4 is a graph of the slopes of the S versus a curves i.e. E_{eff}, for all three samples as a function of δ. The true zero point of each material is circled and the dashed lines represent the linear regression for each data set. Because it is evident that E_{eff} is functionally related to δ, this suggests that an incorrect determination of the zero-point can produce an incorrect determination of the effective moduli. For example, for both iron and sapphire, an error of only $\approx$ 2 nm in the choice of the zero point results in a $\approx$ 7 % error in S, and consequently, E_{eff}.

According to Equation 6, the slope of the indentation stress versus strain should equal $4E_{eff}/3\pi$. The inclined dashed lines shown in Figs. 1(b), 2(b) and 3(b) represent the

$4E_{eff}/3\pi$ line; the solid inclined lines, on the other hand, represents the least squares fit of the data points shown in the linear regime and forced through zero. The closer the correspondence between the inclined dashed lines and the solid inclined lines, the greater the accuracy the of the zero point determination

For silica and sapphire, there is a substantial correlation between the dashed lines and the solid lines, supporting the accuracy of the zero point determination for these materials. This is especially true considering that Equation 6 was derived assuming a perfect sphere indenting a perfectly perpendicular, atomically smooth, elastically isotropic surface. The latter is probably only true here for fused silica. The correspondence would have been greater were the results for larger increments of δ also graphed, as done in Figure 2(b). These factors have also been found to be highly correlated for ZnO,[18,19] Al[18], GaN[20] and more recently, $LiNbO_3$.[24]

Notably, the dashed line for iron is approximately 3 times steeper than its solid line. It has been determined that this difference is not a result of an error in the method of the present application, but rather reflects a physical phenomena most probably related to the elastic anisotropy of iron, which is consistent with previous results.[18]

The present invention may also be implemented in the form of a computer program or by a computer programmed to carry out all or portions of the method of the present invention.

References

The References cited herein are listed below and the disclosures of the listed references are hereby incorporated by reference in their entirety:

1. J. S. Field and M. V. Swain: Determining The Mechanical-Properties Of Small Volumes Of Material From Submicrometer Spherical Indentations. Journal Of Materials Research **10,** 101-112 (1995).
2. J. S. Field and M. V. Swain: The Indentation Characterisation Of The Mechanical Properties Of Various Carbon Materials: Glassy Carbon, Coke And Pyrolytic Graphite. Carbon **34,** 1357 (1996).
3. W. C. Oliver and G. M. Pharr: Measurement of hardness and elastic modulus by instrumented indentation: Advances in understanding and refinements to methodology. Journal of Materials Research **19,** 3-20 (2004).
4. J. L. Bucaille, E. Felder, and G. Hochstetter: Identification of the viscoplastic behavior of a polycarbonate based on experiments and numerical modeling of the nano-indentation test. Journal of Materials Science **37** (2002).
5. P. Grau, G. Berg, W. Fraenzel, and H. Meinhard: Recording hardness testing problems of measurement at small indentation depths PHYS STATUS SOLIDI A **146,** 537-548 (1994).
6. N. Huber and E. Tyulyukovskiy: A new loading history for identification of viscoplastic properties by spherical indentation. Journal of Materials Research **19,** 101-113 (2004).
7. Z. Li, K. Herrmann, and F. Pohlenz: A comparative approach for calibration of the depth measuring system in a nanoindentation instrument. Measurement **39,** 547-552 (2006).
8. B. Rother, A. Steiner, D. A. Dietrich, H. A. Jehn, J. Haupt, and W. Gissler: Depth-sensing indentation measurements with Vickers and Berkovich indenters. Journal of Materials Research **13** (1998).
9. E. Tyulyukovskiy and N. Huber: Neural networks for tip correction of spherical indentation curves from bulk metals and thin metal films. Journal of the Mechanics and Physics of Solids **55,** 391-418 (2007).

10. T. Chudoba, M. Griepentrog, A. Dück, D. Schneider, and F. Richter: Young's modulus measurements on ultra-thin coatings. Journal of Materials Research **19,** 301-314 (2004).

11. T. Chudoba, N. Schwarzer, and F. Richter: Determination of elastic properties of thin films by indentation measurements with a spherical indenter. Surface and Coatings Technology **127,** 9-17 (2000).

12. A. C. Fischer-Cripps: Critical review of analysis and interpretation of nanoindentation test data. Surface and Coatings Technology **200,** 4153-4165 (2006).

13. Y.-H. Liang, Y. Arai, K. Ozasa, M. Ohashi, and E. Tsuchida: Simultaneous measurement of nanoprobe indentation force and photoluminescence of InGaAs/GaAs quantum dots and its simulation. Physica E: Low-dimensional Systems and Nanostructures **36,** 1-11 (2007).

14. Y. Y. Lim and M. Munawar Chaudhri: Indentation of elastic solids with a rigid Vickers pyramidal indenter. Mechanics of Materials **38,** 1213-1228 (2006).

15. V. Linss, N. Schwarzer, T. Chudoba, M. Karniychuk, and F. Richter: Mechanical properties of a graded B-C-N sputtered coating with varying Young's modulus: deposition, theoretical modelling and nanoindentation. Surface and Coatings Technology **195,** 287-297 (2005).

16. F. Richter, M. Herrmann, F. Molnar, T. Chudoba, N. Schwarzer, M. Keunecke, K. Bewilogua, X. W. Zhang, H. G. Boyen, and P. Ziemann: Substrate influence in Young's modulus determination of thin films by indentation methods: Cubic boron nitride as an example. Surface and Coatings Technology **201,** 3577-3587 (2006).

17. C. Ullner: Requirement of a robust method for the precise determination of the contact point in the depth sensing hardness test. Measurement **27,** 43-51 (2000).

18. S. Basu, A. Moseson, and M. W. Barsoum: On the determination of spherical nanoindentation stress-strain curves. Journal of Materials Research **21,** 2628-2637 (2006).

19. S. Basu and M. W. Barsoum: Deformation Micromechanisms of ZnO Single Crystals as Determined From Spherical Nanoindentation Stress-Strain Curves. J. Mater. Res. **Accepted for publication** (2007).
20. S. Basu, M. W. Barsoum, A. D. Williams, and T. D. Moustakas: Spherical nanoindentation and deformation mechanisms in free-standing GaN films. J. App. Phys. **In Print** (2007).
21. J. S. Field and M. V. Swain: A Simple Predictive Model For Spherical Indentation. Journal Of Materials Research **8,** 297-306 (1993).
22. D. Tabor. *Hardness of Metals* (Clarendon, Oxford, U.K., 1951),
23. I. N. Sneddon: The relaxation between load and penetration in the axisymmetric boussinesq problem for a punch of arbitrary profile. Int. J. Engineering Science, **3,** 47 (1965).
24. S. Basu, A. Zhou, and M. W. Barsoum: Micromechanics of Deformation Under a Spherical Indenter and Indirect Observation of Reversible Dislocation Motion in a LiNbO3 Single Crystal. Physics Review Letters **Submitted For Publication** (2007).

CLAIMS

1. A method for determining the zero point of a nano-indented material comprising the steps of:
    a) obtaining continuous stiffness measurement oscillation data for a nano-indented material;
    b) selecting at least one data point;
    c) plotting a stiffness of said material as a function of a contact parameter of said material for said data point to form a plot;
    d) applying a linear regression analysis to plot to determine the degree to which said data point approximates a line that passes through an origin of said plot; and
    e) selecting a zero point from said data point, for which said linear regression most closely approximates a line that passes through the origin of said plot.

2. The method of claim 1, wherein said method may be used to determine the zero point of a material selected from the group consisting of: a solid material and a semi-solid material.

3. The method of claim 1, wherein step e further comprises the step of analyzing a fit of said linear regression.

4. The method of claim 3, wherein said step of analyzing a fit employs a measure selected from a standard error, a correlation coefficient and a combination thereof.

5. The method of claim 4, wherein the selected zero point is a data point that minimizes the standard error and/or maximizes said correlation coefficient.

6. The method of claim 1, wherein said selected zero point is accurate within a resolution of about 2 nm or less.

7. The method of claim 1, wherein said selected zero point is accurate within a resolution of about 1 nm or less.

8. The method of claim 1, further comprising the step of using said zero point to position said material relative to a nano-indenter.

9. A method for determining the zero point of a nano-indented material comprising the steps of:

   a. obtaining continuous stiffness measurement oscillation data for a nanoindented material;
   b. selecting at least one data point;
   c. plotting a first graph of a stiffness of said material as a function of a contact parameter of said material for said data point;
   d. plotting a second graph of indentation stress of said material as a function of indentation strain of said material;
   e. applying a linear regression analysis to said first and second graphs to determine the degree to which said data point approximates a line that passes through an origin of said first and second graphs; and
   f. selecting a zero point from said data point, for which said linear regression most closely approximates a line that passes through the origin of said first and second graphs.

10. The method of claim 9, wherein step (e) further comprises the step of analyzing a fit of said linear regression.

11. The method of claim 10, wherein the step of analyzing a fit of said linear regression uses a measure selected from a standard error, a correlation coefficient and a combination thereof.

12. The method of claim 11, wherein the selected zero point is a data point that minimizes a standard error, maximizes said correlation coefficient or both.

13. The method of claim 9, wherein said selected zero point is accurate within a resolution of about 2 nm or less.

14. The method of claim 9, wherein said selected zero point is accurate within a resolution of about 1 nm or less.

15. A method for determining the zero point of a nano-indented material comprising the steps of:

a. obtaining continuous stiffness measurement oscillation data for a nano-indented material;

b. selecting at least one data point;

c. plotting a first graph of indentation stress of said material as a function of indentation strain of said material;

d. applying a linear regression analysis to said graph to determine the degree to which said data point approximates a line that passes through an origin of said graph; and

e. selecting a zero point from said data point, for which said linear regression most closely approximates a line that passes through the origin of said graph.

16. The method of claim 15, wherein step (e) further comprises the step of analyzing a fit of said linear regression.

17. The method of claim 16, wherein said step of analyzing a fit employs a measure selected from a standard error, a correlation coefficient and a combination thereof.

18. The method of claim 17, wherein the selected zero point is a data point that minimizes a standard error, maximizes said correlation coefficient or both.

19. The method of claim 15, wherein said selected zero point is accurate within a resolution of about 2 nm or less.

20. The method of claim 15, wherein said selected zero point is accurate within a resolution of about 1 nm or less.

ABSTRACT OF THE DISCLOSURE

The present invention relates to a method for the simple, objective and accurate determination the zero point of a material, the point of first contact between an indenter tip and the surface of a material. The zero point is determined by using a sensor having a tip and capable of continuous stiffness measurement. By applying a data shift, which insures that the stiffness versus contact parameter curve is linear and goes through the origin of the graph, it is possible to determine the zero point based on combined data from indentation and from superimposed continuous stiffness measurement oscillations.

fig. 1a

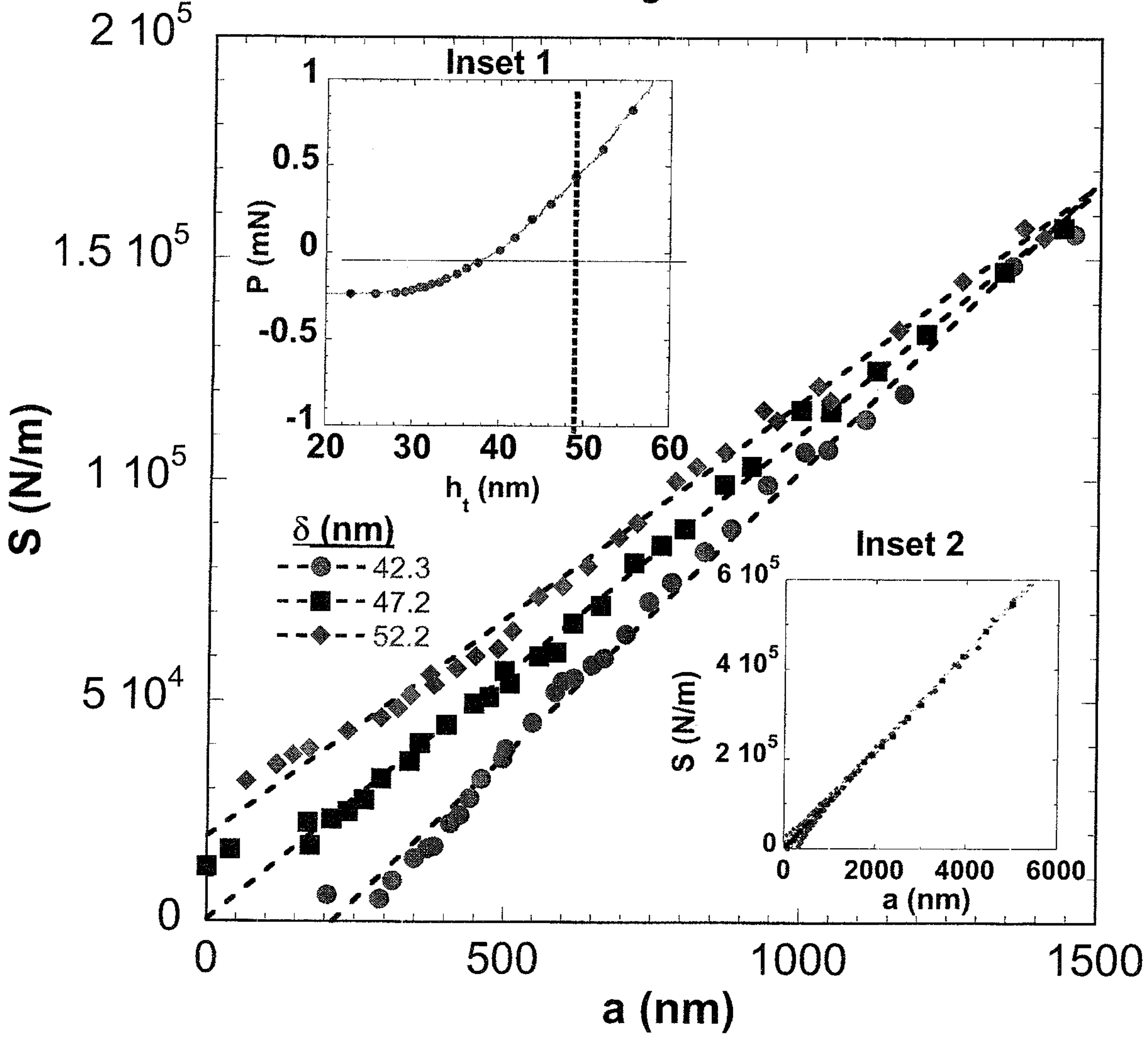
Inset 1
1
0.5
0
-0.5
-1
20
30
40
50
60
P (mN)
h_t (nm)
δ (nm)
42.3
47.2
52.2
Inset 2
6 10^5
4 10^5
2 10^5
0
0
2000
4000
6000
S (N/m)
a (nm)
2 10^5
1.5 10^5
1 10^5
5 10^4
0
0
500
1000
1500
S (N/m)
a (nm)

Fig 1b

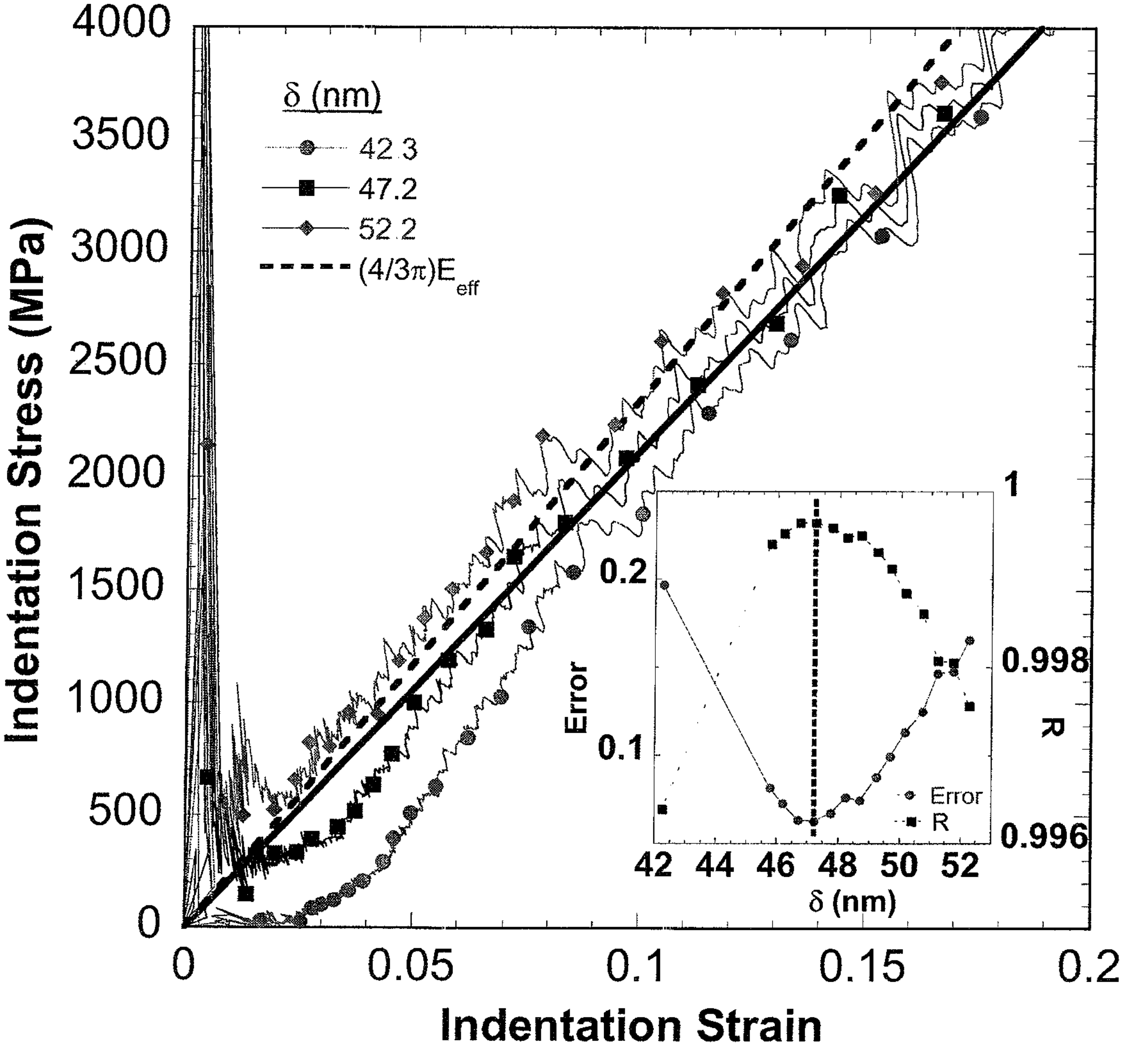
δ (nm)
42.3
47.2
52.2
(4/3π)E_eff
Indentation Stress (MPa)
0
500
1000
1500
2000
2500
3000
3500
4000
Indentation Strain
0
0.05
0.1
0.15
0.2
Error
0.1
0.2
R
1
0.998
0.996
Error
R
42
44
46
48
50
52
δ (nm)

Fig 2a

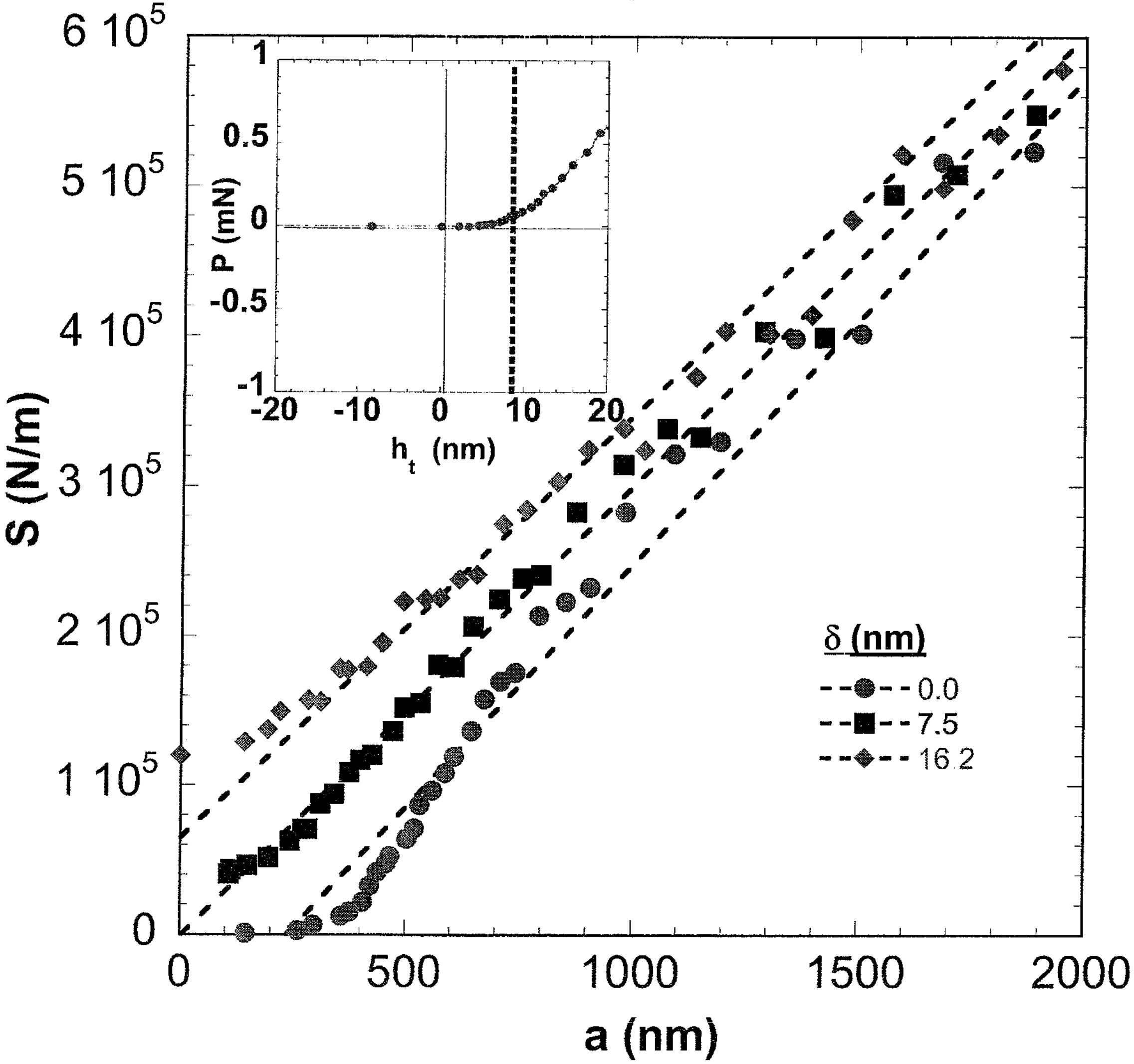
6 10^5
5 10^5
4 10^5
3 10^5
2 10^5
1 10^5
0
S (N/m)
0
500
1000
1500
2000
a (nm)
1
0.5
0
-0.5
-1
P (mN)
-20
-10
0
10
20
h_t (nm)
δ (nm)
0.0
7.5
16.2

Fig. 2b

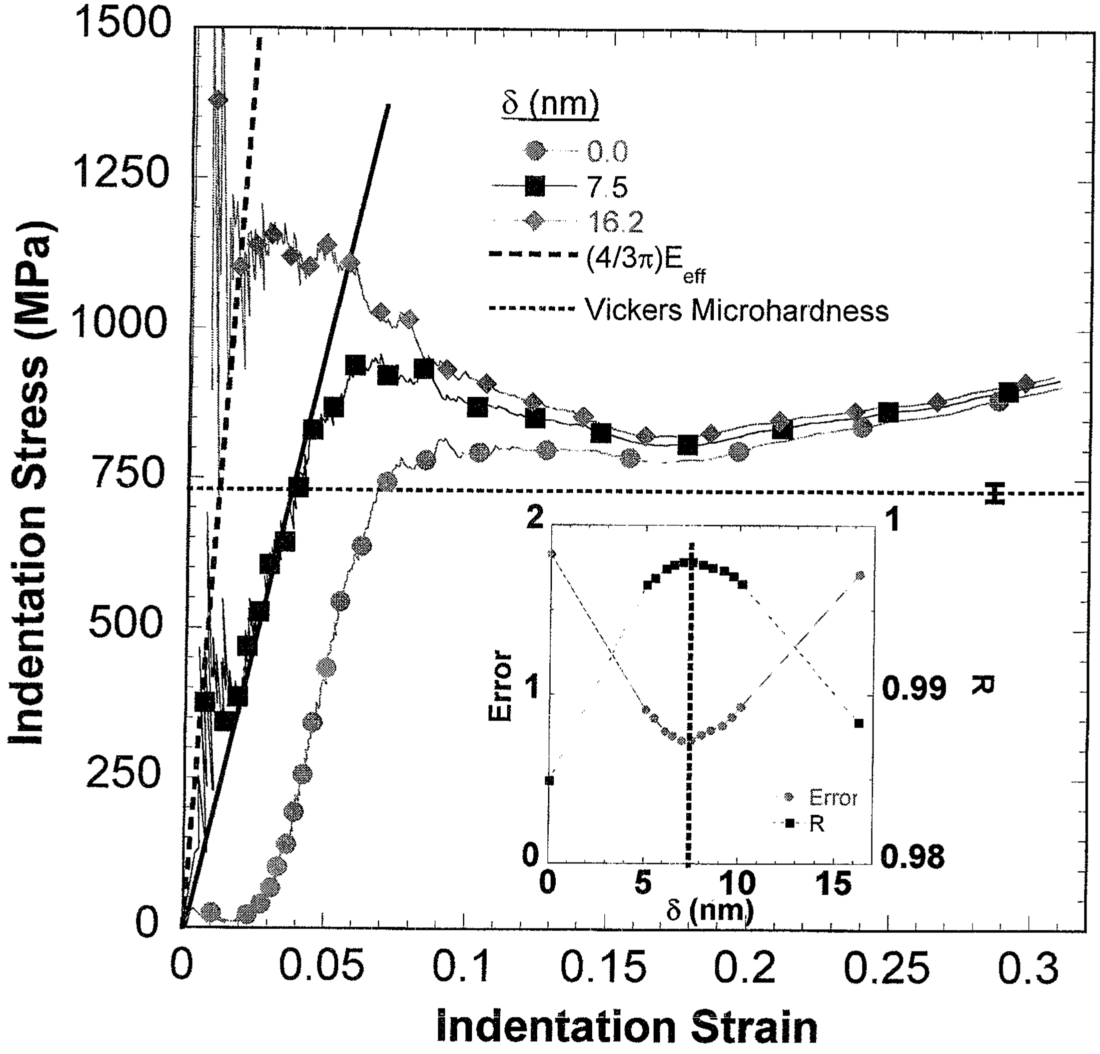

1500
1250
1000
750
500
250
0
Indentation Stress (MPa)
0
0.05
0.1
0.15
0.2
0.25
0.3
Indentation Strain
δ (nm)
0.0
7.5
16.2
(4/3π)E$_{eff}$
Vickers Microhardness
2
1
0
Error
1
0.99
0.98
R
0
5
10
15
δ (nm)
Error
R

Fig 3a

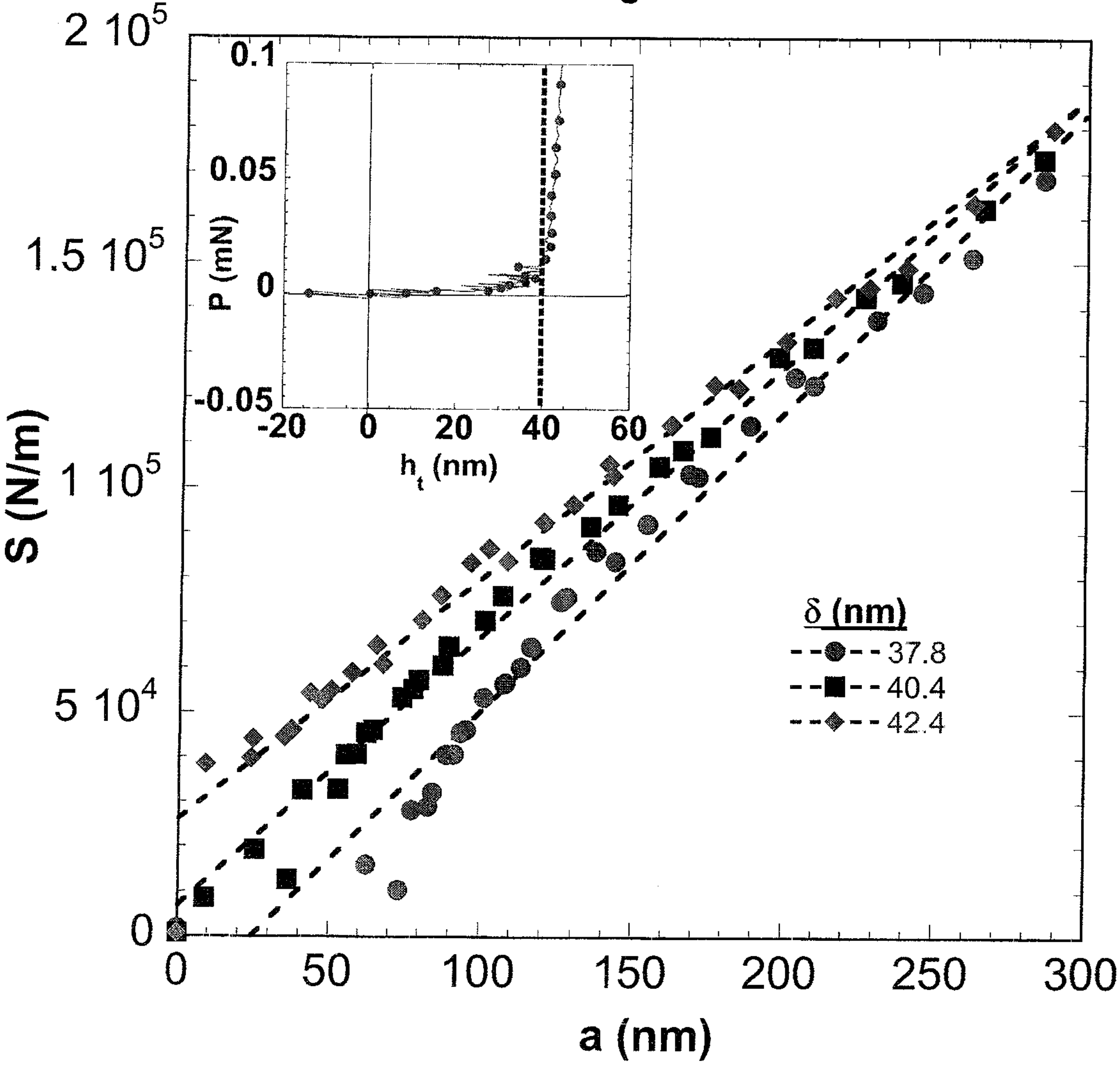
2 10^5
1.5 10^5
1 10^5
5 10^4
0
S (N/m)
0
50
100
150
200
250
300
a (nm)
δ (nm)
37.8
40.4
42.4
0.1
0.05
0
-0.05
P (mN)
-20
0
20
40
60
h_t (nm)

Fig 3b

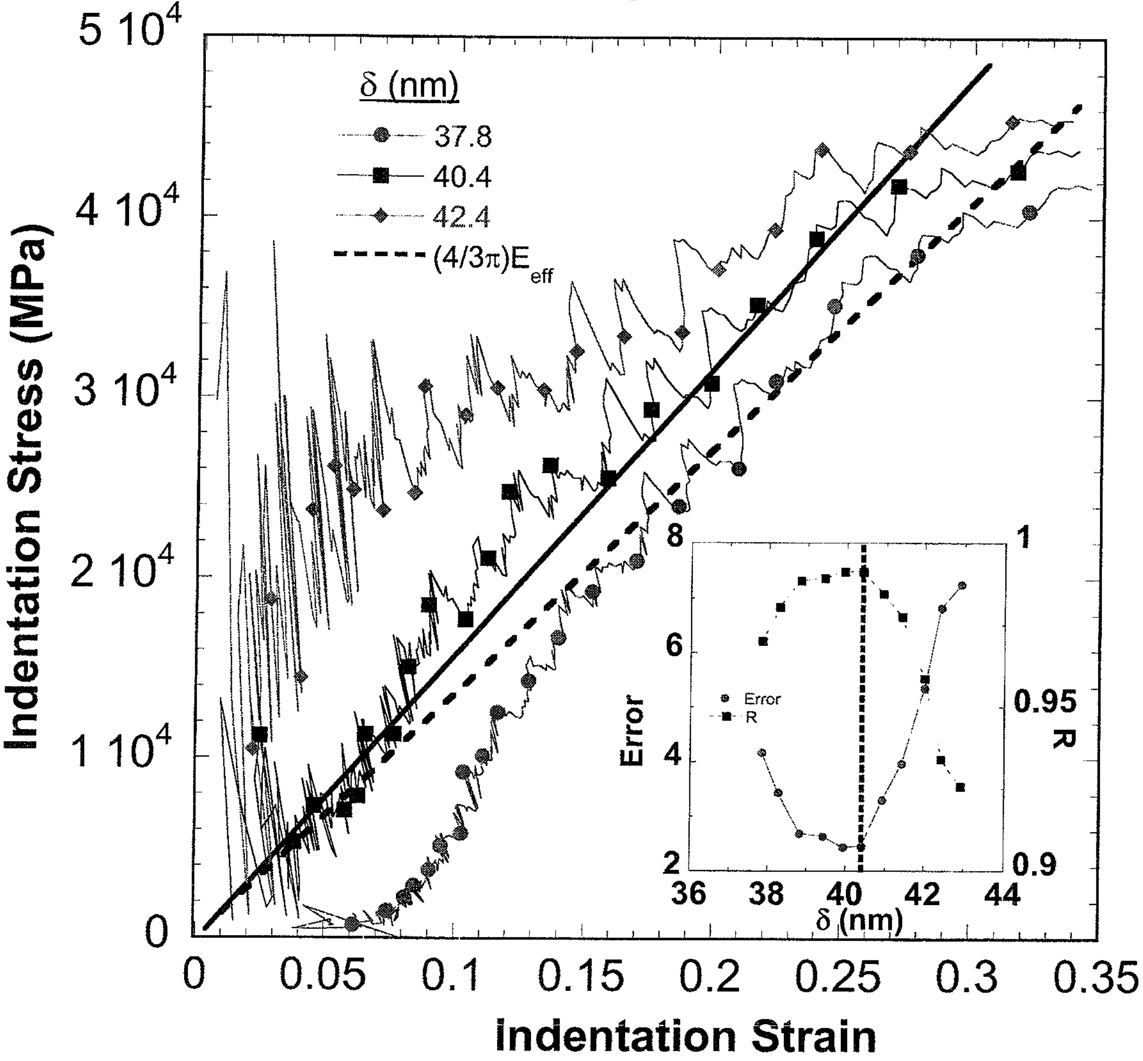
δ (nm)
37.8
40.4
42.4
(4/3π)E_{eff}
Indentation Stress (MPa)
Indentation Strain
5 10^4
4 10^4
3 10^4
2 10^4
1 10^4
0
0.05
0.1
0.15
0.2
0.25
0.3
0.35
Error
R
δ (nm)
36
38
40
42
44
2
4
6
8
0.9
0.95
1

Fig 4

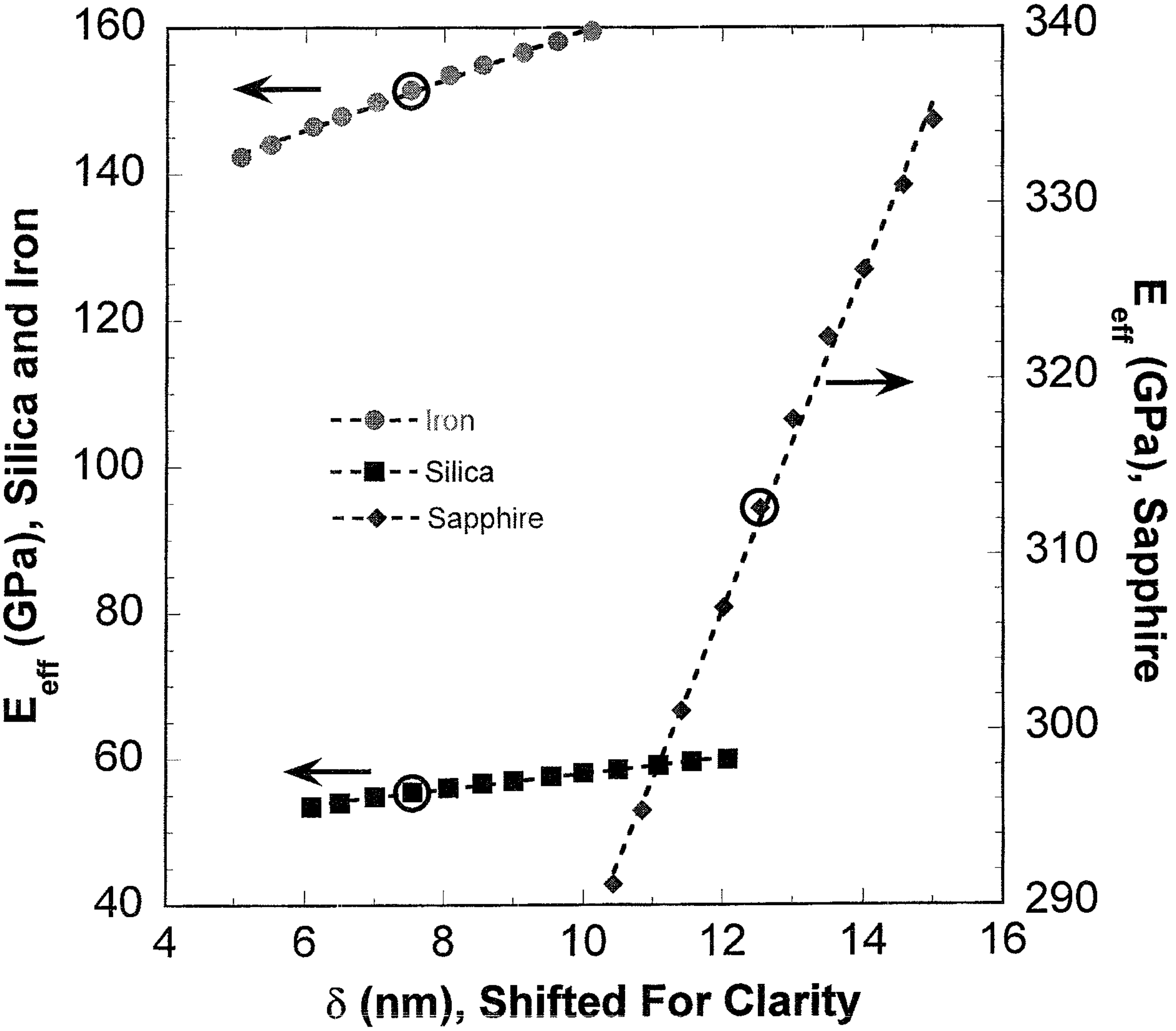
160
140
120
100
80
60
40
340
330
320
310
300
290
4
6
8
10
12
14
16
E_{eff} (GPa), Silica and Iron
E_{eff} (GPa), Sapphire
δ (nm), Shifted For Clarity
Iron
Silica
Sapphire

APPENDIX 2: Detailed Example Of Zero Point Determination Method

This detailed example shows the steps required to implement the effective zero point determination method on Iron$_B$, for the data which appears in Figure 15.

Step 1: Export Raw Data From Instrument File

In our case, the raw data was recorded and analyzed with MTS TestWorks software, version 4.X. It has the feature to export data to Microsoft Excel spreadsheet, which we utilized. We made sure to select the option wherein all data is exported, not just that after the supposed zero point. The raw data for each test location is formatted as below, with rows of ellipses added for this example, to denote a break in the data shown. The "our variable" row has also been added, to aid the reader.

Table 4: Detailed Example - Raw Data

Segment	**Displacement Into Surface**	**Load On Sample**	**Time On Sample**	**Harmonic Contact Stiffness**	**Hardness**	**Modulus**
[Units]	**nm**	**mN**	**s**	**N/m**	**GPa**	**GPa**
[Our Variable]	h_t	P	**---**	S	**---**	**---**
Load Segment Type	-1973.29	-0.02	-212	-225.26	1.8E+308	0
	-1969.64	-0.02014	-211.8	-246.735	1.8E+308	0
	-1967.02	-0.02018	-211.6	-250.99	1.8E+308	0
	-1966	-0.0201	-211.4	-245.4	1.8E+308	0
...	**...**	**...**	**...**	**...**	**...**	**...**
	-1.98364	-0.00032	-0.6	-106.044	1.8E+308	0
	-2.11187	-0.00016	-0.4	-27.3263	1.8E+308	0
	-0.71953	-0.0001	-0.2	58.78342	1.8E+308	0
[X_O]	0	0	0	140.5432	1.8E+308	0
	0.273374	0.000141	0.2	214.2866	1.8E+308	1.2E-158
	0.751746	0.000259	0.4	295.5066	-0.0071	0
	1.2351	0.000382	0.6	412.7958	-0.00545	0
...	**...**	**...**	**...**	**...**	**...**	**...**
	7.448581	0.037264	14.4	32785.48	0.665147	120.5121
	7.461452	0.038363	14.6	34521.27	0.671084	126.2353
	7.489434	0.039619	14.8	37166.23	0.667033	134.2449
[X_j, later X_z]	7.517422	0.040796	15	39448.63	0.66586	141.1131
	7.657895	0.042043	15.2	41880.97	0.6257	143.3232

Segment	Displacement Into Surface	Load On Sample	Time On Sample	Harmonic Contact Stiffness	Hardness	Modulus
	7.783184	0.043291	15.4	42486.57	0.606638	140.7833
	7.752723	0.044473	15.6	43293.42	0.635162	145.391
...	...	...	...	...	...	...
	675.3556	49.58791	82	1225656	1.317608	183.1825
	680.244	50.01821	82.08	1226328	1.318819	182.4708
Hold Segment Type	682.5907	50.23539	82.12	1227530	1.319635	182.2829

The “segment” column includes markers denoting the type of segment which the machine is using. The only two important ones for this work are “Load Segment Type” (begin loading) and “Hold Segment Type” (Hold at the top of the load, even if the time for holding is zero seconds.) Markings in brackets are mine. The other columns are self-explanatory, but the last two (hardness and modulus) are additional CSM data channels, not used in this work. Because they are not used in this method, the Time, Hardness, and Modulus columns are not show in later data tables.

Step 2: Find Point Where P Definitely Increases

Our method involves testing and comparing a number of cases. In order to reduce the quantity of those cases, we look for the point on a plot of the P vs. h_t data to determine where P definitely begins to increase steadily. Such a plot is shown below, in our case within the TestWorks software.

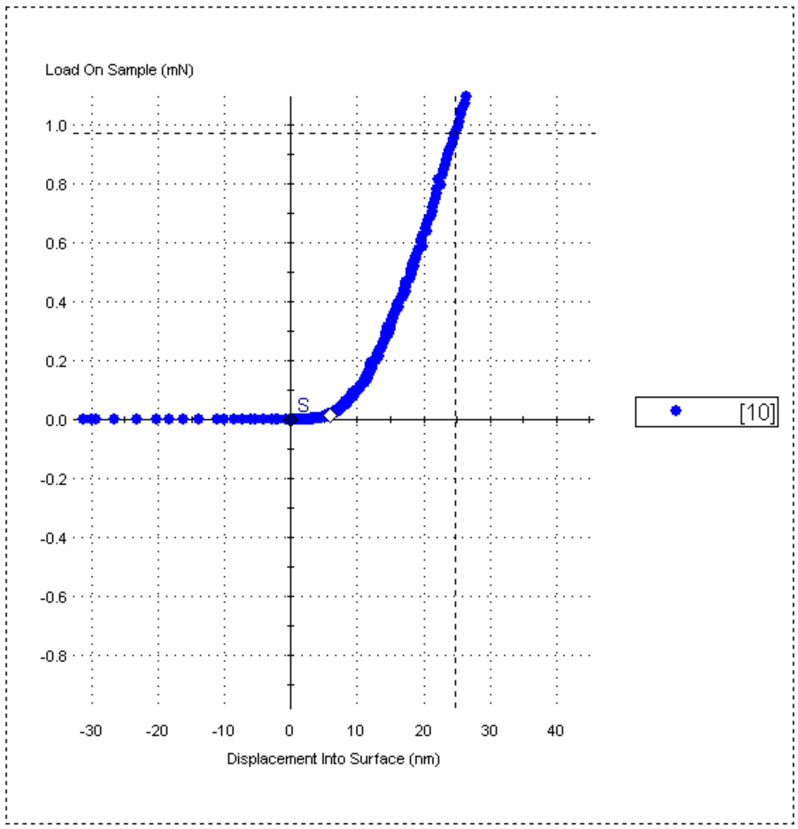

Figure 28: P vs. h_t for raw data

This case is relatively straightforward – the zero point is most likely somewhere in the range 0 nm < h_t < 10 nm. Sometimes this can be deceiving though, as was the case for Silica (Figure 14), where the effective zero point was actually ~ 20 nm away from where P began to increase steadily. This is a demonstration of the fact that choosing a certain range to investigate first is merely a way to reduce the number of cases investigated, and the time and effort involved. The result is by no means subjective though, as we would get the same result by investigating 0 nm < h_t < 10 nm as we would for -1000 nm < h_t < 1000 nm. A smaller range is chosen merely for practical purposes. The range can, and often must, be modified, as described in steps 3 and 4 below.

NOTE: Many of the steps below are repeated in a looping structure. A summary of the steps and how they fit into the looping structure is provided at the end of this appendix.

Step 3: Choose a Zero Point, Subtract $h_{t,j}$ and P_j

We nw choose a zero point X_j to evaluate as if it were the correct zero point X_z. For this example, let us choose the point where ht is 7.517…. We then capture the $h_{t,j}$ and P_j at that point, so in this case $h_{t,j}$ = 7.517422 nm and P_j = 0.040796 mN. We subtract these values (even if they are negative), from the entire h_t and P columns, forcing our X_j point to have zero for both h_t and P. The data after this shift is shown in Table 5: Detailed Example - Data After X_j Shift.

Table 5: Detailed Example - Data After X_j Shift

Segment	**Displacement Into Surface**	**Load On Sample**	**Harmonic Contact Stiffness**
[Units]	**nm**	**mN**	**N/m**
[Our Variable]	h_t	P	S
Load Segment Type	-1980.81	-0.06079	-225.26
	-1977.15	-0.06094	-246.735
	-1974.53	-0.06098	-250.99
	-1973.52	-0.0609	-245.4
...	**...**	**...**	**...**
	-9.50106	-0.04112	-106.044
	-9.62929	-0.04095	-27.3263
	-8.23695	-0.0409	58.78342
[X_O]	-7.51742	-0.0408	140.5432
	-7.24405	-0.04066	214.2866
	-6.76568	-0.04054	295.5066
	-6.28232	-0.04041	412.7958
...	**...**	**...**	**...**
	-0.06884	-0.00353	32785.48
	-0.05597	-0.00243	34521.27
	-0.02799	-0.00118	37166.23
[X_j, later X_z]	0	0	39448.63
	0.140474	0.001247	41880.97
	0.265762	0.002495	42486.57
	0.235302	0.003676	43293.42
...	**...**	**...**	**...**
	667.8382	49.54711	1225656
	672.7265	49.97742	1226328
Hold Segment Type	675.0733	50.19459	1227530

Note that the Stiffness, S, remains unchanged. For example, at X_j, S remains 39448.63 N/m before and after correction.

Step 4: Delete Negative Rows And Calculate Values

We see from Table 5 that there are a number of rows for which ht is less than zero. These are of no interest, being that the tip was not on the surface wherever ht < 0. We thus delete all rows for which that is the case.

Next, we now calculate the values h_c, a, indentation stress, and indentation strain, for each remaining row of data. These are calculated according to Eqs. 11, 13, 4, and 4, respectively. There are constants needed for the calculations, most importantly being the tip radius, which in our case is 13500 nm. The data now appears as follows:

Table 6: Detailed Example - Data With Calculations

Segment	**Displacement Into Surface**	**Load On Sample**	**Harmonic Contact Stiffness**	**Contact Depth**	**Contact Radius**	**Indentation Stress**	**Indentation Strain**
[Units]	**nm**	**mN**	**N/m**	**nm**	**nm**	**MPa**	**Unitless**
[Our Variable]	h_t	P	S	h_c	a	σ	ε
[X_j, later X_z]	0	0	39448.63	0.00	0.00	---	0.00
	0.140474	0.001247	41880.97	0.12	56.48	124.41	0.00
	0.265762	0.002495	42486.57	0.22	77.37	132.65	0.01
	0.235302	0.003676	43293.42	0.17	68.07	252.56	0.01
...	**...**	**...**	**...**	**...**	**...**	**...**	**...**
	667.8382	49.54711	1225656	637.52	4099.58	938.40	0.30
	672.7265	49.97742	1226328	642.16	4114.12	939.87	0.30
Hold Segment Type	675.0733	50.19459	1227530	644.41	4121.13	940.75	0.31

Step 5: Plot S vs. a And Perform Linear Regression

With the data prepared, we now plot S vs. a. Then we use a least-squares linear regression to determine how well the data fits *a straight line forced through the origin.* Such a plot is shown below, as well as the results of the regression.

Figure 29: Detailed Example - S vs. a

The dashed line is the linear regression.

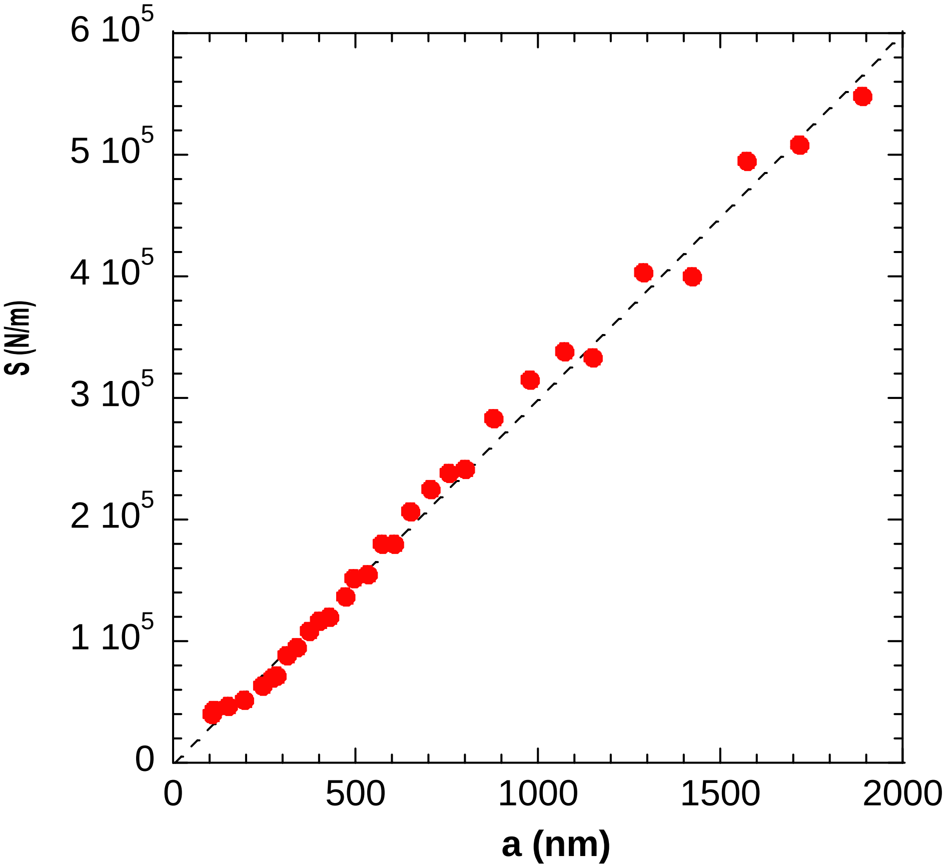

Table 7: Detailed Example - Regression Results - One Case

Delta	E_{eff}	R^2	Standard Error
7.51742	150	0.998031	0.72791

Step 6: Repeat Steps 3, 4, and 5 for Each X_j

Repeat Steps 3, 4, and 5 for each Xj, for the range chosen in Step 2. A certain step between chosen points should be employed. (i.e. every 0.5 nm or every 2 nm) to aid in finding the correct δ. For this step, we sorted the data for the *loading portion* of the curve only , ascending in h_t. Then we chose starting and ending limits for δ, and a step size. Our method allowed us to gain meaningful differentiation between cases down to a step size of 0.5 nm, below which the data usually did not have enough density. The actual points were chosen as the first point which meets or exceeds the δ sought. For example, if we sought 7.5, the first point to satisfy that in this case was 7.51742.

Step 7: Compare S vs. a curves

Now with a range of X_j data sets to consider, we compare the results for their S vs. a curves. This is best done looking at tabular results, but plots can be an aid to the eye, and can be an opportunity to catch any abnormalities. Figure 30 shows a composite S vs. a plot for a number of δ, zoomed in to the early region, where differences are most apparent. The inset shows the full range of the plot, where it can be seen that after some point (in this case a ~ 1500 nm) the difference in δ on longer plays a large role. Table 8 shows the regression results in tabular format, and Figure 31 presents them graphically. Every other case is shown, though we investigated in steps of 0.5 nm.

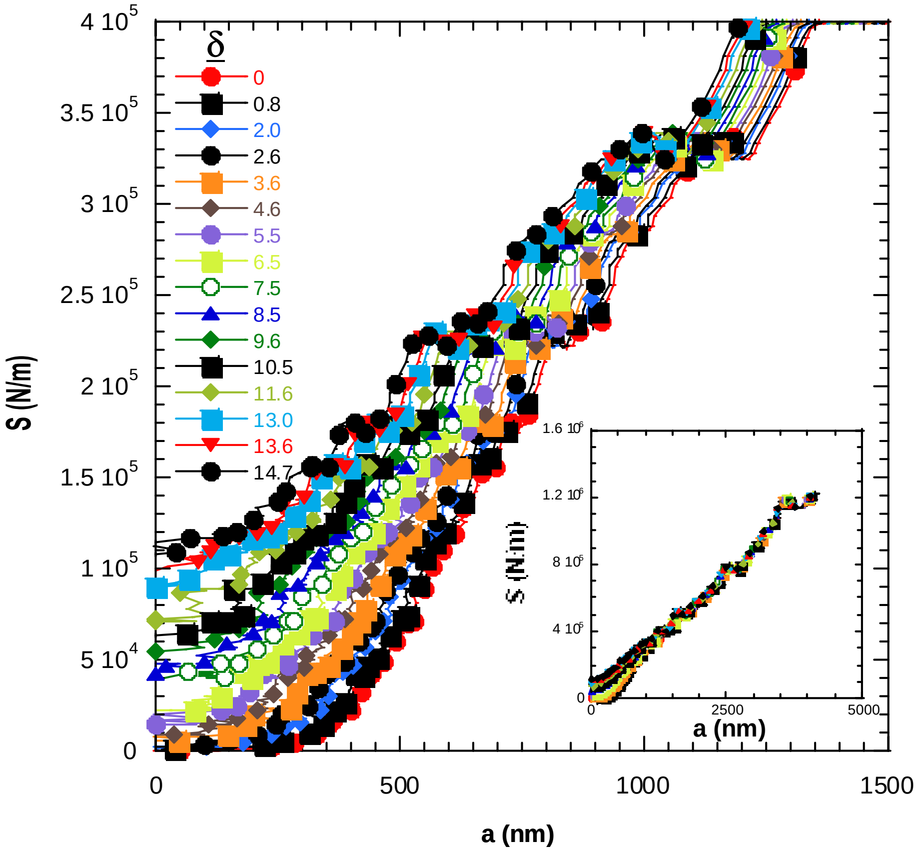

Figure 30: Detailed Example - Composite S vs. a

Table 8: Detailed Example - Composite Regression Results

Delta Sought	Actual Delta	E_{eff}	R^2	F Value	Standard Error
0	0.00000	144	0.98357	88114.18	0.96743
0.5	0.75175	144	0.98601	28904.77	1.69830
1.5	1.99447	146	0.98973	38927.57	1.47628
2.5	2.59167	146	0.99138	46014.45	1.36346
3.5	3.59099	147	0.99378	62283.59	1.17972
4.5	4.60726	148	0.99573	88876.49	0.99388
5.5	5.50213	149	0.99694	120108.57	0.85939
6.5	6.51564	150	0.99776	157377.34	0.75475
7.5	7.51742	150	0.99803	170801.42	0.72791
8.5	8.55621	151	0.99778	146297.51	0.79005
9.5	9.62434	152	0.99749	122430.72	0.86710
10.5	10.52690	152	0.99687	94969.82	0.98770
11.5	11.56399	153	0.99572	66795.71	1.18159
12.5	12.94086	153	0.99478	51420.07	1.35199
13.5	13.63216	154	0.99460	48027.64	1.40140
14.5	14.75381	154	0.99336	37824.55	1.58360

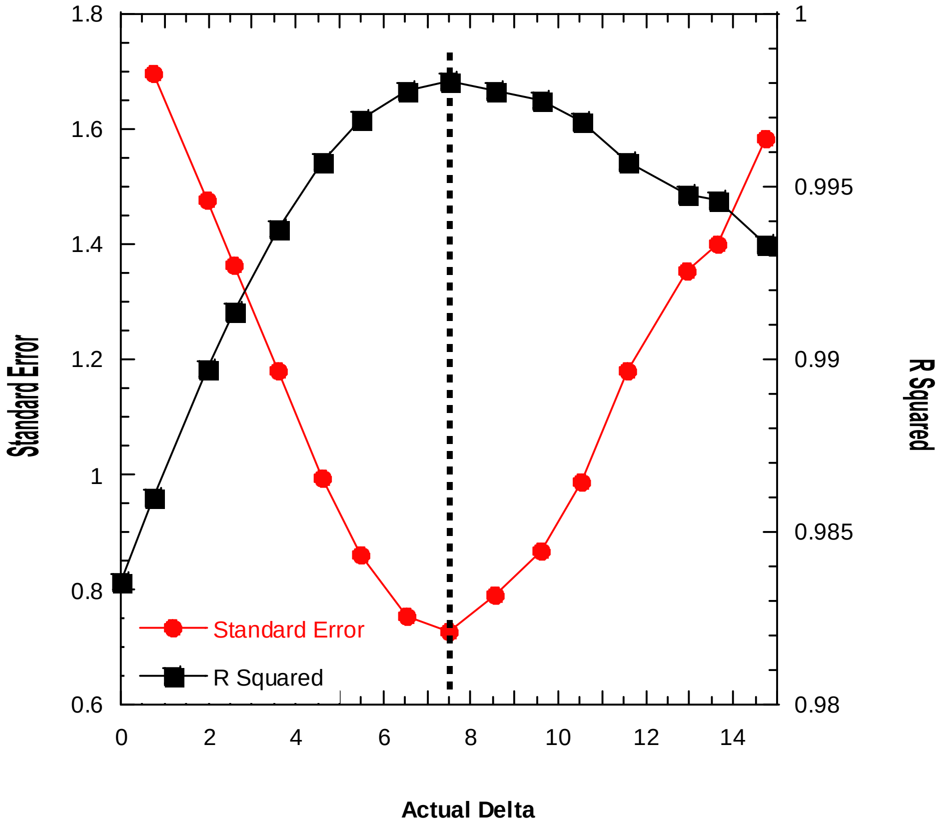

Figure 31: Detailed Example - Regression Results Comparison

We choose as the winner the δ which has the highest R^2 value. The S vs. a plot should thus appear linear and go through the origin. Our winner in this case is clearly δ = 7.5 (most easily identified in the table), the first X_j we chose.

Step 8: Change δ Range And Step Size As Necessary

Note that in the result of Step 7, we found a δ which was clearly the best, and proof that on either side of that δ, the fit was worse. If this is not the case, repeat Step 6 with a new range and/or step size. Using a larger step size, i.e. 2 nm, may be helpful to start identifying the point, but the smallest step size which yields meaningful differentiation should always be used for the final decision. For example, my P vs. h_t plot might have a broad range where X_z could be, say 20 to 80 nm. I would recommend first using a step size of 5nm, so that the number of cases is between 10 and 20. Then one could use 2 nm or 1 nm, and finally 0.5 nm. The driving force for the range would be that at each of these step sizes, the correct delta found should be near the middle of the range. If not, adjust accordingly.

Step 9: Verify Results

As with any numerical method, it is essential to check the results for validity. In our case, this means checking the plots of Load vs. Displacement, S vs. a, and Stress vs. Strain for any gross abnormalities. As Figure 15 shows, the results are indeed reasonable for this sample and location.

Summary Of Steps, Including Looping Structure

Below is a summary of the steps, in a format which highlights their structure.

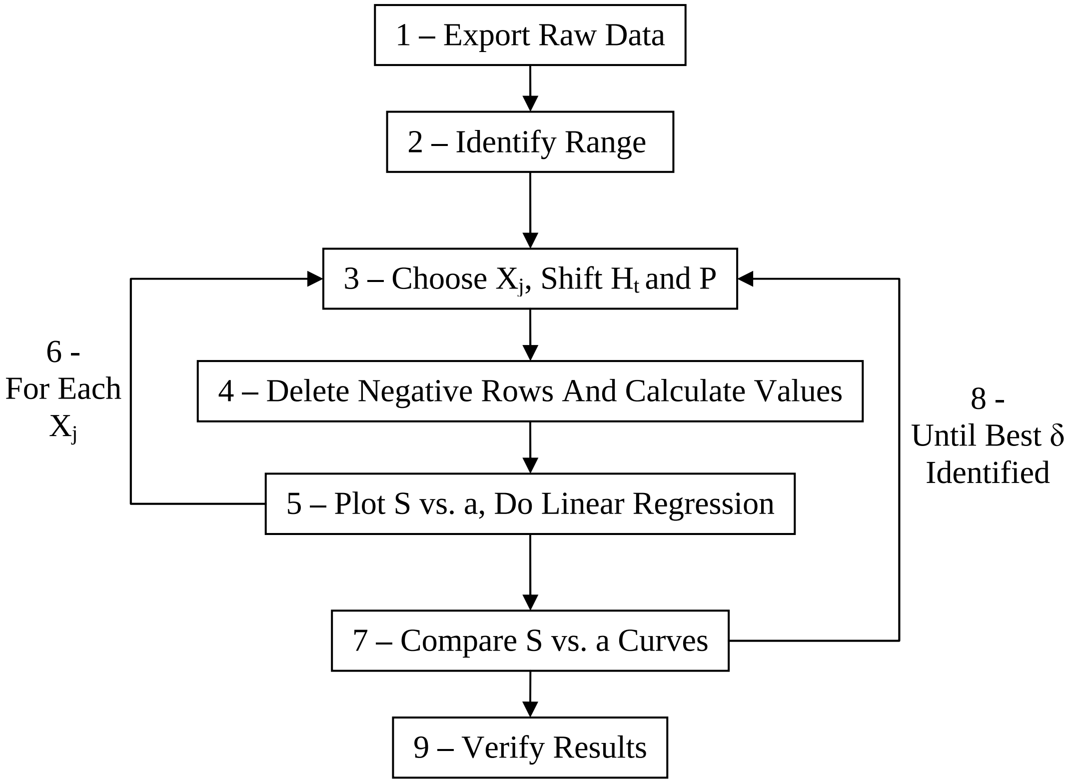

A Note On Automation

This procedure, being entirely objective and numerical, and also being repetitive, lends itself well to programmed automation. For this work, I wrote custom code in Visual Basic For Applications (VBA) within Microsoft Excel to carry out Steps 3 through 7, and then adjusted parameters manually for Step 8. This allowed me to turn a ~ 20 minute process into a 1 minute process. It was a process repeated scores of times so the effort to program was well invested. This process could conceivably be automated, in whole or in part, in any appropriate software or programming language, including Microsoft Excel, Matlab, Java, C++, etc. It could even be integrated into the software of an instrument, allowing it to much more accurately determine the effective zero point. Recall however, that the method is patent pending, so appropriate steps would have to be taken to license it.